Reversing Abnormal Neural Development by Inhibiting OLIG2 in Down Syndrome Human iPSC Brain Organoids and Neuronal Mouse Chimeras

Ranjie Xu[1,2,3], Andrew T Brawner[2], Shenglan Li[4,5], JingJing Liu[6], Hyosung Kim[1], Haipeng Xue[4,5], Zhiping P. Pang[6], Woo-Yang Kim[2,7], Ronald P. Hart[1], Ying Liu[4, 5], Peng Jiang[1,2,3,8, *]

[1]Department of Cell Biology and Neuroscience, Rutgers University, Piscataway, NJ 08854, USA.
[2]Department of Developmental Neuroscience, Munroe-Meyer Institute, University of Nebraska Medical Center, Omaha, NE 68198, USA.
[3]Mary & Dick Holland Regenerative Medicine Program, University of Nebraska Medical Center, Omaha, NE 68198, USA.
[4]Department of Neurosurgery, University of Texas Health Science Center at Houston, Houston, TX 77030, USA.
[5]Center for Stem Cell and Regenerative Medicine, the Brown Foundation Institute of Molecular Medicine for the Prevention of Human Diseases, University of Texas Health Science Center at Houston, Houston, TX 77030, USA.
[6]Department of Neuroscience and Cell Biology and Child Health Institute of New Jersey, Rutgers Robert Wood Johnson Medical School, New Brunswick, NJ 08901, USA.
[7]Biological Sciences, Kent State University, Kent, OH 44242, USA
[8]Lead contact
*Correspondence: peng.jiang@rutgers.edu

Summary

Neurodevelopmental disorder Down syndrome (DS) is the most common genetic origin of intellectual disability. Little has been achieved to reverse the abnormal brain development in DS. Using human induced pluripotent stem cells (hiPSCs), we demonstrate that the population of OLIG2-expressing ventral forebrain neural progenitors is overabundant in the cells derived from DS hiPSCs, which results in excessive production of subclass-specific GABAergic interneurons in DS cerebral organoids and causes impaired recognition memory in DS human neuronal chimeric mice. Overexpression of OLIG2 in DS directly upregulates the expression of interneuron lineage-determining transcription factors. Importantly, knockdown of OLIG2 largely reverses the abnormal global gene expression profile of early stage DS neural progenitors, reduces interneuron population in DS organoids and chimeric mouse brains, and improves behavioral performance of DS chimeric mice. Therefore, OLIG2 is a potential target for developing personalized prenatal therapeutics for intellectual disability in subjects with DS.

Introduction

Down syndrome (DS), resulting from an extra copy of human chromosome 21 (HSA21), is the leading genetic cause of intellectual disability and affects one in every 700-800 live births (Parker et al., 2010). The development of therapies for the rescue of neurocognitive impairment in DS has been limited by the lack of knowledge on the underlying molecular mechanisms (Letourneau and Antonarakis, 2012; Sturgeon and Gardiner, 2011). Previous studies have suggested that an imbalance in excitatory and inhibitory neurotransmission is one of the underlying causes of cognitive deficit of DS (Fernandez et al., 2007; Haydar and Reeves, 2012; Rissman and Mobley, 2011). The inhibitory GABAergic interneurons in the cerebral cortex are derived from the neuroepithelium of the embryonic ventral forebrain (Butt et al., 2005; Kessaris et al., 2006; Marin, 2012; Wonders et al., 2008). Many of these neuroepithelial cells express the HSA21 genes *OLIG1* and *OLIG2*, members of the basic helix-loop-helix family of transcription factors. In mice, both Olig1 and Olig2 are expressed in the embryonic neuroepithelium of the ventral forebrain (Lu et al., 2000; Petryniak et al., 2007). In humans, OLIG2, but not OLIG1, is abundantly expressed in the embryonic ventral forebrain (Jakovcevski and Zecevic, 2005), as opposed to their overlapping expression pattern in mouse embryonic brain. Thus, establishing the role of human *OLIG* genes, in regulating interneuron production is critical for understanding the mechanisms underlying cognitive deficit in DS and may help devise novel therapeutic strategies.

It is highly debatable how the production of GABAergic neurons is altered in DS and how *OLIG* genes are involved as regulators of GABAergic neuron production under normal and DS disease conditions. First, using mouse models, studies examining the functions of *Olig* genes in GABAergic neuron production remain inconclusive. Loss-of-function studies showed that only Olig1 repressed the production of GABAergic interneurons (Furusho et al., 2006; Ono et al., 2008; Petryniak et al., 2007; Silbereis et al., 2014). Gain-of-function studies showed that overexpression of Olig2 promoted the production of GABAergic neurons (Liu et al., 2015). However, this finding is confounded by the fact that the overexpression and mis-expression of Olig2 in inappropriate cells and developmental stages caused massive cell death in the mouse brain (Liu et al., 2015). Second, DS mouse models often show discrepancies in modeling DS-related genotype-phenotype relationships. Genotypically, *Olig* genes are only triplicated in a subset of DS mouse models, because different DS mouse models are trisomic for different HSA21 orthologs. Phenotypically, *Olig* genes are not always overexpressed even if they are triplicated in the genome, due to different epigenetic modifications and chromatin states in mice (Aziz et al., 2018; Belichenko et al., 2015; Goodliffe et al., 2016). The discrepant findings in genotype and phenotypic expression of *Olig* genes, and changes in the number of GABAergic neurons from different DS mouse models are summarized in Table S1. Third, while studies in the Ts65Dn mouse model of DS indicated that GABAergic neurons were overproduced (Chakrabarti et al., 2010) and inhibiting the GABAergic transmission could alleviate cognitive deficit (Fernandez et al., 2007), studies using postmortem brain tissues from elderly DS patients (Kobayashi et al., 1990; Ross et al., 1984) and 2-dimensional (2D) cultures of DS human induced pluripotent stem cells (hiPSCs) (Huo et al., 2018) contradictorily showed reduced production of GABAergic neurons.

The lack of availability of functional human brain tissue from normal or DS patients is preventive for a detailed mechanistic understanding of the pathophysiology of DS. The well-accepted non-invasive approach for prenatal DS screening is usually performed around the end of the first trimester (Malone et al., 2005). Postmortem prenatal DS human brain tissues are scarcely available and are mostly in fetal stages ranging from gestation week (GW) 13-21. Analysis of these tissues yields a limited understanding of early prenatal and embryonic DS brain development (Bhattacharyya et al., 2009; Busciglio et al., 2002; Busciglio and Yankner, 1995; Esposito et al., 2008; Goodliffe et al., 2016; Lu et al., 2012; Mao et al., 2003). Recent studies have demonstrated the utility of hiPSCs derived from individuals with DS as a human cellular model of DS brain development (Briggs et al., 2013; Chen et al., 2014; Jiang et al., 2013b; Shi et al., 2012; Weick et al., 2013). Moreover, the hiPSC-derived 3D brain organoids display structural organizations and cytoarchitecture resembling the developing human brain and have significantly advanced our knowledge on human brain development and pathology (Amin and Pasca, 2018; Brawner et al., 2017; Centeno et al., 2018; Simao et al., 2018).

In this study, we employed brain organoid and *in vivo* chimeric mouse brain models (Chen et al., 2016) to investigate the functions of *OLIG* genes in human interneuron development and pathogenesis. Using ventral forebrain organoids generated from OLIG2-GFP human pluripotent stem cell (hPSC) reporter lines, we demonstrated that human $OLIG2^{+}/GFP^{+}$ ventral forebrain neural progenitor cells (NPCs) generated various subclasses of GABAergic neurons and cholinergic neurons. We found that OLIG2 was overexpressed in DS hiPSC-derived organoids, compared with control hiPSC-derived organoids. Moreover, subclass-specific GABAergic neurons were overproduced in DS brain organoids, as well as in DS chimeric mouse brains. Significantly, DS chimeric mice exhibited impaired recognition memory. We further showed that inhibiting OLIG2 expression by shRNA normalized the overproduction of GABAergic neurons in both organoids and chimeric mouse brains and improved behavioral performance of the DS chimeric mice. Mechanistically, overexpression of OLIG2 resulted in a disrupted gene expression profile in DS organoids. Through direct interactions with GABAergic neuron lineage-determining transcription factors, OLIG2 promoted the production of subclass-specific GABAergic neurons. Development of prenatal therapy for DS has been put forward as a part of 'fetal personalized medicine' strategy (Bianchi, 2012; de Wert et al., 2017; Guedj et al., 2014). Our findings suggest OLIG2 as an excellent potential target for the personalized prenatal therapy for DS.

Results

Human PSC-derived OLIG2$^+$ ventral forebrain NPCs give rise to GABAergic neurons

To test the hypothesis that human OLIG2 is involved in interneuron development, we utilized OLIG2-GFP hPSC (human embryonic stem cell hESC and hiPSC) reporter lines generated in our previous studies (Liu et al., 2011; Xue et al., 2009). Neural differentiation of the hPSCs was induced by dual inhibition of SMAD signaling (Chambers et al., 2009). At week 2, neural rosettes were manually isolated from surrounding cells and expanded as primitive neural progenitor cells (pNPCs), as described in our recent study (Chen et al., 2016). At week 3, we further cultured these pNPCs using an established brain organoid culture protocol (Monzel et al., 2017; Pasca et al., 2015) (Figure 1A). To obtain ventralized brain organoids, we treated the organoids with Sonic Hedgehog (SHH) and purmorphamine (Pur), a small-molecule agonist of SHH signaling pathway (Liu et al., 2013a; Liu et al., 2013b; Maroof et al., 2013; Nicholas et al., 2013), from week 3 to 5. After the treatment of SHH and Pur, many cells in the organoids started to show GFP fluorescence (Figure 1A and Figure S1A). At week 5, most of the cells in the organoids expressed the NPC marker Nestin (97.0 ± 1.4%), forebrain marker FOXG1 (96.6 ± 2.6%), as well as NKX2.1 (80.0 ± 5.6%), a marker of ventral prosencephalic progenitors (Sussel et al., 1999; Xu et al., 2004), but not dorsal brain marker PAX6 (Ma et al., 2012) (n = 4, Figures 1B, 1C), indicating that the vast majority of the cells were ventral forebrain NPCs. In these organoids, we observed distinct rosette-like structures that resembled the proliferative regions of human ventricular zone containing SOX2$^+$ progenitors, and β-III-Tubulin (βIIIT$^+$) immature neurons (Figure S1B). Consistent with our previous studies (Jiang et al., 2013b; Liu et al., 2011), the GFP fluorescence faithfully mirrored the expression of OLIG2 in the NPCs (Figures 1B, 1C; about 38% of the total cells expressed both GFP and OLIG2). Interestingly, only a very small fraction of the NPCs expressed OLIG1 (1.1 ± 0.2%, Figures 1B, 1C). OLIG1 expression did not overlap with OLIG2/GFP and appeared to be localized in the cytoplasm (Figure 1B). This is consistent with a previous report that in human fetal brain tissue, although OLIG2 is expressed in the ventral forebrain throughout the ventricular zone of the ganglionic eminence, OLIG1 is expressed in very few cells (Jakovcevski and Zecevic, 2005). These observations were confirmed by immunoblot analysis. OLIG2 was abundantly expressed and present mostly in the nuclear fraction, whereas OLIG1 was detected at a low level in the cytosolic fraction (Figure 1D). Unexpectedly, qPCR results demonstrated that *OLIG1* and *OLIG*2 mRNAs were both abundantly expressed but with different temporal profiles: during the patterning stage, the levels of both *OLIG* mRNAs were significantly increased from week 3 to 5. The discrepancy between *OLIG1* transcript level and its protein level may suggest the involvement of precise spatiotemporal control of mRNA translation observed in cortical development (Kraushar et al., 2014; Kwan et al., 2012). After initiating neuronal differentiation, *OLIG2* expression started to decrease over time and GFP fluorescence became dim at week 8 (Figure 1A and Figure S1A). Nevertheless, at 8 weeks, some of the βIIIT$^+$ neurons (25.8 ± 2.3%, n = 4), GABA$^+$ neurons (24.8 ± 1.5%, n = 4), and S100β$^+$ astrocytes (2.6 ± 0.5%, n = 4) were labeled by GFP staining, indicating these cells were likely derived from OLIG2$^+$/GFP$^+$ NPCs. However, we did not find any oligodendroglial lineage cells in these organoids cultured under the neuronal differentiation condition, which is consistent with previous reports (Lancaster and Knoblich, 2014; Pasca et al., 2015; Quadrato et al., 2016). The expression of both *OLIG* gene transcripts also significantly decreased at week 8 (Figure 1E). Organoids had been known to lack oligodendrocytes (Pasca, 2018; Quadrato et al., 2016). It was not until recently that the induction of oligodendrogenesis and myelination was achieved, and culture conditions appear to be critical for oligodendroglial differentiation in organoids (Madhavan et al., 2018). In a separate set of experiments, we cultured the 5-week-old organoids under a glial differentiation condition and found MBP$^+$ mature oligodendrocytes in the 8-week-old organoids (Figure S1C), demonstrating that the OLIG2$^+$/GFP$^+$ NPCs in the organoids had the potential to differentiate to oligodendroglial lineage cells if supplied with the appropriate signals.

To further delineate neuronal fate of these OLIG2$^+$ NPCs, we purified the GFP$^+$ cells using fluorescence-activated cell sorting (FACS). At week 5, the SHH and Pur-treated organoids were

disaggregated to single cells and subjected to FACS. About 40% of the total cells were collected as GFP^+ cells (Figures 1H, 1I). The purity of these cells was verified by immunostaining, showing that all of the sorted cells expressed GFP and OLIG2 (Figure S1D). These cells also expressed Nestin, NKX2.1, and the mid/forebrain marker OTX2, confirming that these GFP^+ cells were OLIG2-expressing ventral telencephalic NPCs (Figure S1D). Then we cultured those purified $OLIG2^+/GFP^+$ cells in 3D to generate organoids. GFP fluorescence was strong at week 5 but became dim at week 8, indicating the decreased expression of OLIG2 (Figure S1E). We then assessed cell composition at week 8. We found $NeuN^+$ (89.4 ± 3.7%, n = 4) and $S100\beta^+$ (7.0 ± 0.4%, n = 4) cells in the organoids, but not $NG2^+$ or $PDGFR\alpha^+$ cells (Figures S1F, S1G), demonstrating that the majority of $OLIG2^+/GFP^+$ NPCs differentiated into neurons with a small fraction giving rise to astrocytes, but no differentiation to oligodendroglia under neuronal differentiation condition. Most strikingly, the majority of $OLIG2^+/GFP^+$ NPCs in the organoids efficiently differentiated into GABAergic neurons (57.3 ± 4.9%, n = 4; Figures 1J, 1K). GABAergic interneurons are conventionally categorized based on neuropeptide and Ca^{2+} binding protein expression (Petilla Interneuron Nomenclature Group et al., 2008). We thus examined the subclass composition of the GABAergic neurons derived from $OLIG2^+$ NPCs, by staining the major subclass markers calretinin (CR), calbindin (CB), parvalbumin (PV), somatostatin (SST), and neuropeptide Y (NPY). As shown in Figures 1J, 1K, of these markers, CR was most highly expressed (24.5 ± 3.5%, n = 4), and CB (16.0 ± 1.9%, n = 4), SST (4.9 ± 0.3%, n = 4), and PV (5.2 ± 0.9%, n = 4), were robustly detected. A small percentage of NPY^+ neurons (1.5 ± 0.4%, n = 4) was also detected. After FACS purification, some of the $OLIG2^+/GFP^+$ NPCs were also plated onto coverslips and cultured under 2D conditions in neuronal differentiation medium for 3 weeks. As opposed to 3D cultures, in the 2D cultures maintained for the same period of time, we found that the $OLIG2^+/GFP^+$ NPCs only differentiated into CR^+ neurons and other subclasses of GABAergic neuron were not detected (Figures S1H, S1I), suggesting that the 3D organoid models might be more effective in recapitulating a broader range of GABAergic neuron differentiation as seen in the developing brain. In addition, we interestingly found that a small fraction of $OLIG2^+/GFP^+$ NPCs (2.4 ± 0.7%, n = 4) were able to generate cholinergic neurons identified by the expression of choline acetyltransferase (ChAT) in the organoids (Figures 1J, 1K). Taken together, these results show that the ventral forebrain organoid model in this study recapitulates the expression pattern of OLIG1 and 2 observed in human fetal brain tissue. Moreover, we provide direct evidence demonstrating that human $OLIG2^+/GFP^+$ NPCs give rise to different subclasses of GABAergic neurons and cholinergic neurons in the 3D cultures, in addition to having the potential to differentiate into oligodendrocytes, astrocytes, and motoneurons as reported in our previous studies (Jiang et al., 2013b; Liu et al., 2011).

Abnormal OLIG2 protein expression in DS hiPSC-derived ventral forebrain organoids

Since both *OLIG1* and *OLIG2* are encoded by HSA21, we hypothesized that they would be overexpressed in DS hiPSC-derived organoids because of the increased gene dosage in DS and that this would impact neuronal differentiation. Using the method established with OLIG2-GFP reporter lines (Figure 1A), we derived ventral forebrain organoids from the three pairs of control and hiPSCs generated in our previous study (Chen et al., 2014). As shown in Table S2, the hiPSC lines derived from DS patients include two DS hiPSC lines (DS1, female; and DS2, male) and isogenic disomic (Di)-DS3 and trisomic (Tri)-DS3 hiPSCs that were generated from a single female patient. The isogenic lines were verified by comparative genomic hybridization (CGH) array, which showed no significant insertions or deletions other than full chromosome 21 trisomy (Figures S2A, S2B). As reported in our previous study (Chen et al., 2014), the same age-matched hiPSC lines (control1 and control2 hiPSCs) generated from healthy individuals were used as controls. As shown in Figure 2A, control and DS pNPCs stably exhibited disomy and trisomy of HAS21, respectively. In addition, at the DNA level, all DS pNPCs consistently had ~1.5-fold higher *OLIG1* and *OLIG2* gene copy numbers than the corresponding control pNPCs (Figure S2C). After two weeks of SHH and Pur treatment (week 5), control and DS pNPCs similarly formed organoids with ventricular zone like regions containing $Ki67^+$ and $SOX2^+$ progenitors, and $\beta IIIT^+$ immature neurons (Figure 2B). At week 5, similar expression of brain identity

markers was observed in control vs. DS organoids (Figures 2C, 2D; 99.2 ± 0.2%, vs. 99.3 ± 0.2% for Nestin$^+$ cells; 96.6 ± 1.4% vs. 95.4 ± 1.7% for FOXG1$^+$ cells; 77.1 ± 4.3% vs. 74.9 ± 5.8% for NKX2.1$^+$ cells; and 0.09 ± 0.2% vs. 0.15 ± 0.2% for PAX6$^+$ cells), indicating the efficient patterning of DS and control pNPCs to ventral forebrain identify. The pooled data were generated from experiments repeated for four times (n = 4) using the three pairs of control and DS hiPSCs and for each experiment, 4 to 6 organoids from each cell line (total around 70 control and 70 DS organoids) were used.

As predicted, a significantly higher percentage of OLIG2$^+$ cells was found in DS organoids, compared to control organoids (~ 40% in control vs. 70% in DS, Figure 2E, 2F; n = 4). Consistent with this, we observed a significantly higher expression of *OLIG2* mRNA (6 to14-fold), compared to control organoids (Figure 2G). This finding was verified by western blot analysis (Figures 2E, 2F). In addition, we also observed a higher expression of *OLIG1* transcripts in DS organoids (6 to 17-fold, Figure 2G). However, very few OLIG1$^+$ cells were identified in either DS or control organoids by immunostaining and no significant differences were noted between the two groups (Figures 2C, 2D). Western blot analysis confirmed the similarly low expression of OLIG1 protein in both control and DS organoids (Figures 2H, 2I). These results indicate that our organoid model recapitulates the temporal expression of *OLIG* genes observed in human brain tissue, further implicating the potential role of OLIG2 in neuronal differentiation in early stage NPCs.

To assess the maturity and region specificity of the DS and control organoids, we obtained global transcriptome profiles of organoids by RNA-seq and compared them with BrainSpan, the largest dataset of postmortem human brain transcriptomes from embryonic ages to adulthood (Kang et al., 2011). Remarkably, the transcriptome analyses suggested that the hiPSC-derived 5-week-old organoids were most similar to the human brain in 8 to 9 weeks post-conception (pcw) (Figure 2J). With regards to regional specificity, our preparation best reflected human ventral forebrain, including caudal ganglion eminence (CGE), lateral ganglion eminence (LGE), medial ganglion eminence (MGE), and striatum (STR), with smaller homology to the neocortex (NCX), hippocampus (HIP), amygdala (AMY), and upper rhombic lip (URL) (Figure 2K). We further comprehensively analyzed the maturity and ventral forebrain specificity of our organoids. Consistent results demonstrated that our preparation best reflected the 8 to 9 pcw of MGE, CGE, and LGE, particularly the MGE. However, much less homology was found to STR that only appears after 9 pcw (Figure 2L).

Overabundance of GABAergic neurons in DS ventral forebrain organoids and early postnatal DS human brain tissue

To investigate the generation of GABAergic neurons in DS human brain, particularly in early brain development stages, we cultured the control and DS organoids under the neuronal differentiation condition shown in Figure 1A. Both DS and control organoids similarly increased in size over time in culture (Figures S2D, S2E). The NPCs in DS and control organoids also efficiently differentiated to neurons. At week 8, we saw robust expression of MAP2 (Figure 3A). We next compared the cell compositions in the DS and control organoids (Figures 3B, 3C). Similar percentages of NeuN$^+$ neurons (82.3 ± 3.3% vs. 84.4 ± 3.3% in control and DS organoids, respectively; n = 4) and S100β$^+$ astrocytes (7.7 ± 0.6% vs. 7.9 ± 0.9% in control and DS organoids, respectively; n = 4) were found, indicating similar neural differentiation in the two groups of organoids. Notably, GABA staining robustly labeled neuronal processes in addition to cell bodies in the organoids (Figure 3D and large-area images of organoids in Figure S2F). The GABA fluorescence intensity (FI) in the DS organoids was also significantly higher than that in control organoids (Figure 3E, n = 4). More than half of the cells (~60%) were GABA$^+$ neurons in DS organoids, compared with only ~35% in control organoids (Figures 3D, 3G; n = 4).

We next examined the differentiation to various subclasses of GABAergic neuron in week 8 organoids. There were significantly more CR$^+$ (~35% vs. ~15% in DS and control organoids, respectively; n = 4) and SST$^+$ (~8% vs. ~2% in DS and control organoids, respectively; n = 4) GABAergic neurons in DS organoids than in control organoids (Figure 3F, 3G and Figure S2F). There were no significant differences in the percentage of NPY$^+$, CB$^+$, and PV$^+$ GABAergic neurons (Figures

3F, 3G). In addition, the percentage of ChAT$^+$ cholinergic neurons were also similar in the two groups of organoids (n = 4). To validate these findings, we examined the expression of CR, SST and GAD65/67, an enzyme required for GABA synthesis and a marker of GABAergic neurons, in postmortem cerebral cortex tissue from DS and control subjects at ages of less than one year old (Table S3). These human brain tissues were applicable for western blot analysis, since the denatured SDS-PAGE and Coomassie blue staining showed that the human brain sample preparations exhibited the absence of smear (little or no degradation) and sharp resolution of protein bands (Figure S2G). Strikingly, we observed that protein levels of CR and GAD65/67 in DS patients, as compared to healthy controls, were significantly higher (Figures 3H, 3I). There was a trend of increased expression of SST in DS patients but with large variations, so no statistical significance was detected. This could be due to the relatively much smaller number of SST$^+$ neurons in the cerebral cortex in neonatal human brain, compared to CR$^+$ neurons (Paredes et al., 2016). Taken together, these results demonstrate that the organoid model effectively recapitulates the overabundance of GABAergic neurons seen in the developing DS human brain. We further reveal that among various subclasses of GABAergic neurons, CR$^+$ and SST$^+$ GABAergic neurons are preferentially overproduced in the early developing DS brain.

DS neuronal chimeric mice show overproduction of GABAergic neurons

The *in vitro* data we obtained from the brain organoids was exciting in that the overexpressed OLIG2 in DS appears to bias neuronal differentiation towards inhibitory neurons. However, these neurons represented early developmental stages (Nicholas et al., 2013; Pasca et al., 2015; Patterson et al., 2012). We thus sought to use a human neuronal chimeric mouse brain model (Chen et al., 2016) to examine the stability of the inhibitory neuronal fate of engrafted DS or control NPCs *in vivo*.

We disassociated the 5-week-old, patterned early ventral forebrain DS and control organoids into single progenitor cells and transplanted them into the brains of neonatal r*ag1*$^{-/-}$ immunodeficient mice at regions overlying lateral ventricles (Figure 4A). For the transplantation experiments, two pairs of control and DS hiPSC lines, including control1 and DS1, and isogenic Di-DS3 and Tri-DS3 hiPSC lines, were used, because based on our results in organoids, all DS lines consistently showed similar trends of changes with statistical significance when compared with corresponding control lines (Figures 2G, 3E, 3G, 4J, and 4K). Moreover, inclusion of isogenic hiPSC lines can potentially limit the need for multiple iPSC lines to control for genetic variation (Chen et al., 2014; Maclean et al., 2012; Weick et al., 2013). The donor-derived cells were tracked by staining human nuclei (hN) with specific anti-human nuclei antibody. We found that both engrafted DS and control cells were similarly distributed in mouse brains. At two months post-injection, the engrafted cells were mainly found near the injection sites (Figure 4B1), with some of the cells having migrated to the deep layers of cerebral cortex (Figure 4B2). Occasionally, a small cluster of cells was found in the superficial layers of cerebral cortex (Figure 4B2), which might have been deposited when the injection needle was retracted. The majority of hN$^+$ donor-derived cells expressed NKX2.1, indicating that engrafted cells retained their ventral brain identity *in vivo* (Figures S3A, S3B). At six months post-transplantation, we observed that around 60% of donor-derived cells were LHX6$^+$ in the cerebral cortex in both control and DS groups (Figures S3C, S3D), suggesting that the majority of the cells were post-mitotic interneuron precursors derived from the NKX2.1$^+$ progenitors (Zhao et al., 2008). At six months post-injection, a large population of human cells dispersed widely in the cerebral cortex, as shown by hN staining in both sagittal and coronal brain sections (Figure 4C and Figures S3E-S3K). Notably, there was a high density of donor-derived cells in the superficial layers and a low density in the deep layers (Figure 4C1), suggesting the migration of donor-derived cells from injection sites to the cerebral cortex. Doublecortin (DCX) is a marker of young migrating neurons (Gleeson et al., 1999). At 4 months post-injection, many hN$^+$ cells expressed DCX and had bipolar processes, further suggesting migration of the engrafted cells (Figure S3L). We also tested injecting cells into deeper sites near the subventricular zone (SVZ) and found that the engrafted cells preferentially migrated along the rostral migratory stream to the olfactory bulb and did not lead to distribution and chimerization in the cerebral cortex (Figure S4). This observation is consistent with previous reports (Fricker et al., 1999; Tischfield and Anderson, 2017) that transplanting cells to different

sites leads to different migration and distribution patterns. However, in contrast to our findings in the cerebral cortex, very few of these human cells in the olfactory bulb differentiated into CR^+ cells (Figures S4C, S4F), further suggesting that that the vast majority of the neural progenitors generated using our current protocol were NKX2.1 lineage and mainly gave rise to cortical or striatal interneurons, rather than olfactory bulb interneurons.

To specifically study the human GABAergic neurons developed in the context of cerebral cortex, we focused on analyzing the animals that received cell transplantation to the sites overlying the lateral ventricles and had a wide distribution of donor-derived cells in the cerebral cortex at the age of 6 months. In a separate group of animals, prior to transplantation, we labeled the cells with lentiviral-CMV-GFP and observed wide distribution of GFP^+ processes in the hippocampus, despite the fact that a small population of hN^+ cells were seen in the hippocampus (Figure 4D). In addition, the control and DS cells were highly proliferative before transplantation, as demonstrated by high percentages of $Ki67^+$ cells in both groups (Figures S5A, S5C). We also found that there were more $OLIG2^+/Ki67^+$ cells among total $OLIG2^+$ cells in DS organoids than in control organoids, indicating that DS $OLIG2^+$ ventral forebrain NPCs are more proliferative than control $OLIG2^+$ ventral forebrain NPCs (Figures S5A, S5C). After transplantation, the $Ki67^+/hN^+$ cells dramatically decreased from 2 months (Figures S5B, S5D; 10.2 ± 1.7% and 14.3 ± 3.3% for control and DS group, respectively; n = 7) to 6 months (0.9 ± 0.4% and 1.4 ± 0.6% for control and DS group, respectively; n = 7). We did not observe any tumor formation of the transplanted cells in all the animals examined. Next, we analyzed the differentiation of the engrafted cells in the cerebral cortex of 6-month-old chimeric mice. As shown in Figures 4E, 4I, we found that a large proportion of the engrafted DS and control cells gave rise to $NeuN^+$ neurons. Consistent with previous studies using human samples (Chen et al., 2014; Esposito et al., 2008; Guidi et al., 2008), the DS NPCs exhibited impaired neurogenesis, as indicated by a slightly reduced percentage of $NeuN^+/hN^+$ neurons among total hN^+ cells in the DS cell transplantation group (84.2 ± 3.2%, n = 7), as compared to the control cell transplantation group (76.7 ± 3.3%, n = 7). A small fraction of the engrafted cells gave rise to $GFAP^+$ astrocytes (4.9 ± 3.0% and 4.5 ± 1.7% for control and DS group, respectively) and MBP^+ mature oligodendrocytes (2.0 ± 0.6% and 1.6 ± 0.7% for control and DS group, respectively). No significant differences were noted in the percentages of astrocytes and mature oligodendrocytes in the two groups. In addition, some of the donor-derived cells also expressed OLIG2, most of which at this stage were likely to be oligodendroglia progenitor cells, because no $Nestin^+$ human NPCs were found in these 6-month-old chimeric mouse brains. We observed a higher percentage of $OLIG2^+/hN^+$ cells among total hN^+ cells in the DS cell transplantation group (18.9 ± 3.40%, n = 7) than that in control cell transplantation group (12.5 ± 1.9%, n = 7). To further investigate the differentiation of OPCs from transplanted cells, we examined the expression of OPC marker, PDGFRα. Consistently, we found that there were a higher percentage of $PDGFR\alpha^+/hN^+$ OPCs in DS group than in control group (Figures S5E, S5F). These results might reflect the altered oligodendroglial differentiation seen in Ts65Dn mice and DS human brain tissue (Goodliffe et al., 2016). To examine GABAergic neuron differentiation from the engrafted cells, we double-stained the brain sections with GABA and hN. As shown in Figure 4F and Figures S5G, S5H, GABA staining labeled not only the cell body, but also the processes. As such, the areas that were strongly immunopositive for GABA staining were enriched for hN^+ donor-derived cells, indicating the efficient differentiation of the engrafted cells to GABAergic neurons. These interneurons also expressed vesicular GABA transporter (VGAT) (Figure S5I). We then quantified the FI of GABA staining in the areas that were enriched for hN^+ donor-derived cells to compare the production of GABAergic neurons from transplanted DS and control cells. Consistent with the observations in organoids, engrafted DS cells overproduced GABAergic neurons, indicated by the much higher FI of GABA staining in DS cell transplantation group, as compared to control cell transplantation group (Figures 4G, 4J). Similar results were also obtained by examining the expression of GAD65/67 (Figures S6A, S6F). Furthermore, we examined the different subclasses GABAergic neuron. Significantly higher percentages of CR^+/hN^+ and SST^+/hN^+ neurons among total hN^+ cells were found in DS cell transplantation group than in control cell transplantation group (Figures 4H, 4K), which was similar to the observations in organoids. No significant differences were noted in

the percentage of CB^+/hN^+, PV^+/hN^+, and NPY^+/hN^+ GABAergic neurons, as well as $ChAT^+/hN^+$ cholinergic neurons (Figures 4H, 4K). Previous studies in mice show that a subpopulation of neocortical interneurons co-express CR and SST (Xu et al., 2006). To further examine whether this subpopulation of interneurons was overly produced from transplanted DS cells, we triple-stained control and DS chimeric mouse brains with CR, SST, and hN. At 6 months post-transplantation, none of the human interneurons in control chimeric mice co-expressed CR and SST, whereas in DS chimeric mice, CR^+/SST^+ human interneurons were occasionally seen (Figure S6B; less than 1% of total hN^+ cells). These results suggest that the subclass of CR^+/SST^+ interneurons is increased in the DS chimeric mice, but they only represent a very small population. The overly produced interneurons from the engrafted DS cells are mainly CR^+/SST^- and CR^-/SST^+ interneurons.

We further immunostained synaptic markers in the brain sections. As shown in Figure S6C, many of the hN^+ cells in the cerebral cortex were surrounded by the presynaptic marker synapsin I. Then, we double-stained human-specific MAP2 (hMAP2), which selectively labels dendrites of donor-derived human neurons, and postsynaptic density protein 95 (PSD-95), a postsynaptic marker. The $PSD\text{-}95^+$ puncta were found to distribute along the $hMAP2^+$ dendrites (Figure S6D). These results suggest that the human neurons likely form synapses in the mouse brain. Furthermore, we examined the expression of c-Fos, an activity-dependent immediate early gene that is expressed in neurons following depolarization and often used as a marker for mapping neuronal activity (Loebrich and Nedivi, 2009). As shown in Figures S6E, S6G, about 20% of the hN^+ neurons at 6 months were positive for c-Fos, indicating that they were functionally active in the mouse brain. Moreover, in a separate group of animals, we labeled donor cells with lentiviral-CMV-GFP before transplantation. At 6 months post-transplantation, we performed electron microscopic analysis. We observed synaptic terminals formed between human neurons labeled by diaminobenzidine (DAB) staining against GFP or a human-specific cytoplasmic marker STEM121 and mouse neurons that were not labeled by the DAB staining (Figure S6H). In addition, we performed patch-clamp recording in brain slices and backfilled the recorded cells with fluorescent dye Dextran Alexa 594 through the recording pipettes. The identity of recorded cells was revealed by *post hoc* immunostaining with hN antibody and detected colocalization with the fluorescent dye. Among 22 recorded cells from 4 mice, 7 were identified as human neurons (Figure 4L). Out of the 7 hN^+ donor-derived neurons, 6 neurons fired action potentials upon ramp current injections (Figure 4M) and all 7 neurons exhibited spontaneous postsynaptic currents (sPSCs) and potentials (sPSPs) (Figure 4N). These responses had sharp rises and slow decays, which are characteristics of synaptic events. In addition, both excitatory and inhibitory postsynaptic current responses were seen, based on their respective kinetics (Figure 4N, upper panel), suggesting that donor cell-derived GABAergic neurons might have interactions with host neuronal cells in the mouse brain. Taken together, these results indicate that this human neuronal chimeric mouse model, in which ventral forebrain NPCs are engrafted, recapitulates the overproduction of GABAergic neurons from DS NPCs in brain organoids.

OLIG2 overexpression in DS biases gene expression attributed to GABAergic neurons

To gain mechanistic insight into how DS ventral brain NPCs were biased to GABAergic neuron generation, we performed next-generation whole-genome deep sequencing and analyzed the transcriptomic profiles of 5-week-old DS and control organoids, including one pair of control and DS organoids (control1 and DS1), and the pair of isogenic Di-DS3 and Tri-DS3 organoids. A dendrogram demonstrated that two control organoids (control1 and Di-DS3 organoids) and two DS organoids (DS1 and Tri-DS3 organoids) clustered closer to each other, respectively, indicating that they had similar biological properties within the same group, while the gene expression of DS organoids was distinct from that of control organoids (Figure 5A). Next, we did two-step analyses to narrow down to the most prominent differentially expressed genes (DEGs) that were identified in common between control1 vs. DS1 and Di-DS3 vs. Tri-DS3 organoids. Previous studies have shown that comparisons of RNA-seq data between isogenic pairs are often distinct from those between cell lines with different genetic backgrounds (Lin et al., 2015). Thus, choosing only transcripts overlapping between the two pairs of

cultures provides an added level of confidence in their reproducibility. As shown in Figures 5A, 5B, we began with comparing expression of transcripts between control1 and DS1 organoids. We identified a total of 2,920 DEGs, including 1,796 up-regulated genes and 1,124 down-regulated genes. To reduce the potential interference of different genetic background between control1 and DS1 cells, we then examined the 2,920 DEGs in the organoids generated from isogenic Di-DS3 and Tri-DS3 hiPSCs. We identified that a total of 610 overlapping DEGs, including 398 up-regulated genes and 212 down-regulated genes. Notably, there were 943 DEGs (506 up-regulated genes and 437 down-regulated genes) in the comparison between Di-DS3 and Tri-DS3 organoids that were not seen in the comparison between control1 and DS1 organoids. Next, we analyzed the distribution of the overlapping 610 DEGs on each human chromosome. As shown in Figure 5C, we found that the majority of the DEGs were non-HSA21 genes (577 of 610 DEGs), similar to previous studies using human samples (Goodliffe et al., 2016; Weick et al., 2013). However, HSA21 had the highest percentage of DEGs among all the chromosomes. We also observed that all of the DEGs on HSA21 were upregulated in DS samples and the overexpression of these genes on HSA21 resulted in both positive and negative regulation of the genes on other chromosomes. To further investigate how inhibiting the expression of *OLIG2* would change the global gene expression profile in DS during early embryonic brain development, we generated Tri-DS3 hiPSCs expressing OLIG2 shRNA (Tri-DS3 + OLIG2^{shRNA} hiPSCs) by infecting these hiPSCs with lentivirus carrying the OLIG2 shRNA. Then we generated organoids from the hiPSCs (Tri-DS3 + OLIG2^{shRNA} organoids). RNA-seq results revealed that many DEGs were reversed after OLIG2 knockdown, as compared to the organoids derived from the Tri-DS3 hiPSCs received control shRNA with scrambled and non-targeting sequences (Tri-DS3 + Cont^{shRNA} organoids) and control1 organoids (Figure 5D). A Venn diagram showed that the expression of 255 of 398 upregulated overlapping DEGs and 166 of 212 downregulated overlapping DEGs was effectively reversed (Figure 5E). We also analyzed the reversed DEGs after OLIG2 knockdown compared between Di-DS3 and Tri-DS3 and their distribution on chromosomes (Figures S7A, S7B). To explore the possible biological processes altered by the overlapping DEGs, gene ontology (GO) analyses of the upregulated and downregulated genes were performed. Biological processes such as myelin sheath, transcription, and cell proliferation were significantly enriched, consistent with previous findings (Goodliffe et al., 2016; Lockstone et al., 2007; Lu et al., 2012) (Figures 5F, 5G). Interestingly, GO and top 20 annotated pathways revealed that an enrichment of downregulated genes in DS organoids was particularly related to neurodevelopmental terms such as nervous system development, synaptic vesicle recycling, axon guidance, synaptic vesicle, axon extension, dendrite and neuron projection guidance, indicating that the embryonic neuronal development as early as 8 to 9 pcw is altered in DS (Figure 5F). In addition, we found that the upregulated genes in DS organoids were enriched in extracellular matrix terms, such as extracellular matrix organization, extracellular matrix structural constituent, extracellular matrix disassembly, indicating that the altered cells' dynamic behavior in DS might affect cell adhesion, communication, and differentiation and fate specification (Figure 5G). Moreover, the GO analyses demonstrated that most of the changed pathways in both DS1 and Tri-DS3 groups were also significantly rescued, such as nervous system development, axon guidance, and extracellular matrix organization, suggesting that inhibiting OLIG2 expression in DS effectively reversed the tendency for abnormal neurodevelopment (Figures 5F, 5G).

In order to investigate the molecular mechanisms underlying the overproduction of GABAergic neurons in DS, we examined the expression of transcription factors that play critical roles in GABAergic neuron development and specification (Cobos et al., 2006; Kelsom and Lu, 2013). RNA-seq results indicated that expression of many of these transcription factors was altered in DS organoids, as compared to control organoids. Among this group, *DLX1/2*, *LHX6/8*, and *SOX6* are reported to regulate specification of CR^{+} and SST^{+} interneurons (Azim et al., 2009; Flandin et al., 2011; Hanson et al., 2007). *NPAS1/3*, which also regulates interneuron fate (Stanco et al., 2014), was abnormally increased in the DS organoids. In addition, we also found that other genes that regulate interneuron neurogenesis and migration, such as *ASCL1*(Casarosa et al., 1999; Castro et al., 2011), *ARX* (Colasante et al., 2008), and *NR2F2* (Kanatani et al., 2008) were also altered in DS organoids. Furthermore, we analyzed

expression of these transcription factors after *OLIG2* knockdown. Strikingly, the majority of them were effectively reversed (Figure 5H). We further performed qPCR to verify RNA-seq results using brain organoids from the isogenic pair of hiPSCs. As shown Figure 5I, qPCR results showed that the expression of all the transcripts was increased in DS. Among all the genes we examined, only *DLX 5* and *6* showed inconsistent results between RNA-seq and qRT-PCR verification. Notably, unlike other genes in the RNA-seq analysis (Figure 5H), only *DLX 5* and *6* exhibited different expression levels between Tri-DS3 organoids and Tri-DS3+Cont^{shRNA} organoids which were derived from the same Tri-DS3 hiPSCs but received infection of lentivirus carrying control shRNA. This result suggests that expression levels of *DLX5* and *6* might not be able to be stably detected by RNA-seq. This could be caused by the low expression levels of *DLX5* and *6,* because our qRT-PCR analysis indicated that *DLX5* and *6* were present at very low abundance in all the cell preparations (< 0.015% and 0.004% of GAPDH for *DLX5* and *6*, respectively in control organoids, as compared to 0.48% and 0.73% of GAPDH for *DLX1* and *2*, respectively). Moreover, our qPCR results demonstrated that inhibiting OLIG2 expression reversed the increased expression of the majority of the transcription factors, such as *DLX1/2*, *LHX6/8* and *SOX6* (Figure 5I).

As a transcription factor, OLIG2 was reported to regulate gene expression through activating the promoter and enhancer (Kuspert et al., 2011; Ligon et al., 2007). To further test our hypothesis that OLIG2 could regulate the expression of these transcriptional factors directly through interacting with the promoters of these genes, we performed a chromatin immunoprecipitation (ChIP) assay. We focused on examining the interactions between OLIG2 with *LHX8* or *DLX1* promoter sequences, because *LHX8* had the highest fold-change in the DS (Figure 5I) and *DLX1* was reported to be crucial for the production and longevity of CR^{+} and SST^{+} GABAergic neuron (Hanson et al., 2007). We designed 6 to 7 pairs of primers to span the 2000bp promoter sequences of upstream of the transcriptional start sites (TSS) of *LHX8* and *DLX1*. As shown in Figure 5J, OLIG2 antibody immunoprecipitated the regions from -162 to -345, -1149 to -1321, and -1756 to -1890 in *LHX8* promoter region and from -320 to -452 in *DLX1* promoter region, demonstrating direct interactions of OLIG2 with promoters of *LHX8* and *DLX1*. We further performed dual luciferase reporter assay to examine the functionality of OLIG2 interactions with *DLX1* and *LHX8*. Based on our ChIP-PCR assay results, we cloned the promoter sequences of *DLX1* (-10 to -1250) and *LHX*8 (-1 to -2000) and inserted them into pGL3-Basic luciferase reporter vector. We then transfected these plasmids into control hiPSC-derived pNPCs. As shown in Figure 5K, when an OLIG2 expression vector was co-transfected into these cells, compared to co-transfection with a control vector, nearly 2.6 or 2.1-fold upregulation of luciferase activity was induced for *DLX1* or *LHX8*, respectively (Figure 5K). Thus, these data provide direct evidence indicating that OLIG2 functions upstream of DLX1 and LHX8 and promotes their expression by regulating their promoter activity.

Collectively, all these results demonstrate that OLIG2 overexpression is likely associated with the abnormal gene expression profiles and that altered biological processes are critically involved in early DS embryonic brain development. More importantly, we find that OLIG2 directly binds and regulates the promoter regions of pro-inhibitory neuronal differentiation transcription factors, which might be the molecular underpinnings for a biased neural differentiation in DS.

Inhibiting OLIG2 expression rescues overproduction of GABAergic neurons in DS organoids and chimeric mouse brains

Given the mechanistic insight presented in this study that overexpressed OLIG2 was responsible for the abnormal neuronal differentiation, we hypothesized that inhibiting the expression of OLIG2 would reverse the overproduction phenotypes under trisomy 21 conditions. To test this hypothesis, again we took the RNAi knockdown approach and used two DS hiPSC lines expressing OLIG2 shRNA or control shRNA (In addition to the Tri-DS3 hiPSCs, we also generated DS1 hiPSCs expressing OLIG2 shRNA or control shRNA). Knockdown efficiency was confirmed by examining OLIG2 expression at both mRNA and protein levels (Figures S7C, S7D, S7E). We cultured the 5-week-old DS + OLIG2^{shRNA} and DS + Cont^{shRNA} ventral forebrain organoids under neuronal differentiation conditions and also generated chimeric mouse brains by engrafting the NPCs dissociated from those organoids. After 3 weeks (8-

week-old organoids), we examined the cell compositions and found that NeuN, S100β, PDGFRα, and NG2 expression were similar in disomic control, DS + OLIG2^{shRNA}, and DS + Cont^{shRNA} organoids (Figures S7F, S7G). Then we examined the population of GABAergic neurons. The percentages of GABA^{+} cells and FI of GABA staining were significantly decreased in DS + OLIG2^{shRNA} organoids, as compared to DS + Cont^{shRNA} organoids (Figures 6A, 6B). Moreover, the percentages of CR^{+} and SST^{+} GABAergic neurons were decreased after inhibition of OLIG2 expression (Figures 6C, 6D). The percentages of other subclasses of GABAergic neurons and cholinergic neurons were not significantly changed. In 6-month-old chimeric mouse brains, we found that the percentage of NeuN^{+}/hN^{+} among total hN^{+} cells increased in the mouse brains which received DS + OLIG2^{shRNA} NPC transplant, as compared to the mouse brains which received DS + Cont^{shRNA} NPC transplant (Figures S7H, S7I). Consistent with the results in organoids, FI of GABA staining was decreased after inhibiting OLIG2 expression (Figures 6E and 6F). The overproduction of CR^{+} and SST^{+} GABAergic neurons was rescued and no significant differences of the population of CB^{+}, PV^{+}, NPY^{+}, and ChAT^{+} neurons were noted (Figures 6E and 6F). Therefore, overexpression of OLIG2 in DS results in overproduction of subclass-specific GABAergic neurons, which can be rescued by inhibiting OLIG2 expression.

DS chimeric mice exhibit impaired recognition memory that can be improved by inhibiting OLIG2 expression

Cognitive impairment**,** characterized by learning and memory deficits, is a primary phenotypic manifestation of DS patients and mouse models of DS (Contestabile et al., 2010). Based on the findings that the donor cell-derived neurons might interact with host neurons in the mouse brain, we hypothesized that engrafted control and DS cells might differently impact the behavioral performance of the animals and inhibiting the expression of OLIG2 in DS cells would reverse the different behavior phenotypes. To test our hypothesis, we examined five groups of mice: (1) vehicle control group that received injection of phosphate-buffered saline (PBS); (2) control chimeric mice that received transplantation of control1 or Di-DS1 cells; (3) DS chimeric mice that received transplantation of DS1 or Tri-DS3 cells; (4) DS + Cont^{shRNA} chimeric mice that received transplantation of DS1+Cont^{shRNA} or Tri-DS3+Cont^{shRNA} cells ; and (5) DS + OLIG2^{shRNA} chimeric mice that received transplantation of DS1+OLIG2^{shRNA} or Tri-DS3+OLIG2^{shRNA} cells. We performed histological assessment after behavioral testing and assessed the engraftment efficiency and degree of chimerization by quantifying the percentage of hN^{+} cells among total DAPI^{+} cells in sagittal brain sections covering regions from 0.3 to 2.4 mm lateral to midline, as reported in the previous studies (Chen et al., 2015; Han et al., 2013). We found that the degree of chimerization was similar among the four groups of animals that received cell transplant (Figure S7J).

We performed the open field test to evaluate basal global activity in the five groups of mice. Mice were placed into a chamber under dim ambient light conditions and activity was monitored for 5 minutes. We found no significant difference in the total traveling distance and time in the center area (Figure 7A; n = 10 - 15), suggesting no significant difference in locomotor activity and exploratory behavior among the four groups. Next, we performed the novel object recognition test to assess the learning and memory that is associated with the prefrontal cortex and hippocampus (Antunes and Biala, 2012; Wan et al., 1999). Mice were placed in the center of the acquisition box and allowed for 10 min to investigate two identical objects during the training day. 24 hours later, one old object was replaced with a novel object and the time spent on each object was recorded on the testing day (Figure 7B). Similarly, no difference in the total traveling distance was observed (Figure 7B). We did not observe any significant behavioral changes in the preference ratio to the novel object between the PBS control group and control chimeric mouse group (Figure 7B). Interestingly, DS chimeric mice spent less time with the novel object, compared to control chimeric mice and PBS control mice (Figure 7B; 0.62 ± 0.024, 0.68 ± 0.028, 0.50± 0.017 for PBS control mice, control chimeric mice, and DS chimeric mice, respectively; n = 10-15), suggesting that DS chimeric mice had impaired recognition memory. Moreover, this impairment was effectively rescued by inhibiting OLIG2 expression (Figure 7B; 0.49 ± 0.020 and 0.60 ± 0.016 for DS + Cont^{shRNA} and DS + OLIG2^{shRNA} chimeric mice, respectively; n = 10-

15). Next, we performed the elevated plus maze test to assess anxiety of the chimeric mice to further rule out the effects of anxiety on learning performance. Based on the rodents' tendency toward dark, enclosed spaces, and an unconditioned fear of heights/open spaces, mice were placed in the center of the apparatus with two open and two enclosed elevated arms and allowed to explore the apparatus for 5 min. We did not observe any significant difference in the total traveling distance, the number of entries, and time spent in the open arms (Figure 7C; n = 10-15), suggesting the anxiety was similar among the five groups.

Discussion

The development of species-specific research tools to investigate the functions of HAS21 genes in human brain development and pathology is important. In this study, we unravel the contribution of *OLIG2* overexpression in DS to developmental abnormalities in humans by using a unique hiPSC-based paradigm to precisely model DS. In this paradigm, we employ a complementary combination of human iPSC-derived cerebral organoid and developmentally-appropriate chimeric mouse brain model systems. These systems embrace the complexity of human neural cells developed in 3D conditions that retain cell-cell/cell-matrix interactions.

Compared to conventional 2D monolayer cultures, the 3D cerebral organoid model possesses significant advantages for modeling human embryonic ventral forebrain development and neuronal differentiation. The ventral forebrain organoids closely recapitulate the expression pattern of OLIG1 and OLIG2 in the human embryonic brain under healthy and DS disease states. As opposed to 2D cultures, the OLIG2$^+$ NPCs in the 3D cultures are capable of efficiently generating distinct subclasses of neurons. Differentiation of human cholinergic neurons is rarely seen from ventral forebrain NPCs in 2D cultures (Ma et al., 2012; Maroof et al., 2013; Nicholas et al., 2013), unless nerve growth factor, a survival factor for cholinergic neurons, is added (Liu et al., 2013b). Interestingly, we find that without adding nerve growth factor, the purified OLIG2$^+$ NPCs also generate cholinergic neurons in the organoids. The comparison between our organoid samples and the BrainSpan dataset confirms that the gene expression patterns in the organoids exhibit similarities with human embryonic brain at 8 to 9 pcw (equivalent to GW 10 to 11) that precede fetal stages (Engle et al., 2004). Thus, these organoids provide unprecedented opportunities to investigate DS human brain development at embryonic stages.

The development of the human chimeric mouse model permits the study of human interneuron development and disease pathogenesis *in vivo,* which allows specifying *1)* whether the inhibitory neuron cell fate remains stable under long-term survival conditions; and *2)* whether grafted “disordered” neurons cause any behavioral abnormalities*.* Recent studies in human brain tissue have demonstrated the widespread and extensive migration of immature neurons for several months in the neonatal brain (Paredes et al., 2016; Sanai et al., 2011). In particular, a study identifies that these immature neurons are mainly young GABAergic neurons, which form an arching or “Arc” structure adjacent to the anterior body of lateral ventricle and within the neighboring subcortical white matter. This “Arc” migratory stream takes the human GABAergic neurons to the frontal lobe of infants and young children (Paredes et al., 2016). In our study, at 2 months post-transplantation, most of the engrafted cells migrate away from injection sites and integrate into the brain regions overlying the lateral ventricles, which might mimic the “Arc” structure seen in the infant human brain. Very interestingly, at 6 months, the donor-derived cells, mostly GABAergic neurons, reside predominantly in the cerebral cortex. Previous studies have documented the transplantation of hPSC-derived progenitors of GABAergic neurons into rodent developing brains and demonstrated active migration of these GABAergic neurons to the cerebral cortex (Maroof et al., 2013; Nicholas et al., 2013). However, enrichment of human GABAergic neuron in the cerebral cortex, as shown in the present study, has not been reported previously. In our study, injection of the cells to the selected sites (anterior anlagen of the corpus callosum that overlies lateral ventricles, but not the deeper sites near the SVZ) of the neonatal mouse brain within a day of birth may facilitate the migration of the engrafted cells and generation of chimeric brains. Moreover, these cells are also expected to divide for at least 6 months in the mouse host (Chen et al., 2016; Windrem et al., 2014), which may result in the large number of human donor cells in the mouse brain seen at 6 months. Notably, the majority of transplanted neural progenitors differentiated to neurons, with a small population giving rise to glial cells. We propose that the following two reasons may account for this observation. First, the engrafted neural progenitors have great neurogenic potential, because those organoid-derived neural progenitors are differentiated from rosette-type pNPCs which are highly neurogenic (Elkabetz et al., 2008; Li et al., 2011) and stay at a primitive stage, as they are highly responsive to instructive neural patterning cues *in vitro*. Moreover, the organoids developed from pNPCs are only cultured for a short period of time (2 weeks) in the presence of FGF-2 and then are dissociated for transplantation. NPCs usually progress toward a definitive stage with increased

gliogenic bias and concomitant loss of neurogenic potential after a few passages in the presence of FGF-2 and EGF (Elkabetz et al., 2008; Li et al., 2011). Second, we transplant cells into the mouse brain at the earliest postnatal age, P0, as there is an age-related decline of the neurogenic niche in the brain (Katsimpardi et al., 2014; Villeda et al., 2011). The neurogenic niche in the neonatal mouse brain may promote neurogenesis from the transplanted cells, further facilitating neuronal differentiation (Chen et al., 2016).

In both DS organoids and DS chimeric mouse brains, we find that by directly interacting with GABAergic neuron lineage-determining transcription factors, overexpression of OLIG2 leads to overproduction of the subclass-specific GABAergic neurons. We propose that the increased expression of *DLX1* in DS organoids may be largely responsible for the overproduction of CR^+ interneurons, because previous studies in mice have shown that *Dlx1* is involved in production of CR^+ interneurons (Hanson et al., 2007); and that increased expression of *LHX6/8* and *SOX6* may be largely responsible for the overproduction of SST^+ interneurons, because *Lhx6/8* and *Sox6* regulate specification of SST^+ interneurons (Azim et al., 2009; Flandin et al., 2011). In addition, these transcription factors may also work together to fine-tune the production of different subclasses of interneurons, since previous studies have also shown that Dlx5/6 are directly downstream of Dlx1/2 (Anderson et al., 1997a; Anderson et al., 1997b; Zerucha et al., 2000) and Sox6 functions downstream of Lhx6 (Batista-Brito et al., 2009). Interestingly, our RNA-seq analyses also show abnormal expression of genes involved in oligodendrocytes differentiation and myelination in DS, which is in consistence with a recent study that reported defective oligodendrocyte differentiation and myelination in Ts65Dn mice and human brain tissue (Goodliffe et al., 2016). Future gene network analysis of the RNA-seq data may help guide the investigation of the regulatory effects of OLIG2 on downstream interneuronal as well as oligodendroglial transcriptional targets.

Notably, a recent study in human brain tissue (Paredes et al., 2016) demonstrates that from postnatal 1 day to 5 months, among various subclasses of GABAergic neurons, CR^+ neurons are the predominant subclasses that migrate to the cingulate gyrus from the “Arc” structure, with the most drastic addition to the cortex (over 4-fold increase from 100,000 to over 400,000 CR^+ cells/cingulate segment). This finding suggests that those CR^+ neurons may play important roles associated with the critical period of brain plasticity in the early postnatal developing human brain. Intriguingly, our immunoblot results show an overabundance of CR in DS cortical brain tissue, collected from patients less than one-year old. We find that DS NPCs overproduce CR^+ and SST^+ GABAergic neurons in the chimeric mouse brain. Although a large number of human cells are seen in the mouse brains, there is no significant behavioral change between the PBS control group and control chimeric mouse. We further find that only around 20% of the total human cells are c-Fos^+ and likely to be functionally active. Thus, the low percentage of active cells among the total control human interneurons may not be able to cause significant behavioral changes in control chimeric mouse group, as compared to the PBS control group. Furthermore, DS chimeric mice exhibit impaired recognition memory in the novel object recognition test, compared to control chimeric mice and PBS vehicle control mice, despite the fact that similarly around 20% of total DS cells are c-Fos^+ active interneurons. These data suggest that the impaired recognition memory in DS chimeric mice is very likely caused by the addition of these subclasses-specific human interneurons. This is further supported by our observations that inhibiting OLIG2 in DS cells corrects the abnormal production of the CR^+ and SST^+ interneurons and that DS+OLIG2^{shRNA} chimeric mice have improved recognition memory, compared to the DS+control^{shRNA} chimeric mice. Collectively, these results suggest that cognitive impairments in DS may be associated with the abnormal production of subclass-specific GABAergic neurons from embryonic ventral forebrain NPCs.

We also discovered findings that are distinct from those identified previously in mice and in human samples. Studies using postmortem brain tissues from elderly DS patients (Kobayashi et al., 1990; Ross et al., 1984) and 2D cultures of DS iPSCs (Huo et al., 2018) showed reduced production of GABAergic neurons. The previous studies only used postmortem brain tissues from elderly patients with Alzheimer-like degeneration (Kobayashi et al., 1990; Ross et al., 1984), which may confound the

evaluation of the cell counts of GABAergic neurons (Contestabile et al., 2017). Our results using DS hiPSCs and human brain tissues from DS patients less than one year old clearly demonstrate overproduction of SST^+ and CR^+ GABAergic neurons. A recent study (Huo et al., 2018) using DS hiPSCs reported discrepant findings that DS cells produced less CR^+ neurons, although they similarly overproduced SST^+ neurons. We propose that the discrepancy may result from the fact that 2D cultures were used in that study. In addition, the different transplantation strategies may also result in the discrepant *in vivo* findings. Our transplantation strategy was designed to mimic the GABAergic neuron development in an immature brain in the context of cerebral cortex, as opposed to the strategy of transplantation of young GABAergic neurons into a mature brain (8 to 10 weeks old mice) at sites very deep in the brain (medial septum), used in the recent study (Huo et al., 2018). In addition, we find that human OLIG2, but not OLIG1, determines the overproduction of GABAergic neurons in DS, mainly of the CR^+ subclass. These findings also distinct from the observations in mice, in which mouse Olig1, rather than Olig2, regulates GABAergic neuron differentiation (Furusho et al., 2006; Ono et al., 2008; Petryniak et al., 2007; Silbereis et al., 2014), and overexpression of Olig1 and Olig2 results in mainly overproduction of PV^+ GABAergic neurons in Ts65Dn mice (Chakrabarti et al., 2010). In this study, although around 80% of engrafted human NPCs are $NKX2.1^+$, we observe that in control chimeric mice, nearly all of the human donor-derived CR^+ GABAergic neurons are CR^+/SST^- and in DS chimeric mice, the vast majority of the overly produced CR^+ neurons are also CR^+/SST^-. In contrast, in normal mouse brain, there are exceedingly few CR^+/SST^- interneurons that are derived from $Nkx2.1^+$ MGE progenitor cells, because the vast majority of these interneurons are CGE/non-Nkx2.1 lineage derived (Butt et al., 2005; Lopez-Bendito et al., 2004; Wonders and Anderson, 2006; Xu et al., 2004). This discrepancy may reflect a species difference, because a previous study shows that CR^+/SST^+ neurons are virtually absent in human brain and nearly all of the CR^+ neurons are CR^+/SST^- (Gonzalez-Albo et al., 2001). However, we also cannot exclude the possibility that OLIG2 overexpression in DS may result in conversion of MGE-like progenitors to CGE-like progenitors after the downregulation of Nkx2.1. Further studies are required to address this question.

There is a growing interest in the development of prenatal therapy for DS, as part of a 'fetal personalized medicine' strategy (Bianchi, 2012; de Wert et al., 2017; Guedj et al., 2014). A prenatal therapy approach may be more effective at rebalancing inhibition and excitation, considering that GABAergic neurons are born during the prenatal period. The hiPSC-based models developed in this study will complement DS transgenic mouse models and provide powerful tools to develop personalized medicine and precision prenatal treatment for DS.

STAR METHODS

Detailed methods are provided in the online version of this paper and include the following:

- KEY RESOURCES TABLE
- CONTACT FOR REAGENT AND RESOURCE SHARING
- EXPERIMENTAL MODEL AND SUBJECT DETAILS
    - Generation, culture, and quality control of hPSC lines and their neural derivatives
    - Animals
- METHOD DETAILS
    - Cell transplantation
    - Electrophysiology
    - RNA isolation and qPCR
    - ChIP
    - RNA sequencing
    - Immunostaining and cell counting
    - Electron microscopy
    - Western blotting
    - Coomassie blue staining
    - shRNA knockdown experiments
    - FACS
    - Cell fractionation
    - Open field test
    - Elevated plus maze
    - Novel object recognition
    - Vector construction, transfection, and luciferase reporter assay
    - CGH array.
- QUANTIFICATION AND STATISTICAL ANALYSIS
- DATA AND SOFTWARE AVAILABILITY SUPPLEMENTAL

Acknowledgements

This work was in part supported by grants from the NIH (R21HD091512 and R01NS102382 to P.J.), an Institutional Development Award (IDeA) from the National Institute of General Medical Sciences of the NIH under grant number P30GM110768 (to P.J.), and Edna Ittner Pediatric Research Support Fund (to P.J.). Y.L. was supported by R01NS110707, Memorial Hermann Foundation-Staman Ogilvie Fund, the Bentsen Stroke Center, and the TIRR Foundation through Mission Connect (014-115), the Craig H. Neilsen Foundation (338617). R.P.H. was supported by R01ES026057, R01AT008458, and R21DA039686. We thank DNA Sequencing Core at UNMC for performing RNA-seq experiment, which receives partial support from the National Institute for General Medical Science INBRE - P20GM103427-14 and COBRE - 1P30GM110768-01 grants as well as The Fred & Pamela Buffett Cancer Center Support Grant - P30CA036727. We thank the Bioinformatics and Systems Biology Core at UNMC for providing RNA-seq data analysis services, which receives support from Nebraska Research Initiative and NIH (2P20GM103427 and 5P30CA036727). We thank Dr. Minhan Ka from UNMC for technical assistance with ChIP-PCR assay and thank Dr. Alice Liu from Rutgers University and Dr. Guang Yang from Beckman Research Institute of City of Hope for suggestions and technical assistance with luciferase reporter assay. We also thank Mr. Andrew Boreland from Rutgers University for the help with drawing graphic abstract.

Author Contributions

R.X. and P.J. designed experiments and interpreted data; R.X. carried out most of experiments with technical assistance from A.T.B., H.K., H.X., and W.K.; S.L., Y.L., and R.P.H. performed the gene expression analysis; J.L. and Z.P.P. performed electrophysiological recordings; Z.P.P. and R.P.H. provided critical suggestions to the overall research direction; P.J. directed the project and wrote the manuscript together with R.X. and input from all co-authors.

Competing Financial Interests

The authors declare no competing financial interests.

References:

Alton, G., and Kesari, S. (2016). Novel small molecule inhibitors of the OLIG2 transcription factor: promising new therapeutics for glioblastoma. Future Oncol *12*, 1001-1004.

Amin, N.D., and Pasca, S.P. (2018). Building Models of Brain Disorders with Three-Dimensional Organoids. Neuron *100*, 389-405.

Anderson, S.A., Eisenstat, D.D., Shi, L., and Rubenstein, J.L. (1997a). Interneuron migration from basal forebrain to neocortex: dependence on Dlx genes. Science *278*, 474-476.

Anderson, S.A., Qiu, M., Bulfone, A., Eisenstat, D.D., Meneses, J., Pedersen, R., and Rubenstein, J.L. (1997b). Mutations of the homeobox genes Dlx-1 and Dlx-2 disrupt the striatal subventricular zone and differentiation of late born striatal neurons. Neuron *19*, 27-37.

Antunes, M., and Biala, G. (2012). The novel object recognition memory: neurobiology, test procedure, and its modifications. Cogn Process *13*, 93-110.

Azim, E., Jabaudon, D., Fame, R.M., and Macklis, J.D. (2009). SOX6 controls dorsal progenitor identity and interneuron diversity during neocortical development. Nat Neurosci *12*, 1238-1247.

Aziz, N.M., Guedj, F., Pennings, J.L.A., Olmos-Serrano, J.L., Siegel, A., Haydar, T.F., and Bianchi, D.W. (2018). Lifespan analysis of brain development, gene expression and behavioral phenotypes in the Ts1Cje, Ts65Dn and Dp(16)1/Yey mouse models of Down syndrome. Dis Model Mech *11*.

Batista-Brito, R., Rossignol, E., Hjerling-Leffler, J., Denaxa, M., Wegner, M., Lefebvre, V., Pachnis, V., and Fishell, G. (2009). The cell-intrinsic requirement of Sox6 for cortical interneuron development. Neuron *63*, 466-481.

Belichenko, N.P., Belichenko, P.V., Kleschevnikov, A.M., Salehi, A., Reeves, R.H., and Mobley, W.C. (2009). The "Down syndrome critical region" is sufficient in the mouse model to confer behavioral, neurophysiological, and synaptic phenotypes characteristic of Down syndrome. J Neurosci *29*, 5938-5948.

Belichenko, P.V., Kleschevnikov, A.M., Becker, A., Wagner, G.E., Lysenko, L.V., Yu, Y.E., and Mobley, W.C. (2015). Down Syndrome Cognitive Phenotypes Modeled in Mice Trisomic for All HSA 21 Homologues. PLoS One *10*, e0134861.

Bevins, R.A., and Besheer, J. (2006). Object recognition in rats and mice: a one-trial non-matching-to-sample learning task to study 'recognition memory'. Nat Protoc *1*, 1306-1311.

Bhattacharyya, A., McMillan, E., Chen, S.I., Wallace, K., and Svendsen, C.N. (2009). A critical period in cortical interneuron neurogenesis in down syndrome revealed by human neural progenitor cells. Dev Neurosci *31*, 497-510.

Bianchi, D.W. (2012). From prenatal genomic diagnosis to fetal personalized medicine: progress and challenges. Nat Med *18*, 1041-1051.

Blair, J.A., Wang, C., Hernandez, D., Siedlak, S.L., Rodgers, M.S., Achar, R.K., Fahmy, L.M., Torres, S.L., Petersen, R.B., Zhu, X., *et al.* (2016). Individual Case Analysis of Postmortem Interval Time on Brain Tissue Preservation. PLoS One *11*, e0151615.

Brawner, A.T., Xu, R., Liu, D., and Jiang, P. (2017). Generating CNS organoids from human induced pluripotent stem cells for modeling neurological disorders. Int J Physiol Pathophysiol Pharmacol *9*, 101-111.

Briggs, J.A., Sun, J., Shepherd, J., Ovchinnikov, D.A., Chung, T.L., Nayler, S.P., Kao, L.P., Morrow, C.A., Thakar, N.Y., Soo, S.Y., *et al.* (2013). Integration-free induced pluripotent stem cells model genetic and neural developmental features of down syndrome etiology. Stem Cells *31*, 467-478.

Busciglio, J., Pelsman, A., Wong, C., Pigino, G., Yuan, M., Mori, H., and Yankner, B.A. (2002). Altered metabolism of the amyloid beta precursor protein is associated with mitochondrial dysfunction in Down's syndrome. Neuron *33*, 677-688.

Busciglio, J., and Yankner, B.A. (1995). Apoptosis and increased generation of reactive oxygen species in Down's syndrome neurons in vitro. Nature *378*, 776-779.

Butt, S.J., Fuccillo, M., Nery, S., Noctor, S., Kriegstein, A., Corbin, J.G., and Fishell, G. (2005). The temporal and spatial origins of cortical interneurons predict their physiological subtype. Neuron *48*, 591-604.

Casarosa, S., Fode, C., and Guillemot, F. (1999). Mash1 regulates neurogenesis in the ventral telencephalon. Development *126*, 525-534.

Castro, D.S., Martynoga, B., Parras, C., Ramesh, V., Pacary, E., Johnston, C., Drechsel, D., Lebel-Potter, M., Garcia, L.G., Hunt, C., *et al.* (2011). A novel function of the proneural factor Ascl1 in progenitor proliferation identified by genome-wide characterization of its targets. Genes Dev *25*, 930-945.

Centeno, E.G.Z., Cimarosti, H., and Bithell, A. (2018). 2D versus 3D human induced pluripotent stem cell-derived cultures for neurodegenerative disease modelling. Mol Neurodegener *13*, 27.

Chakrabarti, L., Best, T.K., Cramer, N.P., Carney, R.S., Isaac, J.T., Galdzicki, Z., and Haydar, T.F. (2010). Olig1 and Olig2 triplication causes developmental brain defects in Down syndrome. Nat Neurosci *13*, 927-934.

Chambers, S.M., Fasano, C.A., Papapetrou, E.P., Tomishima, M., Sadelain, M., and Studer, L. (2009). Highly efficient neural conversion of human ES and iPS cells by dual inhibition of SMAD signaling. Nat Biotechnol *27*, 275-280.

Chen, C., Jiang, P., Xue, H., Peterson, S.E., Tran, H.T., McCann, A.E., Parast, M.M., Li, S., Pleasure, D.E., Laurent, L.C., *et al.* (2014). Role of astroglia in Down's syndrome revealed by patient-derived human-induced pluripotent stem cells. Nat Commun *5*, 4430.

Chen, C., Kim, W.Y., and Jiang, P. (2016). Humanized neuronal chimeric mouse brain generated by neonatally engrafted human iPSC-derived primitive neural progenitor cells. JCI Insight *1*, e88632.

Chen, H., Qian, K., Chen, W., Hu, B., Blackbourn, L.W.t., Du, Z., Ma, L., Liu, H., Knobel, K.M., Ayala, M., *et al.* (2015). Human-derived neural progenitors functionally replace astrocytes in adult mice. J Clin Invest *125*, 1033-1042.

Cobos, I., Long, J.E., Thwin, M.T., and Rubenstein, J.L. (2006). Cellular patterns of transcription factor expression in developing cortical interneurons. Cereb Cortex *16 Suppl 1*, i82-88.

Colasante, G., Collombat, P., Raimondi, V., Bonanomi, D., Ferrai, C., Maira, M., Yoshikawa, K., Mansouri, A., Valtorta, F., Rubenstein, J.L., *et al.* (2008). Arx is a direct target of Dlx2 and thereby contributes to the tangential migration of GABAergic interneurons. J Neurosci *28*, 10674-10686.

Contestabile, A., Benfenati, F., and Gasparini, L. (2010). Communication breaks-Down: from neurodevelopment defects to cognitive disabilities in Down syndrome. Prog Neurobiol *91*, 1-22.

Contestabile, A., Magara, S., and Cancedda, L. (2017). The GABAergic Hypothesis for Cognitive Disabilities in Down Syndrome. Front Cell Neurosci *11*, 54.

Das, I., and Reeves, R.H. (2011). The use of mouse models to understand and improve cognitive deficits in Down syndrome. Dis Model Mech *4*, 596-606.

de Wert, G., Dondorp, W., and Bianchi, D.W. (2017). Fetal therapy for Down syndrome: an ethical exploration. Prenat Diagn *37*, 222-228.

Elkabetz, Y., Panagiotakos, G., Al Shamy, G., Socci, N.D., Tabar, V., and Studer, L. (2008). Human ES cell-derived neural rosettes reveal a functionally distinct early neural stem cell stage. Genes Dev *22*, 152-165.

Engle, W.A., American Academy of Pediatrics Committee on, F., and Newborn (2004). Age terminology during the perinatal period. Pediatrics *114*, 1362-1364.

Esposito, G., Imitola, J., Lu, J., De Filippis, D., Scuderi, C., Ganesh, V.S., Folkerth, R., Hecht, J., Shin, S., Iuvone, T., *et al.* (2008). Genomic and functional profiling of human Down syndrome neural progenitors implicates S100B and aquaporin 4 in cell injury. Hum Mol Genet *17*, 440-457.

Fernandez, F., Morishita, W., Zuniga, E., Nguyen, J., Blank, M., Malenka, R.C., and Garner, C.C. (2007). Pharmacotherapy for cognitive impairment in a mouse model of Down syndrome. Nat Neurosci *10*, 411-413.

Flandin, P., Zhao, Y., Vogt, D., Jeong, J., Long, J., Potter, G., Westphal, H., and Rubenstein, J.L. (2011). Lhx6 and Lhx8 coordinately induce neuronal expression of Shh that controls the generation of interneuron progenitors. Neuron *70*, 939-950.

Fricker, R.A., Carpenter, M.K., Winkler, C., Greco, C., Gates, M.A., and Bjorklund, A. (1999). Site-specific migration and neuronal differentiation of human neural progenitor cells after transplantation in the adult rat brain. J Neurosci *19*, 5990-6005.

Furusho, M., Ono, K., Takebayashi, H., Masahira, N., Kagawa, T., Ikeda, K., and Ikenaka, K. (2006). Involvement of the Olig2 transcription factor in cholinergic neuron development of the basal forebrain. Dev Biol *293*, 348-357.

Gleeson, J.G., Lin, P.T., Flanagan, L.A., and Walsh, C.A. (1999). Doublecortin is a microtubule-associated protein and is expressed widely by migrating neurons. Neuron *23*, 257-271.

Gonzalez-Albo, M.C., Elston, G.N., and DeFelipe, J. (2001). The human temporal cortex: characterization of neurons expressing nitric oxide synthase, neuropeptides and calcium-binding proteins, and their glutamate receptor subunit profiles. Cereb Cortex *11*, 1170-1181.

Goodliffe, J.W., Olmos-Serrano, J.L., Aziz, N.M., Pennings, J.L., Guedj, F., Bianchi, D.W., and Haydar, T.F. (2016). Absence of Prenatal Forebrain Defects in the Dp(16)1Yey/+ Mouse Model of Down Syndrome. J Neurosci *36*, 2926-2944.

Guedj, F., Bianchi, D.W., and Delabar, J.M. (2014). Prenatal treatment of Down syndrome: a reality? Curr Opin Obstet Gynecol *26*, 92-103.

Guidi, S., Bonasoni, P., Ceccarelli, C., Santini, D., Gualtieri, F., Ciani, E., and Bartesaghi, R. (2008). Neurogenesis impairment and increased cell death reduce total neuron number in the hippocampal region of fetuses with Down syndrome. Brain pathology *18*, 180-197.

Han, X., Chen, M., Wang, F., Windrem, M., Wang, S., Shanz, S., Xu, Q., Oberheim, N.A., Bekar, L., Betstadt, S., *et al.* (2013). Forebrain engraftment by human glial progenitor cells enhances synaptic plasticity and learning in adult mice. Cell Stem Cell *12*, 342-353.

Hanson, J.E., Blank, M., Valenzuela, R.A., Garner, C.C., and Madison, D.V. (2007). The functional nature of synaptic circuitry is altered in area CA3 of the hippocampus in a mouse model of Down's syndrome. J Physiol *579*, 53-67.

Haydar, T.F., and Reeves, R.H. (2012). Trisomy 21 and early brain development. Trends Neurosci *35*, 81-91.

Huang da, W., Sherman, B.T., and Lempicki, R.A. (2009a). Bioinformatics enrichment tools: paths toward the comprehensive functional analysis of large gene lists. Nucleic Acids Res *37*, 1-13.

Huang da, W., Sherman, B.T., and Lempicki, R.A. (2009b). Systematic and integrative analysis of large gene lists using DAVID bioinformatics resources. Nat Protoc *4*, 44-57.

Huo, H.Q., Qu, Z.Y., Yuan, F., Ma, L., Yao, L., Xu, M., Hu, Y., Ji, J., Bhattacharyya, A., Zhang, S.C., *et al.* (2018). Modeling Down Syndrome with Patient iPSCs Reveals Cellular and Migration Deficits of GABAergic Neurons. Stem Cell Reports.

Ichiki, T., Labosky, P.A., Shiota, C., Okuyama, S., Imagawa, Y., Fogo, A., Niimura, F., Ichikawa, I., Hogan, B.L., and Inagami, T. (1995). Effects on blood pressure and exploratory behaviour of mice lacking angiotensin II type-2 receptor. Nature *377*, 748-750.

Jakovcevski, I., and Zecevic, N. (2005a). Olig transcription factors are expressed in oligodendrocyte and neuronal cells in human fetal CNS. J Neurosci *25*, 10064-10073.

Jakovcevski, I., and Zecevic, N. (2005b). Sequence of oligodendrocyte development in the human fetal telencephalon. Glia *49*, 480-491.

Jiang, P., Chen, C., Liu, X.B., Pleasure, D.E., Liu, Y., and Deng, W. (2016). Human iPSC-Derived Immature Astroglia Promote Oligodendrogenesis by Increasing TIMP-1 Secretion. Cell Rep.

Jiang, P., Chen, C., Liu, X.B., Selvaraj, V., Liu, W., Feldman, D.H., Liu, Y., Pleasure, D.E., Li, R.A., and Deng, W. (2013a). Generation and characterization of spiking and nonspiking oligodendroglial progenitor cells from embryonic stem cells. Stem Cells *31*, 2620-2631.

Jiang, P., Chen, C., Wang, R., Chechneva, O.V., Chung, S.H., Rao, M.S., Pleasure, D.E., Liu, Y., Zhang, Q., and Deng, W. (2013b). hESC-derived Olig2+ progenitors generate a subtype of astroglia with protective effects against ischaemic brain injury. Nat Commun *4*, 2196.

Kanatani, S., Yozu, M., Tabata, H., and Nakajima, K. (2008). COUP-TFII is preferentially expressed in the caudal ganglionic eminence and is involved in the caudal migratory stream. J Neurosci *28*, 13582-13591.

Kang, H.J., Kawasawa, Y.I., Cheng, F., Zhu, Y., Xu, X., Li, M., Sousa, A.M., Pletikos, M., Meyer, K.A., Sedmak, G., *et al.* (2011). Spatio-temporal transcriptome of the human brain. Nature *478*, 483-489.

Katsimpardi, L., Litterman, N.K., Schein, P.A., Miller, C.M., Loffredo, F.S., Wojtkiewicz, G.R., Chen, J.W., Lee, R.T., Wagers, A.J., and Rubin, L.L. (2014). Vascular and neurogenic rejuvenation of the aging mouse brain by young systemic factors. Science *344*, 630-634.

Kelsom, C., and Lu, W. (2013). Development and specification of GABAergic cortical interneurons. Cell Biosci *3*, 19.

Kessaris, N., Fogarty, M., Iannarelli, P., Grist, M., Wegner, M., and Richardson, W.D. (2006). Competing waves of oligodendrocytes in the forebrain and postnatal elimination of an embryonic lineage. Nat Neurosci *9*, 173-179.

Kim, H., Xu, R., Ragunathan, P., Dunaevsky, A., Liu, Y., Dreyfus, C., and Jiang, P. (2018). Pluripotent Stem Cell-derived Cerebral Organoids Reveal Human Oligodendrogenesis with Dorsal and Ventral Origins. BioRxiv.

Kobayashi, K., Emson, P.C., Mountjoy, C.Q., Thornton, S.N., Lawson, D.E., and Mann, D.M. (1990). Cerebral cortical calbindin D28K and parvalbumin neurones in Down's syndrome. Neurosci Lett *113*, 17-22.

Kraushar, M.L., Thompson, K., Wijeratne, H.R., Viljetic, B., Sakers, K., Marson, J.W., Kontoyiannis, D.L., Buyske, S., Hart, R.P., and Rasin, M.R. (2014). Temporally defined neocortical translation and polysome assembly are determined by the RNA-binding protein Hu antigen R. Proc Natl Acad Sci U S A *111*, E3815-3824.

Kuspert, M., Hammer, A., Bosl, M.R., and Wegner, M. (2011). Olig2 regulates Sox10 expression in oligodendrocyte precursors through an evolutionary conserved distal enhancer. Nucleic Acids Res *39*, 1280-1293.

Kwan, K.Y., Lam, M.M., Johnson, M.B., Dube, U., Shim, S., Rasin, M.R., Sousa, A.M., Fertuzinhos, S., Chen, J.G., Arellano, J.I.*, et al.* (2012). Species-dependent posttranscriptional regulation of NOS1 by FMRP in the developing cerebral cortex. Cell *149*, 899-911.

Lancaster, M.A., and Knoblich, J.A. (2014). Generation of cerebral organoids from human pluripotent stem cells. Nat Protoc *9*, 2329-2340.

Lancaster, M.A., Renner, M., Martin, C.A., Wenzel, D., Bicknell, L.S., Hurles, M.E., Homfray, T., Penninger, J.M., Jackson, A.P., and Knoblich, J.A. (2013). Cerebral organoids model human brain development and microcephaly. Nature *501*, 373-379.

Letourneau, A., and Antonarakis, S.E. (2012). Genomic determinants in the phenotypic variability of Down syndrome. Prog Brain Res *197*, 15-28.

Li, W., Sun, W., Zhang, Y., Wei, W., Ambasudhan, R., Xia, P., Talantova, M., Lin, T., Kim, J., Wang, X.*, et al.* (2011). Rapid induction and long-term self-renewal of primitive neural precursors from human embryonic stem cells by small molecule inhibitors. Proc Natl Acad Sci U S A *108*, 8299-8304.

Ligon, K.L., Huillard, E., Mehta, S., Kesari, S., Liu, H., Alberta, J.A., Bachoo, R.M., Kane, M., Louis, D.N., Depinho, R.A.*, et al.* (2007). Olig2-regulated lineage-restricted pathway controls replication competence in neural stem cells and malignant glioma. Neuron *53*, 503-517.

Lin, L., Swerdel, M.R., Lazaropoulos, M.P., Hoffman, G.S., Toro-Ramos, A.J., Wright, J., Lederman, H., Chen, J., Moore, J.C., and Hart, R.P. (2015). Spontaneous ATM Gene Reversion in A-T iPSC to Produce an Isogenic Cell Line. Stem Cell Reports *5*, 1097-1108.

Liu, J.J., Bello, N.T., and Pang, Z.P. (2017). Presynaptic Regulation of Leptin in a Defined Lateral Hypothalamus-Ventral Tegmental Area Neurocircuitry Depends on Energy State. J Neurosci *37*, 11854-11866.

Liu, W., Zhou, H., Liu, L., Zhao, C., Deng, Y., Chen, L., Wu, L., Mandrycky, N., McNabb, C.T., Peng, Y., *et al.* (2015). Disruption of neurogenesis and cortical development in transgenic mice misexpressing Olig2, a gene in the Down syndrome critical region. Neurobiol Dis *77*, 106-116.

Liu, Y., Jiang, P., and Deng, W. (2011). OLIG gene targeting in human pluripotent stem cells for motor neuron and oligodendrocyte differentiation. Nat Protoc *6*, 640-655.

Liu, Y., Liu, H., Sauvey, C., Yao, L., Zarnowska, E.D., and Zhang, S.C. (2013a). Directed differentiation of forebrain GABA interneurons from human pluripotent stem cells. Nat Protoc *8*, 1670-1679.

Liu, Y., Weick, J.P., Liu, H., Krencik, R., Zhang, X., Ma, L., Zhou, G.M., Ayala, M., and Zhang, S.C. (2013b). Medial ganglionic eminence-like cells derived from human embryonic stem cells correct learning and memory deficits. Nat Biotechnol *31*, 440-447.

Lockstone, H.E., Harris, L.W., Swatton, J.E., Wayland, M.T., Holland, A.J., and Bahn, S. (2007). Gene expression profiling in the adult Down syndrome brain. Genomics *90*, 647-660.

Loebrich, S., and Nedivi, E. (2009). The function of activity-regulated genes in the nervous system. Physiol Rev *89*, 1079-1103.

Lopez-Bendito, G., Sturgess, K., Erdelyi, F., Szabo, G., Molnar, Z., and Paulsen, O. (2004). Preferential origin and layer destination of GAD65-GFP cortical interneurons. Cereb Cortex *14*, 1122-1133.

Lu, J., Lian, G., Zhou, H., Esposito, G., Steardo, L., Delli-Bovi, L.C., Hecht, J.L., Lu, Q.R., and Sheen, V. (2012). OLIG2 over-expression impairs proliferation of human Down syndrome neural progenitors. Hum Mol Genet *21*, 2330-2340.

Lu, Q.R., Yuk, D., Alberta, J.A., Zhu, Z., Pawlitzky, I., Chan, J., McMahon, A.P., Stiles, C.D., and Rowitch, D.H. (2000). Sonic hedgehog--regulated oligodendrocyte lineage genes encoding bHLH proteins in the mammalian central nervous system. Neuron *25*, 317-329.

Ma, L., Hu, B., Liu, Y., Vermilyea, S.C., Liu, H., Gao, L., Sun, Y., Zhang, X., and Zhang, S.C. (2012). Human embryonic stem cell-derived GABA neurons correct locomotion deficits in quinolinic acid-lesioned mice. Cell Stem Cell *10*, 455-464.

Maclean, G.A., Menne, T.F., Guo, G., Sanchez, D.J., Park, I.H., Daley, G.Q., and Orkin, S.H. (2012). Altered hematopoiesis in trisomy 21 as revealed through in vitro differentiation of isogenic human pluripotent cells. Proc Natl Acad Sci U S A *109*, 17567-17572.

Madhavan, M., Nevin, Z.S., Shick, H.E., Garrison, E., Clarkson-Paredes, C., Karl, M., Clayton, B.L.L., Factor, D.C., Allan, K.C., Barbar, L., *et al.* (2018). Induction of myelinating oligodendrocytes in human cortical spheroids. Nat Methods.

Malone, F.D., Canick, J.A., Ball, R.H., Nyberg, D.A., Comstock, C.H., Bukowski, R., Berkowitz, R.L., Gross, S.J., Dugoff, L., Craigo, S.D., *et al.* (2005). First-trimester or second-trimester screening, or both, for Down's syndrome. N Engl J Med *353*, 2001-2011.

Mao, R., Zielke, C.L., Zielke, H.R., and Pevsner, J. (2003). Global up-regulation of chromosome 21 gene expression in the developing Down syndrome brain. Genomics *81*, 457-467.

Mariani, J., Coppola, G., Zhang, P., Abyzov, A., Provini, L., Tomasini, L., Amenduni, M., Szekely, A., Palejev, D., Wilson, M., *et al.* (2015). FOXG1-Dependent Dysregulation of GABA/Glutamate Neuron Differentiation in Autism Spectrum Disorders. Cell *162*, 375-390.

Mariani, J., Simonini, M.V., Palejev, D., Tomasini, L., Coppola, G., Szekely, A.M., Horvath, T.L., and Vaccarino, F.M. (2012). Modeling human cortical development in vitro using induced pluripotent stem cells. Proc Natl Acad Sci U S A *109*, 12770-12775.

Marin, O. (2012). Brain development: The neuron family tree remodelled. Nature *490*, 185-186.

Maroof, A.M., Keros, S., Tyson, J.A., Ying, S.W., Ganat, Y.M., Merkle, F.T., Liu, B., Goulburn, A., Stanley, E.G., Elefanty, A.G., *et al.* (2013). Directed differentiation and functional maturation of cortical interneurons from human embryonic stem cells. Cell Stem Cell *12*, 559-572.

Monzel, A.S., Smits, L.M., Hemmer, K., Hachi, S., Moreno, E.L., van Wuellen, T., Jarazo, J., Walter, J., Bruggemann, I., Boussaad, I., *et al.* (2017). Derivation of Human Midbrain-Specific Organoids from Neuroepithelial Stem Cells. Stem Cell Reports *8*, 1144-1154.

Muller, F.J., Schuldt, B.M., Williams, R., Mason, D., Altun, G., Papapetrou, E.P., Danner, S., Goldmann, J.E., Herbst, A., Schmidt, N.O., *et al.* (2011). A bioinformatic assay for pluripotency in human cells. Nat Methods *8*, 315-317.

Nicholas, C.R., Chen, J., Tang, Y., Southwell, D.G., Chalmers, N., Vogt, D., Arnold, C.M., Chen, Y.J., Stanley, E.G., Elefanty, A.G., *et al.* (2013). Functional maturation of hPSC-derived forebrain interneurons requires an extended timeline and mimics human neural development. Cell Stem Cell *12*, 573-586.

Ono, K., Takebayashi, H., Ikeda, K., Furusho, M., Nishizawa, T., Watanabe, K., and Ikenaka, K. (2008). Regional- and temporal-dependent changes in the differentiation of Olig2 progenitors in the forebrain, and the impact on astrocyte development in the dorsal pallium. Dev Biol *320*, 456-468.

Paredes, M.F., James, D., Gil-Perotin, S., Kim, H., Cotter, J.A., Ng, C., Sandoval, K., Rowitch, D.H., Xu, D., McQuillen, P.S., *et al.* (2016). Extensive migration of young neurons into the infant human frontal lobe. Science *354*.

Parker, S.E., Mai, C.T., Canfield, M.A., Rickard, R., Wang, Y., Meyer, R.E., Anderson, P., Mason, C.A., Collins, J.S., Kirby, R.S., *et al.* (2010). Updated National Birth Prevalence estimates for selected birth defects in the United States, 2004-2006. Birth Defects Res A Clin Mol Teratol *88*, 1008-1016.

Pasca, A.M., Sloan, S.A., Clarke, L.E., Tian, Y., Makinson, C.D., Huber, N., Kim, C.H., Park, J.Y., O'Rourke, N.A., Nguyen, K.D., *et al.* (2015). Functional cortical neurons and astrocytes from human pluripotent stem cells in 3D culture. Nat Methods *12*, 671-678.

Pasca, S.P. (2018). The rise of three-dimensional human brain cultures. Nature *553*, 437-445.

Patterson, M., Chan, D.N., Ha, I., Case, D., Cui, Y., Van Handel, B., Mikkola, H.K., and Lowry, W.E. (2012). Defining the nature of human pluripotent stem cell progeny. Cell Res *22*, 178-193.

Petilla Interneuron Nomenclature Group, G., Ascoli, G.A., Alonso-Nanclares, L., Anderson, S.A., Barrionuevo, G., Benavides-Piccione, R., Burkhalter, A., Buzsaki, G., Cauli, B., Defelipe, J., *et al.* (2008). Petilla terminology: nomenclature of features of GABAergic interneurons of the cerebral cortex. Nat Rev Neurosci *9*, 557-568.

Petryniak, M.A., Potter, G.B., Rowitch, D.H., and Rubenstein, J.L. (2007). Dlx1 and Dlx2 control neuronal versus oligodendroglial cell fate acquisition in the developing forebrain. Neuron *55*, 417-433.

Quadrato, G., Brown, J., and Arlotta, P. (2016). The promises and challenges of human brain organoids as models of neuropsychiatric disease. Nat Med *22*, 1220-1228.

Rissman, R.A., and Mobley, W.C. (2011). Implications for treatment: GABAA receptors in aging, Down syndrome and Alzheimer's disease. J Neurochem *117*, 613-622.

Rodrigues, G.M.C., Gaj, T., Adil, M.M., Wahba, J., Rao, A.T., Lorbeer, F.K., Kulkarni, R.U., Diogo, M.M., Cabral, J.M.S., Miller, E.W., *et al.* (2017). Defined and Scalable Differentiation of Human Oligodendrocyte Precursors from Pluripotent Stem Cells in a 3D Culture System. Stem Cell Reports *8*, 1770-1783.

Ross, M.H., Galaburda, A.M., and Kemper, T.L. (1984). Down's syndrome: is there a decreased population of neurons? Neurology *34*, 909-916.

Sanai, N., Nguyen, T., Ihrie, R.A., Mirzadeh, Z., Tsai, H.H., Wong, M., Gupta, N., Berger, M.S., Huang, E., Garcia-Verdugo, J.M., *et al.* (2011). Corridors of migrating neurons in the human brain and their decline during infancy. Nature *478*, 382-386.

Shi, Y., Kirwan, P., Smith, J., Robinson, H.P., and Livesey, F.J. (2012). Human cerebral cortex development from pluripotent stem cells to functional excitatory synapses. Nat Neurosci *15*, 477-486, S471.

Silbereis, J.C., Nobuta, H., Tsai, H.H., Heine, V.M., McKinsey, G.L., Meijer, D.H., Howard, M.A., Petryniak, M.A., Potter, G.B., Alberta, J.A., *et al.* (2014). Olig1 function is required to repress dlx1/2 and interneuron production in Mammalian brain. Neuron *81*, 574-587.

Simao, D., Silva, M.M., Terrasso, A.P., Arez, F., Sousa, M.F.Q., Mehrjardi, N.Z., Saric, T., Gomes-Alves, P., Raimundo, N., Alves, P.M., *et al.* (2018). Recapitulation of Human Neural Microenvironment Signatures in iPSC-Derived NPC 3D Differentiation. Stem Cell Reports *11*, 552-564.

Stanco, A., Pla, R., Vogt, D., Chen, Y., Mandal, S., Walker, J., Hunt, R.F., Lindtner, S., Erdman, C.A., Pieper, A.A., *et al.* (2014). NPAS1 represses the generation of specific subtypes of cortical interneurons. Neuron *84*, 940-953.

Sturgeon, X., and Gardiner, K.J. (2011). Transcript catalogs of human chromosome 21 and orthologous chimpanzee and mouse regions. Mamm Genome *22*, 261-271.

Sussel, L., Marin, O., Kimura, S., and Rubenstein, J.L. (1999). Loss of Nkx2.1 homeobox gene function results in a ventral to dorsal molecular respecification within the basal telencephalon: evidence for a transformation of the pallidum into the striatum. Development *126*, 3359-3370.

Tischfield, D.J., and Anderson, S.A. (2017). Differentiation of Mouse Embryonic Stem Cells into Cortical Interneuron Precursors. J Vis Exp.

Tosic, M., Rakic, S., Matthieu, J., and Zecevic, N. (2002). Identification of Golli and myelin basic proteins in human brain during early development. Glia *37*, 219-228.

Tsigelny, I.F., Mukthavaram, R., Kouznetsova, V.L., Chao, Y., Babic, I., Nurmemmedov, E., Pastorino, S., Jiang, P., Calligaris, D., Agar, N., *et al.* (2017). Multiple spatially related pharmacophores define small molecule inhibitors of OLIG2 in glioblastoma. Oncotarget *8*, 22370-22384.

Villeda, S.A., Luo, J., Mosher, K.I., Zou, B., Britschgi, M., Bieri, G., Stan, T.M., Fainberg, N., Ding, Z., Eggel, A., *et al.* (2011). The ageing systemic milieu negatively regulates neurogenesis and cognitive function. Nature *477*, 90-94.

Walf, A.A., and Frye, C.A. (2007). The use of the elevated plus maze as an assay of anxiety-related behavior in rodents. Nat Protoc *2*, 322-328.

Wan, H., Aggleton, J.P., and Brown, M.W. (1999). Different contributions of the hippocampus and perirhinal cortex to recognition memory. J Neurosci *19*, 1142-1148.

Wang, S., Bates, J., Li, X., Schanz, S., Chandler-Militello, D., Levine, C., Maherali, N., Studer, L., Hochedlinger, K., Windrem, M., *et al.* (2013). Human iPSC-derived oligodendrocyte progenitor cells can myelinate and rescue a mouse model of congenital hypomyelination. Cell Stem Cell *12*, 252-264.

Weick, J.P., Held, D.L., Bonadurer, G.F., 3rd, Doers, M.E., Liu, Y., Maguire, C., Clark, A., Knackert, J.A., Molinarolo, K., Musser, M., *et al.* (2013). Deficits in human trisomy 21 iPSCs and neurons. Proc Natl Acad Sci U S A *110*, 9962-9967.

Windrem, M.S., Osipovitch, M., Liu, Z., Bates, J., Chandler-Militello, D., Zou, L., Munir, J., Schanz, S., McCoy, K., Miller, R.H., *et al.* (2017). Human iPSC Glial Mouse Chimeras Reveal Glial Contributions to Schizophrenia. Cell Stem Cell *21*, 195-208 e196.

Windrem, M.S., Schanz, S.J., Guo, M., Tian, G.F., Washco, V., Stanwood, N., Rasband, M., Roy, N.S., Nedergaard, M., Havton, L.A., *et al.* (2008). Neonatal chimerization with human glial progenitor cells can both remyelinate and rescue the otherwise lethally hypomyelinated shiverer mouse. Cell Stem Cell *2*, 553-565.

Windrem, M.S., Schanz, S.J., Morrow, C., Munir, J., Chandler-Militello, D., Wang, S., and Goldman, S.A. (2014). A competitive advantage by neonatally engrafted human glial progenitors yields mice whose brains are chimeric for human glia. J Neurosci *34*, 16153-16161.

Wonders, C.P., and Anderson, S.A. (2006). The origin and specification of cortical interneurons. Nat Rev Neurosci *7*, 687-696.

Wonders, C.P., Taylor, L., Welagen, J., Mbata, I.C., Xiang, J.Z., and Anderson, S.A. (2008). A spatial bias for the origins of interneuron subgroups within the medial ganglionic eminence. Dev Biol *314*, 127-136.

Xiang, Y., Tanaka, Y., Patterson, B., Kang, Y.J., Govindaiah, G., Roselaar, N., Cakir, B., Kim, K.Y., Lombroso, A.P., Hwang, S.M., *et al.* (2017). Fusion of Regionally Specified hPSC-Derived Organoids Models Human Brain Development and Interneuron Migration. Cell Stem Cell *21*, 383-398 e387.

Xu, Q., Cobos, I., De La Cruz, E., Rubenstein, J.L., and Anderson, S.A. (2004). Origins of cortical interneuron subtypes. J Neurosci *24*, 2612-2622.

Xu, R., Hu, Q., Ma, Q., Liu, C., and Wang, G. (2014). The protease Omi regulates mitochondrial biogenesis through the GSK3beta/PGC-1alpha pathway. Cell Death Dis *5*, e1373.

Xu, X., Roby, K.D., and Callaway, E.M. (2006). Mouse cortical inhibitory neuron type that coexpresses somatostatin and calretinin. J Comp Neurol *499*, 144-160.

Xue, H., Wu, S., Papadeas, S.T., Spusta, S., Swistowska, A.M., MacArthur, C.C., Mattson, M.P., Maragakis, N.J., Capecchi, M.R., Rao, M.S., *et al.* (2009). A targeted neuroglial reporter line generated by homologous recombination in human embryonic stem cells. Stem Cells *27*, 1836-1846.

Zerucha, T., Stuhmer, T., Hatch, G., Park, B.K., Long, Q., Yu, G., Gambarotta, A., Schultz, J.R., Rubenstein, J.L., and Ekker, M. (2000). A highly conserved enhancer in the Dlx5/Dlx6 intergenic region is the site of cross-regulatory interactions between Dlx genes in the embryonic forebrain. J Neurosci *20*, 709-721.

Zhao, Y., Flandin, P., Long, J.E., Cuesta, M.D., Westphal, H., and Rubenstein, J.L. (2008). Distinct molecular pathways for development of telencephalic interneuron subtypes revealed through analysis of Lhx6 mutants. J Comp Neurol *510*, 79-99.

Alton, G., and Kesari, S. (2016). Novel small molecule inhibitors of the OLIG2 transcription factor: promising new therapeutics for glioblastoma. Future Oncol *12*, 1001-1004.

Amin, N.D., and Pasca, S.P. (2018). Building Models of Brain Disorders with Three-Dimensional Organoids. Neuron *100*, 389-405.

Anderson, S.A., Eisenstat, D.D., Shi, L., and Rubenstein, J.L. (1997a). Interneuron migration from basal forebrain to neocortex: dependence on Dlx genes. Science *278*, 474-476.

Anderson, S.A., Qiu, M., Bulfone, A., Eisenstat, D.D., Meneses, J., Pedersen, R., and Rubenstein, J.L. (1997b). Mutations of the homeobox genes Dlx-1 and Dlx-2 disrupt the striatal subventricular zone and differentiation of late born striatal neurons. Neuron *19*, 27-37.

Antunes, M., and Biala, G. (2012). The novel object recognition memory: neurobiology, test procedure, and its modifications. Cogn Process *13*, 93-110.

Azim, E., Jabaudon, D., Fame, R.M., and Macklis, J.D. (2009). SOX6 controls dorsal progenitor identity and interneuron diversity during neocortical development. Nat Neurosci *12*, 1238-1247.

Aziz, N.M., Guedj, F., Pennings, J.L.A., Olmos-Serrano, J.L., Siegel, A., Haydar, T.F., and Bianchi, D.W. (2018). Lifespan analysis of brain development, gene expression and behavioral phenotypes in the Ts1Cje, Ts65Dn and Dp(16)1/Yey mouse models of Down syndrome. Dis Model Mech *11*.

Batista-Brito, R., Rossignol, E., Hjerling-Leffler, J., Denaxa, M., Wegner, M., Lefebvre, V., Pachnis, V., and Fishell, G. (2009). The cell-intrinsic requirement of Sox6 for cortical interneuron development. Neuron *63*, 466-481.

Belichenko, N.P., Belichenko, P.V., Kleschevnikov, A.M., Salehi, A., Reeves, R.H., and Mobley, W.C. (2009). The "Down syndrome critical region" is sufficient in the mouse model to confer behavioral, neurophysiological, and synaptic phenotypes characteristic of Down syndrome. J Neurosci *29*, 5938-5948.

Belichenko, P.V., Kleschevnikov, A.M., Becker, A., Wagner, G.E., Lysenko, L.V., Yu, Y.E., and Mobley, W.C. (2015). Down Syndrome Cognitive Phenotypes Modeled in Mice Trisomic for All HSA 21 Homologues. PLoS One *10*, e0134861.

Bevins, R.A., and Besheer, J. (2006). Object recognition in rats and mice: a one-trial non-matching-to-sample learning task to study 'recognition memory'. Nat Protoc *1*, 1306-1311.

Bhattacharyya, A., McMillan, E., Chen, S.I., Wallace, K., and Svendsen, C.N. (2009). A critical period in cortical interneuron neurogenesis in down syndrome revealed by human neural progenitor cells. Dev Neurosci *31*, 497-510.

Bianchi, D.W. (2012). From prenatal genomic diagnosis to fetal personalized medicine: progress and challenges. Nat Med *18*, 1041-1051.

Blair, J.A., Wang, C., Hernandez, D., Siedlak, S.L., Rodgers, M.S., Achar, R.K., Fahmy, L.M., Torres, S.L., Petersen, R.B., Zhu, X., *et al.* (2016). Individual Case Analysis of Postmortem Interval Time on Brain Tissue Preservation. PLoS One *11*, e0151615.

Brawner, A.T., Xu, R., Liu, D., and Jiang, P. (2017). Generating CNS organoids from human induced pluripotent stem cells for modeling neurological disorders. Int J Physiol Pathophysiol Pharmacol *9*, 101-111.

Briggs, J.A., Sun, J., Shepherd, J., Ovchinnikov, D.A., Chung, T.L., Nayler, S.P., Kao, L.P., Morrow, C.A., Thakar, N.Y., Soo, S.Y., *et al.* (2013). Integration-free induced pluripotent stem cells model genetic and neural developmental features of down syndrome etiology. Stem Cells *31*, 467-478.

Busciglio, J., Pelsman, A., Wong, C., Pigino, G., Yuan, M., Mori, H., and Yankner, B.A. (2002). Altered metabolism of the amyloid beta precursor protein is associated with mitochondrial dysfunction in Down's syndrome. Neuron *33*, 677-688.

Busciglio, J., and Yankner, B.A. (1995). Apoptosis and increased generation of reactive oxygen species in Down's syndrome neurons in vitro. Nature *378*, 776-779.

Butt, S.J., Fuccillo, M., Nery, S., Noctor, S., Kriegstein, A., Corbin, J.G., and Fishell, G. (2005). The temporal and spatial origins of cortical interneurons predict their physiological subtype. Neuron *48*, 591-604.

Casarosa, S., Fode, C., and Guillemot, F. (1999). Mash1 regulates neurogenesis in the ventral telencephalon. Development *126*, 525-534.

Castro, D.S., Martynoga, B., Parras, C., Ramesh, V., Pacary, E., Johnston, C., Drechsel, D., Lebel-Potter, M., Garcia, L.G., Hunt, C., *et al.* (2011). A novel function of the proneural factor Ascl1 in progenitor proliferation identified by genome-wide characterization of its targets. Genes Dev *25*, 930-945.

Centeno, E.G.Z., Cimarosti, H., and Bithell, A. (2018). 2D versus 3D human induced pluripotent stem cell-derived cultures for neurodegenerative disease modelling. Mol Neurodegener *13*, 27.

Chakrabarti, L., Best, T.K., Cramer, N.P., Carney, R.S., Isaac, J.T., Galdzicki, Z., and Haydar, T.F. (2010). Olig1 and Olig2 triplication causes developmental brain defects in Down syndrome. Nat Neurosci *13*, 927-934.

Chambers, S.M., Fasano, C.A., Papapetrou, E.P., Tomishima, M., Sadelain, M., and Studer, L. (2009). Highly efficient neural conversion of human ES and iPS cells by dual inhibition of SMAD signaling. Nat Biotechnol *27*, 275-280.

Chen, C., Jiang, P., Xue, H., Peterson, S.E., Tran, H.T., McCann, A.E., Parast, M.M., Li, S., Pleasure, D.E., Laurent, L.C., *et al.* (2014). Role of astroglia in Down's syndrome revealed by patient-derived human-induced pluripotent stem cells. Nat Commun *5*, 4430.

Chen, C., Kim, W.Y., and Jiang, P. (2016). Humanized neuronal chimeric mouse brain generated by neonatally engrafted human iPSC-derived primitive neural progenitor cells. JCI Insight *1*, e88632.

Chen, H., Qian, K., Chen, W., Hu, B., Blackbourn, L.W.t., Du, Z., Ma, L., Liu, H., Knobel, K.M., Ayala, M., *et al.* (2015). Human-derived neural progenitors functionally replace astrocytes in adult mice. J Clin Invest *125*, 1033-1042.

Cobos, I., Long, J.E., Thwin, M.T., and Rubenstein, J.L. (2006). Cellular patterns of transcription factor expression in developing cortical interneurons. Cereb Cortex *16 Suppl 1*, i82-88.

Colasante, G., Collombat, P., Raimondi, V., Bonanomi, D., Ferrai, C., Maira, M., Yoshikawa, K., Mansouri, A., Valtorta, F., Rubenstein, J.L., *et al.* (2008). Arx is a direct target of Dlx2 and thereby contributes to the tangential migration of GABAergic interneurons. J Neurosci *28*, 10674-10686.

Contestabile, A., Benfenati, F., and Gasparini, L. (2010). Communication breaks-Down: from neurodevelopment defects to cognitive disabilities in Down syndrome. Prog Neurobiol *91*, 1-22.

Contestabile, A., Magara, S., and Cancedda, L. (2017). The GABAergic Hypothesis for Cognitive Disabilities in Down Syndrome. Front Cell Neurosci *11*, 54.

Das, I., and Reeves, R.H. (2011). The use of mouse models to understand and improve cognitive deficits in Down syndrome. Dis Model Mech *4*, 596-606.

de Wert, G., Dondorp, W., and Bianchi, D.W. (2017). Fetal therapy for Down syndrome: an ethical exploration. Prenat Diagn *37*, 222-228.

Elkabetz, Y., Panagiotakos, G., Al Shamy, G., Socci, N.D., Tabar, V., and Studer, L. (2008). Human ES cell-derived neural rosettes reveal a functionally distinct early neural stem cell stage. Genes Dev *22*, 152-165.

Engle, W.A., American Academy of Pediatrics Committee on, F., and Newborn (2004). Age terminology during the perinatal period. Pediatrics *114*, 1362-1364.

Esposito, G., Imitola, J., Lu, J., De Filippis, D., Scuderi, C., Ganesh, V.S., Folkerth, R., Hecht, J., Shin, S., Iuvone, T., *et al.* (2008). Genomic and functional profiling of human Down syndrome neural progenitors implicates S100B and aquaporin 4 in cell injury. Hum Mol Genet *17*, 440-457.

Fernandez, F., Morishita, W., Zuniga, E., Nguyen, J., Blank, M., Malenka, R.C., and Garner, C.C. (2007). Pharmacotherapy for cognitive impairment in a mouse model of Down syndrome. Nat Neurosci *10*, 411-413.

Flandin, P., Zhao, Y., Vogt, D., Jeong, J., Long, J., Potter, G., Westphal, H., and Rubenstein, J.L. (2011). Lhx6 and Lhx8 coordinately induce neuronal expression of Shh that controls the generation of interneuron progenitors. Neuron *70*, 939-950.

Fricker, R.A., Carpenter, M.K., Winkler, C., Greco, C., Gates, M.A., and Bjorklund, A. (1999). Site-specific migration and neuronal differentiation of human neural progenitor cells after transplantation in the adult rat brain. J Neurosci *19*, 5990-6005.

Furusho, M., Ono, K., Takebayashi, H., Masahira, N., Kagawa, T., Ikeda, K., and Ikenaka, K. (2006). Involvement of the Olig2 transcription factor in cholinergic neuron development of the basal forebrain. Dev Biol *293*, 348-357.

Gleeson, J.G., Lin, P.T., Flanagan, L.A., and Walsh, C.A. (1999). Doublecortin is a microtubule-associated protein and is expressed widely by migrating neurons. Neuron *23*, 257-271.

Gonzalez-Albo, M.C., Elston, G.N., and DeFelipe, J. (2001). The human temporal cortex: characterization of neurons expressing nitric oxide synthase, neuropeptides and calcium-binding proteins, and their glutamate receptor subunit profiles. Cereb Cortex *11*, 1170-1181.

Goodliffe, J.W., Olmos-Serrano, J.L., Aziz, N.M., Pennings, J.L., Guedj, F., Bianchi, D.W., and Haydar, T.F. (2016). Absence of Prenatal Forebrain Defects in the Dp(16)1Yey/+ Mouse Model of Down Syndrome. J Neurosci *36*, 2926-2944.

Guedj, F., Bianchi, D.W., and Delabar, J.M. (2014). Prenatal treatment of Down syndrome: a reality? Curr Opin Obstet Gynecol *26*, 92-103.

Guidi, S., Bonasoni, P., Ceccarelli, C., Santini, D., Gualtieri, F., Ciani, E., and Bartesaghi, R. (2008). Neurogenesis impairment and increased cell death reduce total neuron number in the hippocampal region of fetuses with Down syndrome. Brain pathology *18*, 180-197.

Han, X., Chen, M., Wang, F., Windrem, M., Wang, S., Shanz, S., Xu, Q., Oberheim, N.A., Bekar, L., Betstadt, S.*, et al.* (2013). Forebrain engraftment by human glial progenitor cells enhances synaptic plasticity and learning in adult mice. Cell Stem Cell *12*, 342-353.

Hanson, J.E., Blank, M., Valenzuela, R.A., Garner, C.C., and Madison, D.V. (2007). The functional nature of synaptic circuitry is altered in area CA3 of the hippocampus in a mouse model of Down's syndrome. J Physiol *579*, 53-67.

Haydar, T.F., and Reeves, R.H. (2012). Trisomy 21 and early brain development. Trends Neurosci *35*, 81-91.

Huang da, W., Sherman, B.T., and Lempicki, R.A. (2009a). Bioinformatics enrichment tools: paths toward the comprehensive functional analysis of large gene lists. Nucleic Acids Res *37*, 1-13.

Huang da, W., Sherman, B.T., and Lempicki, R.A. (2009b). Systematic and integrative analysis of large gene lists using DAVID bioinformatics resources. Nat Protoc *4*, 44-57.

Huo, H.Q., Qu, Z.Y., Yuan, F., Ma, L., Yao, L., Xu, M., Hu, Y., Ji, J., Bhattacharyya, A., Zhang, S.C.*, et al.* (2018). Modeling Down Syndrome with Patient iPSCs Reveals Cellular and Migration Deficits of GABAergic Neurons. Stem Cell Reports.

Ichiki, T., Labosky, P.A., Shiota, C., Okuyama, S., Imagawa, Y., Fogo, A., Niimura, F., Ichikawa, I., Hogan, B.L., and Inagami, T. (1995). Effects on blood pressure and exploratory behaviour of mice lacking angiotensin II type-2 receptor. Nature *377*, 748-750.

Jakovcevski, I., and Zecevic, N. (2005). Olig transcription factors are expressed in oligodendrocyte and neuronal cells in human fetal CNS. J Neurosci *25*, 10064-10073.

Jiang, P., Chen, C., Liu, X.B., Pleasure, D.E., Liu, Y., and Deng, W. (2016). Human iPSC-Derived Immature Astroglia Promote Oligodendrogenesis by Increasing TIMP-1 Secretion. Cell Rep.

Jiang, P., Chen, C., Liu, X.B., Selvaraj, V., Liu, W., Feldman, D.H., Liu, Y., Pleasure, D.E., Li, R.A., and Deng, W. (2013a). Generation and characterization of spiking and nonspiking oligodendroglial progenitor cells from embryonic stem cells. Stem Cells *31*, 2620-2631.

Jiang, P., Chen, C., Wang, R., Chechneva, O.V., Chung, S.H., Rao, M.S., Pleasure, D.E., Liu, Y., Zhang, Q., and Deng, W. (2013b). hESC-derived Olig2+ progenitors generate a subtype of astroglia with protective effects against ischaemic brain injury. Nat Commun *4*, 2196.

Kanatani, S., Yozu, M., Tabata, H., and Nakajima, K. (2008). COUP-TFII is preferentially expressed in the caudal ganglionic eminence and is involved in the caudal migratory stream. J Neurosci *28*, 13582-13591.

Kang, H.J., Kawasawa, Y.I., Cheng, F., Zhu, Y., Xu, X., Li, M., Sousa, A.M., Pletikos, M., Meyer, K.A., Sedmak, G., *et al.* (2011). Spatio-temporal transcriptome of the human brain. Nature *478*, 483-489.

Katsimpardi, L., Litterman, N.K., Schein, P.A., Miller, C.M., Loffredo, F.S., Wojtkiewicz, G.R., Chen, J.W., Lee, R.T., Wagers, A.J., and Rubin, L.L. (2014). Vascular and neurogenic rejuvenation of the aging mouse brain by young systemic factors. Science *344*, 630-634.

Kelsom, C., and Lu, W. (2013). Development and specification of GABAergic cortical interneurons. Cell Biosci *3*, 19.

Kessaris, N., Fogarty, M., Iannarelli, P., Grist, M., Wegner, M., and Richardson, W.D. (2006). Competing waves of oligodendrocytes in the forebrain and postnatal elimination of an embryonic lineage. Nat Neurosci *9*, 173-179.

Kobayashi, K., Emson, P.C., Mountjoy, C.Q., Thornton, S.N., Lawson, D.E., and Mann, D.M. (1990). Cerebral cortical calbindin D28K and parvalbumin neurones in Down's syndrome. Neurosci Lett *113*, 17-22.

Kraushar, M.L., Thompson, K., Wijeratne, H.R., Viljetic, B., Sakers, K., Marson, J.W., Kontoyiannis, D.L., Buyske, S., Hart, R.P., and Rasin, M.R. (2014). Temporally defined neocortical translation and polysome assembly are determined by the RNA-binding protein Hu antigen R. Proc Natl Acad Sci U S A *111*, E3815-3824.

Kuspert, M., Hammer, A., Bosl, M.R., and Wegner, M. (2011). Olig2 regulates Sox10 expression in oligodendrocyte precursors through an evolutionary conserved distal enhancer. Nucleic Acids Res *39*, 1280-1293.

Kwan, K.Y., Lam, M.M., Johnson, M.B., Dube, U., Shim, S., Rasin, M.R., Sousa, A.M., Fertuzinhos, S., Chen, J.G., Arellano, J.I.*, et al.* (2012). Species-dependent posttranscriptional regulation of NOS1 by FMRP in the developing cerebral cortex. Cell *149*, 899-911.

Lancaster, M.A., and Knoblich, J.A. (2014). Generation of cerebral organoids from human pluripotent stem cells. Nat Protoc *9*, 2329-2340.

Letourneau, A., and Antonarakis, S.E. (2012). Genomic determinants in the phenotypic variability of Down syndrome. Prog Brain Res *197*, 15-28.

Li, W., Sun, W., Zhang, Y., Wei, W., Ambasudhan, R., Xia, P., Talantova, M., Lin, T., Kim, J., Wang, X.*, et al.* (2011). Rapid induction and long-term self-renewal of primitive neural precursors from human embryonic stem cells by small molecule inhibitors. Proc Natl Acad Sci U S A *108*, 8299-8304.

Ligon, K.L., Huillard, E., Mehta, S., Kesari, S., Liu, H., Alberta, J.A., Bachoo, R.M., Kane, M., Louis, D.N., Depinho, R.A.*, et al.* (2007). Olig2-regulated lineage-restricted pathway controls replication competence in neural stem cells and malignant glioma. Neuron *53*, 503-517.

Lin, L., Swerdel, M.R., Lazaropoulos, M.P., Hoffman, G.S., Toro-Ramos, A.J., Wright, J., Lederman, H., Chen, J., Moore, J.C., and Hart, R.P. (2015). Spontaneous ATM Gene Reversion in A-T iPSC to Produce an Isogenic Cell Line. Stem Cell Reports *5*, 1097-1108.

Liu, J.J., Bello, N.T., and Pang, Z.P. (2017). Presynaptic Regulation of Leptin in a Defined Lateral Hypothalamus-Ventral Tegmental Area Neurocircuitry Depends on Energy State. J Neurosci *37*, 11854-11866.

Liu, W., Zhou, H., Liu, L., Zhao, C., Deng, Y., Chen, L., Wu, L., Mandrycky, N., McNabb, C.T., Peng, Y.*, et al.* (2015). Disruption of neurogenesis and cortical development in transgenic mice misexpressing Olig2, a gene in the Down syndrome critical region. Neurobiol Dis *77*, 106-116.

Liu, Y., Jiang, P., and Deng, W. (2011). OLIG gene targeting in human pluripotent stem cells for motor neuron and oligodendrocyte differentiation. Nat Protoc *6*, 640-655.

Liu, Y., Liu, H., Sauvey, C., Yao, L., Zarnowska, E.D., and Zhang, S.C. (2013a). Directed differentiation of forebrain GABA interneurons from human pluripotent stem cells. Nat Protoc *8*, 1670-1679.

Liu, Y., Weick, J.P., Liu, H., Krencik, R., Zhang, X., Ma, L., Zhou, G.M., Ayala, M., and Zhang, S.C. (2013b). Medial ganglionic eminence-like cells derived from human embryonic stem cells correct learning and memory deficits. Nat Biotechnol *31*, 440-447.

Lockstone, H.E., Harris, L.W., Swatton, J.E., Wayland, M.T., Holland, A.J., and Bahn, S. (2007). Gene expression profiling in the adult Down syndrome brain. Genomics *90*, 647-660.

Loebrich, S., and Nedivi, E. (2009). The function of activity-regulated genes in the nervous system. Physiol Rev *89*, 1079-1103.

Lopez-Bendito, G., Sturgess, K., Erdelyi, F., Szabo, G., Molnar, Z., and Paulsen, O. (2004). Preferential origin and layer destination of GAD65-GFP cortical interneurons. Cereb Cortex *14*, 1122-1133.

Lu, J., Lian, G., Zhou, H., Esposito, G., Steardo, L., Delli-Bovi, L.C., Hecht, J.L., Lu, Q.R., and Sheen, V. (2012). OLIG2 over-expression impairs proliferation of human Down syndrome neural progenitors. Hum Mol Genet *21*, 2330-2340.

Lu, Q.R., Yuk, D., Alberta, J.A., Zhu, Z., Pawlitzky, I., Chan, J., McMahon, A.P., Stiles, C.D., and Rowitch, D.H. (2000). Sonic hedgehog--regulated oligodendrocyte lineage genes encoding bHLH proteins in the mammalian central nervous system. Neuron *25*, 317-329.

Ma, L., Hu, B., Liu, Y., Vermilyea, S.C., Liu, H., Gao, L., Sun, Y., Zhang, X., and Zhang, S.C. (2012). Human embryonic stem cell-derived GABA neurons correct locomotion deficits in quinolinic acid-lesioned mice. Cell Stem Cell *10*, 455-464.

Maclean, G.A., Menne, T.F., Guo, G., Sanchez, D.J., Park, I.H., Daley, G.Q., and Orkin, S.H. (2012). Altered hematopoiesis in trisomy 21 as revealed through in vitro differentiation of isogenic human pluripotent cells. Proc Natl Acad Sci U S A *109*, 17567-17572.

Madhavan, M., Nevin, Z.S., Shick, H.E., Garrison, E., Clarkson-Paredes, C., Karl, M., Clayton, B.L.L., Factor, D.C., Allan, K.C., Barbar, L., *et al.* (2018). Induction of myelinating oligodendrocytes in human cortical spheroids. Nat Methods.

Malone, F.D., Canick, J.A., Ball, R.H., Nyberg, D.A., Comstock, C.H., Bukowski, R., Berkowitz, R.L., Gross, S.J., Dugoff, L., Craigo, S.D., *et al.* (2005). First-trimester or second-trimester screening, or both, for Down's syndrome. N Engl J Med *353*, 2001-2011.

Mao, R., Zielke, C.L., Zielke, H.R., and Pevsner, J. (2003). Global up-regulation of chromosome 21 gene expression in the developing Down syndrome brain. Genomics *81*, 457-467.

Mariani, J., Coppola, G., Zhang, P., Abyzov, A., Provini, L., Tomasini, L., Amenduni, M., Szekely, A., Palejev, D., Wilson, M., *et al.* (2015). FOXG1-Dependent Dysregulation of GABA/Glutamate Neuron Differentiation in Autism Spectrum Disorders. Cell *162*, 375-390.

Mariani, J., Simonini, M.V., Palejev, D., Tomasini, L., Coppola, G., Szekely, A.M., Horvath, T.L., and Vaccarino, F.M. (2012). Modeling human cortical development in vitro using induced pluripotent stem cells. Proc Natl Acad Sci U S A *109*, 12770-12775.

Marin, O. (2012). Brain development: The neuron family tree remodelled. Nature *490*, 185-186.

Maroof, A.M., Keros, S., Tyson, J.A., Ying, S.W., Ganat, Y.M., Merkle, F.T., Liu, B., Goulburn, A., Stanley, E.G., Elefanty, A.G., *et al.* (2013). Directed differentiation and functional maturation of cortical interneurons from human embryonic stem cells. Cell Stem Cell *12*, 559-572.

Monzel, A.S., Smits, L.M., Hemmer, K., Hachi, S., Moreno, E.L., van Wuellen, T., Jarazo, J., Walter, J., Bruggemann, I., Boussaad, I., *et al.* (2017). Derivation of Human Midbrain-Specific Organoids from Neuroepithelial Stem Cells. Stem Cell Reports *8*, 1144-1154.

Muller, F.J., Schuldt, B.M., Williams, R., Mason, D., Altun, G., Papapetrou, E.P., Danner, S., Goldmann, J.E., Herbst, A., Schmidt, N.O., *et al.* (2011). A bioinformatic assay for pluripotency in human cells. Nat Methods *8*, 315-317.

Nicholas, C.R., Chen, J., Tang, Y., Southwell, D.G., Chalmers, N., Vogt, D., Arnold, C.M., Chen, Y.J., Stanley, E.G., Elefanty, A.G., *et al.* (2013). Functional maturation of hPSC-derived forebrain interneurons requires an extended timeline and mimics human neural development. Cell Stem Cell *12*, 573-586.

Ono, K., Takebayashi, H., Ikeda, K., Furusho, M., Nishizawa, T., Watanabe, K., and Ikenaka, K. (2008). Regional- and temporal-dependent changes in the differentiation of Olig2 progenitors in the forebrain, and the impact on astrocyte development in the dorsal pallium. Dev Biol *320*, 456-468.

Paredes, M.F., James, D., Gil-Perotin, S., Kim, H., Cotter, J.A., Ng, C., Sandoval, K., Rowitch, D.H., Xu, D., McQuillen, P.S., *et al.* (2016). Extensive migration of young neurons into the infant human frontal lobe. Science *354*.

Parker, S.E., Mai, C.T., Canfield, M.A., Rickard, R., Wang, Y., Meyer, R.E., Anderson, P., Mason, C.A., Collins, J.S., Kirby, R.S., *et al.* (2010). Updated National Birth Prevalence estimates for selected birth defects in the United States, 2004-2006. Birth Defects Res A Clin Mol Teratol *88*, 1008-1016.

Pasca, A.M., Sloan, S.A., Clarke, L.E., Tian, Y., Makinson, C.D., Huber, N., Kim, C.H., Park, J.Y., O'Rourke, N.A., Nguyen, K.D., *et al.* (2015). Functional cortical neurons and astrocytes from human pluripotent stem cells in 3D culture. Nat Methods *12*, 671-678.

Pasca, S.P. (2018). The rise of three-dimensional human brain cultures. Nature *553*, 437-445.

Patterson, M., Chan, D.N., Ha, I., Case, D., Cui, Y., Van Handel, B., Mikkola, H.K., and Lowry, W.E. (2012). Defining the nature of human pluripotent stem cell progeny. Cell Res *22*, 178-193.

Petilla Interneuron Nomenclature Group, G., Ascoli, G.A., Alonso-Nanclares, L., Anderson, S.A., Barrionuevo, G., Benavides-Piccione, R., Burkhalter, A., Buzsaki, G., Cauli, B., Defelipe, J., *et al.* (2008). Petilla terminology: nomenclature of features of GABAergic interneurons of the cerebral cortex. Nat Rev Neurosci *9*, 557-568.

Petryniak, M.A., Potter, G.B., Rowitch, D.H., and Rubenstein, J.L. (2007). Dlx1 and Dlx2 control neuronal versus oligodendroglial cell fate acquisition in the developing forebrain. Neuron *55*, 417-433.

Quadrato, G., Brown, J., and Arlotta, P. (2016). The promises and challenges of human brain organoids as models of neuropsychiatric disease. Nat Med *22*, 1220-1228.

Rissman, R.A., and Mobley, W.C. (2011). Implications for treatment: GABAA receptors in aging, Down syndrome and Alzheimer's disease. J Neurochem *117*, 613-622.

Ross, M.H., Galaburda, A.M., and Kemper, T.L. (1984). Down's syndrome: is there a decreased population of neurons? Neurology *34*, 909-916.

Sanai, N., Nguyen, T., Ihrie, R.A., Mirzadeh, Z., Tsai, H.H., Wong, M., Gupta, N., Berger, M.S., Huang, E., Garcia-Verdugo, J.M., *et al.* (2011). Corridors of migrating neurons in the human brain and their decline during infancy. Nature *478*, 382-386.

Shi, Y., Kirwan, P., Smith, J., Robinson, H.P., and Livesey, F.J. (2012). Human cerebral cortex development from pluripotent stem cells to functional excitatory synapses. Nat Neurosci *15*, 477-486, S471.

Silbereis, J.C., Nobuta, H., Tsai, H.H., Heine, V.M., McKinsey, G.L., Meijer, D.H., Howard, M.A., Petryniak, M.A., Potter, G.B., Alberta, J.A., *et al.* (2014). Olig1 function is required to repress dlx1/2 and interneuron production in Mammalian brain. Neuron *81*, 574-587.

Simao, D., Silva, M.M., Terrasso, A.P., Arez, F., Sousa, M.F.Q., Mehrjardi, N.Z., Saric, T., Gomes-Alves, P., Raimundo, N., Alves, P.M., *et al.* (2018). Recapitulation of Human Neural Microenvironment Signatures in iPSC-Derived NPC 3D Differentiation. Stem Cell Reports *11*, 552-564.

Stanco, A., Pla, R., Vogt, D., Chen, Y., Mandal, S., Walker, J., Hunt, R.F., Lindtner, S., Erdman, C.A., Pieper, A.A., *et al.* (2014). NPAS1 represses the generation of specific subtypes of cortical interneurons. Neuron *84*, 940-953.

Sturgeon, X., and Gardiner, K.J. (2011). Transcript catalogs of human chromosome 21 and orthologous chimpanzee and mouse regions. Mamm Genome *22*, 261-271.

Sussel, L., Marin, O., Kimura, S., and Rubenstein, J.L. (1999). Loss of Nkx2.1 homeobox gene function results in a ventral to dorsal molecular respecification within the basal telencephalon: evidence for a transformation of the pallidum into the striatum. Development *126*, 3359-3370.

Tischfield, D.J., and Anderson, S.A. (2017). Differentiation of Mouse Embryonic Stem Cells into Cortical Interneuron Precursors. J Vis Exp.

Tsigelny, I.F., Mukthavaram, R., Kouznetsova, V.L., Chao, Y., Babic, I., Nurmemmedov, E., Pastorino, S., Jiang, P., Calligaris, D., Agar, N., *et al.* (2017). Multiple spatially related pharmacophores define small molecule inhibitors of OLIG2 in glioblastoma. Oncotarget *8*, 22370-22384.

Villeda, S.A., Luo, J., Mosher, K.I., Zou, B., Britschgi, M., Bieri, G., Stan, T.M., Fainberg, N., Ding, Z., Eggel, A., *et al.* (2011). The ageing systemic milieu negatively regulates neurogenesis and cognitive function. Nature *477*, 90-94.

Walf, A.A., and Frye, C.A. (2007). The use of the elevated plus maze as an assay of anxiety-related behavior in rodents. Nat Protoc *2*, 322-328.

Wan, H., Aggleton, J.P., and Brown, M.W. (1999). Different contributions of the hippocampus and perirhinal cortex to recognition memory. J Neurosci *19*, 1142-1148.

Weick, J.P., Held, D.L., Bonadurer, G.F., 3rd, Doers, M.E., Liu, Y., Maguire, C., Clark, A., Knackert, J.A., Molinarolo, K., Musser, M., *et al.* (2013). Deficits in human trisomy 21 iPSCs and neurons. Proc Natl Acad Sci U S A *110*, 9962-9967.

Windrem, M.S., Osipovitch, M., Liu, Z., Bates, J., Chandler-Militello, D., Zou, L., Munir, J., Schanz, S., McCoy, K., Miller, R.H., *et al.* (2017). Human iPSC Glial Mouse Chimeras Reveal Glial Contributions to Schizophrenia. Cell Stem Cell *21*, 195-208 e196.

Windrem, M.S., Schanz, S.J., Guo, M., Tian, G.F., Washco, V., Stanwood, N., Rasband, M., Roy, N.S., Nedergaard, M., Havton, L.A., *et al.* (2008). Neonatal chimerization with human glial progenitor cells can both remyelinate and rescue the otherwise lethally hypomyelinated shiverer mouse. Cell Stem Cell *2*, 553-565.

Windrem, M.S., Schanz, S.J., Morrow, C., Munir, J., Chandler-Militello, D., Wang, S., and Goldman, S.A. (2014). A competitive advantage by neonatally engrafted human glial progenitors yields mice whose brains are chimeric for human glia. J Neurosci *34*, 16153-16161.

Wonders, C.P., and Anderson, S.A. (2006). The origin and specification of cortical interneurons. Nat Rev Neurosci *7*, 687-696.

Wonders, C.P., Taylor, L., Welagen, J., Mbata, I.C., Xiang, J.Z., and Anderson, S.A. (2008). A spatial bias for the origins of interneuron subgroups within the medial ganglionic eminence. Dev Biol *314*, 127-136.

Xiang, Y., Tanaka, Y., Patterson, B., Kang, Y.J., Govindaiah, G., Roselaar, N., Cakir, B., Kim, K.Y., Lombroso, A.P., Hwang, S.M., *et al.* (2017). Fusion of Regionally Specified hPSC-Derived Organoids Models Human Brain Development and Interneuron Migration. Cell Stem Cell *21*, 383-398 e387.

Xu, Q., Cobos, I., De La Cruz, E., Rubenstein, J.L., and Anderson, S.A. (2004). Origins of cortical interneuron subtypes. J Neurosci *24*, 2612-2622.

Xu, R., Hu, Q., Ma, Q., Liu, C., and Wang, G. (2014). The protease Omi regulates mitochondrial biogenesis through the GSK3beta/PGC-1alpha pathway. Cell Death Dis *5*, e1373.

Xu, X., Roby, K.D., and Callaway, E.M. (2006). Mouse cortical inhibitory neuron type that coexpresses somatostatin and calretinin. J Comp Neurol *499*, 144-160.

Xue, H., Wu, S., Papadeas, S.T., Spusta, S., Swistowska, A.M., MacArthur, C.C., Mattson, M.P., Maragakis, N.J., Capecchi, M.R., Rao, M.S., *et al.* (2009). A targeted neuroglial reporter line generated by homologous recombination in human embryonic stem cells. Stem Cells *27*, 1836-1846.

Zerucha, T., Stuhmer, T., Hatch, G., Park, B.K., Long, Q., Yu, G., Gambarotta, A., Schultz, J.R., Rubenstein, J.L., and Ekker, M. (2000). A highly conserved enhancer in the Dlx5/Dlx6 intergenic region is the site of cross-regulatory interactions between Dlx genes in the embryonic forebrain. J Neurosci *20*, 709-721.

Zhao, Y., Flandin, P., Long, J.E., Cuesta, M.D., Westphal, H., and Rubenstein, J.L. (2008). Distinct molecular pathways for development of telencephalic interneuron subtypes revealed through analysis of Lhx6 mutants. J Comp Neurol *510*, 79-99.

STAR METHODS

KEY RESOURCES TABLE

REAGENT or RESOURCE	SOURCE	IDENTIFIER
Antibodies		
Mouse anti-βIIItubulin	Millipore	Cat# MAB1637; RRID: AB_2210524
Mouse anti-β-tubulin	DSHB	Cat# E7; RRID: AB_528499
Rabbit anti-Calbindin (CB)	Millipore	Cat# AB1778; RRID: AB_2068336
Rabbit anti-Calretinin (CR)	Swant	Cat# 7697; RRID: AB_2619710
Rabbit anti-c-FOS	Santa Cruz	Cat# SC-52; RRID: AB_2106783
Goat anti-ChAT	Millipore	Cat# AB144P; RRID: AB_90650
Rabbit anti-FOXG1	Abcam	Cat# ab18259; RRID: AB_732415
Rabbit anti-GABA	Sigma	Cat# A2052; RRID: AB_477652
Rabbit anti-GAD65/67	Millipore	Cat# AB1511; RRID: AB_90715
Mouse anti-GAPDH	Santa Cruz	Cat# SC-32233; RRID: AB_627679
Rabbit anti-GFAP	Boster	Cat# PA1239; RRID: AB_10892391
Goat anti-GFP	Rockland	Cat# 600-141-215; RRID: AB_1961516
Mouse anti-GFP	Thermo	Cat# MA5-15256; RRID: AB_10979281
Mouse anti-Human nuclei (hN)	Millipore	Cat# MAB4383; RRID: AB_827439
Mouse anti-Ki67	Cell signaling	Cat# 9449; RRID: AB_2715512
Rabbit anti-Ki67	Thermo Fisher Scientific	Cat# SP6; RRID: AB_2314700
Mouse anti-MAP2	Millipore	Cat# MAB3418; RRID: AB_94856
Mouse anti-Human MAP2	Santa Cruz	Cat# SC-74420; RRID: AB_1126219
Rabbit anti-LHX6	Abcam	Cat# ab22885; RRID: AB_447345
Rat anti-MBP	Millipore	Cat# MAB386; RRID: AB_94975
Rabbit anti-NeuN	Millipore	Cat# ABN78; RRID: AB_10807945
Mouse anti-NeuN	Millipore	Cat# MAB377; RRID: AB_2298772
Rabbit anti-Neuropeptide Y (NPY)	Abcam	Cat# AB10980; RRID: AB_297635
Goat anti-Nestin	Santa Cruz	Cat# SC-21249; RRID: AB_2267112
Rabbit anti-NG2	Millipore	Cat# AB5320; RRID: AB_91789
Rabbit anti-NKX2.1(TTF1)	Abcam	Cat# ab76013; RRID: AB_1310784
Rabbit anti-OLIG2	Phosphosolutions	Cat# 1538; RRID: AB_2492193
Mouse anti-OLIG1	Millipore	Cat# MAB5540; RRID: AB_2157530
Rabbit anti-OLIG1	Phosphosolutions	Cat# 1537; RRID: AB_2492192
Rabbit anti-OLIG1	Abcam	Cat#124908; RRID: AB_10972689
Mouse anti-OTX2	R&D	Cat# AF2418; RRID: AB_2157554
Rabbit anti-Parvalbumin (PV)	Abcam	Cat# AB11427; RRID: AB_298032
Rabbit anti-PAX6	GeneTex	Cat# GTX113241; RRID: AB_1951119
Rabbit anti-PDGFRα	Santa Cruz	Cat# SC-338; RRID: AB_631064
Rabbit anti-Phospho-Histone H3	Thermo Fisher Scientific	Cat# PA5–17869; RRID: AB_10984484
Rabbit anti-PSD95	Invitrogen	Cat# 51-6900; RRID: AB_2533914
Mouse anti-S100β	Sigma	Cat# S2532; RRID: AB_477499
Rat anti-Somatostatin (SST)	Millipore	Cat# AB354; RRID: AB_303889
Rabbit anti-Somatostatin (SST)	Peninsula Laboratories International	Cat# T-4102.0400; RRID: AB_518613
Rabbit anti-SOX2	Millipore	Cat# AB5603; RRID: AB_2286686
Mouse anti-STEM121	Takara	Cat# Y40410; RRID: AB_2632385

Rabbit anti-Synapsin I	Millipore	Cat# AB1543P; RRID: AB_90757
Rabbit anti-VGAT	Millipore	Cat# AB5062P; RRID: AB_2301998
Bacterial and virus Strains		
OLIG2 shRNA	Santa Cruz	Cat# sc-38147-V
copGFP		Cat# sc-108084
Biological Samples		
Postmortem human brain tissues	See Table S3	
Chemicals, Peptides, and Recombinant Proteins		
SB431542	Stemgent	Cat# 04-0010-05
noggin	Peprotech	Cat# 120-10C
DMEM/F12	HyClone	Cat# SH3002201
N2	Thermo Fisher Scientific	Cat# 17502048
growth factor-reduced Matrigel	Corning	Cat# 354230
laminin	Corning	Cat# 354232
Neurobasal	Thermo Fisher Scientific	Cat# 21103-049
B27-RA	Thermo Fisher Scientific	Cat# 12587010
FGF2	Peprotech	Cat# 100-18B
hLIF	Millipore	Cat# 300-05
CHIR99021	Biogems	Cat# 2520691
Y-27632	Tocris	Cat# 125410
TrypLE Express	Thermo Fisher Scientific	Cat# 12605028
sonic hedgehog (SHH)	Peprotech	Cat# 100-45
purmorphamine	Cayman Chem	Cat# 10009634
BDNF	Peprotech	Cat# 450-02
GDNF	Peprotech	Cat# 450-10
dibutyryl-cyclic AMP	Sigma	Cat# D0260
ascorbic acid	Sigma	Cat# A4403
Critical Commercial Assays		
TaqMan Gene Expression Master Mix	Thermo Fisher Scientific	Cat# 4369016
Nuclear/Cytosolic Fractionation Kit	Cell Biolabs Inc	Cat# AKR171
Deposited data		
RNA-seq data	This paper	GEO: GSE124513
Experimental Models: Cell Lines		
See Table S2 for details		
Experimental Models: Organisms/Strains		
Rag1$^{-/-}$ mice	Jackson Laboratory	Mouse strain datasheet: 002216, RRID:IMSR_JAX:003145
Oligonucleotides		
See Table S4 for list of Taqman primers		
See Table S5 for list of ChIP-PCR primers		
See Table S6 for list of luciferase report assay primers		
Software and Algorithms		
Zen 2.3	Carl Zeiss	N/A
Fiji	ImageJ	https://imagej.net/Fiji/Downloads N/A
GraphPad Prism 7.01	GraphPad Software	N/A

CONTACT FOR REAGENT AND RESOURCE SHARING

Further information and requests for resources and reagents should be directed to and will be fulfilled by the Lead Contact, Peng Jiang (peng.jiang@rutgers.edu).

EXPERIMENTAL MODEL AND SUBJECT DETAILS

Generation, culture, and quality control of hPSC lines and their neural derivatives.

The control and DS hiPSC lines were generated from patient-derived fibroblasts using the "Yamanaka" reprogramming factors, as reported in our previous study (Chen et al., 2014). DS fibroblasts were obtained from Coriell Institute for Medical Research (Table S2). The hiPSC lines derived from DS patients include two DS hiPSC lines (DS1, female; and DS2, male) and isogenic Di-DS3 and Tri-DS3 hiPSCs that were generated from a single female patient. Previous studies reported the generation of DS isogenic disomic and trisomic subclones either from the same parental iPSC lines during serial passage (Maclean et al., 2012) or from reprogramming mosaic DS fibroblasts (Weick et al., 2013). As reported in our previous study (Chen et al., 2014), we did not observe mosaicism in the fibroblasts from patient DS3 and the disomic subclones were identified during passaging similar to the study (Maclean et al., 2012). The isogenic Di- and Tri-DS3 iPSCs were then isolated and established by clonal expansion. Moreover, all the hiPSC lines derived from DS patients have been fully characterized by performing karyotyping, teratoma assay, DNA fingerprinting STR (short tandem repeat) analysis, gene expression profiling, and Pluritest (www.PluriTest.org), a robust open-access bioinformatic assay of pluripotency in human cells based on their gene expression profiles (Muller et al., 2011), as described in our previous study (Chen et al., 2014). Comparative genomic hybridization (CGH) array was used to verify the isogenicity of the Di-DS3 and Tri-DS3 hiPSCs. In the current study, fluorescence in situ hybridization (FISH) analysis with a human chromosome 21 (HSA21)-specific probe (Vysis LSI 21 probe; Abbott Molecular) was routinely performed to examine the copy number of HSA21 in the DS and control hiPSC-derived pNPCs, as previously described (Chen et al., 2014). In addition, *OLIG1* and O*LIG2* relative DNA copy number were examined routinely by using TaqMan Copy Number Assay (Applied Biosystems). Briefly, genomic DNA from DS and control pNPCs was collected by using DNA Extract All Reagents Kit (Applied Biosystems) and gene copy number of *OLIG1*, *OLIG2*, and RNase P were examined with primers Hs05549528, Hs02041572 or Copy Number Reference Assay human RNase P, respectively, using TaqMan Gene Expression Master Mix kit (Applied Biosystems). *OLIG1* and *OLIG2* relative DNA copy number were calculated by normalizing to RNase P DNA copy number, according to the manufacturer's instructions. The OLIG2-GFP knockin hESC and hiPSC reporter lines were generated using a gene-targeting protocol as reported in our previous studies (Liu et al., 2011; Xue et al., 2009). The hPSCs were maintained under feeder-free condition and cultured on dishes coated with hESC-qualified Matrigel (Corning) in mTeSR1 media (STEMCELL Technologies). The hPSCs were passaged approximately once per week with ReLeSR media (STEMCELL Technologies). All the hPSC studies were approved by the committees on stem cell research at Rutgers University.

Animals

Rag1$^{-/-}$ mice (B6.129S7-*Rag1*^{tm1Mom}/J, The Jackson Laboratory) were used for cell transplantation. All animal work was performed without gender bias under the Institutional Animal Care and Use Committee (IACUC) protocol approved by Rutgers University IACUC Committee.

METHOD DETAILS

Ventral forebrain organoid generation and culture

To generate ventral forebrain organoids, we used pNPCs as the starting population, because utilization of these neural fate-restricted progenitors has the advantage of efficient differentiation into desired brain regions (Monzel et al., 2017). Similar to previous studies (Mariani et al., 2012; Pasca et al., 2015; Xiang et al., 2017), we did not include Matrigel as supportive matrix in forming organoids, as we did not find significant improvement in the formation of ventral forebrain organoids by Matrigel embedding in

our system. Briefly, the pNPCs were derived from hPSCs using small molecule-based protocols (Chen et al., 2016; Li et al., 2011). Neural differentiation in the embryoid bodies (EB) was induced by dual inhibition of SMAD signaling (Chambers et al., 2009), using inhibitors SB431542 (5 μM, Stemgent) and noggin (50 ng/ml, Peprotech) in neural induction medium composed of DMEM/F12 (HyClone) and 1× N2 (Thermo Fisher Scientific) for 1 week. EBs were then grown on dishes coated with growth factor-reduced Matrigel (BD Biosciences) in the medium consisting of DMEM/F12, 1× N2, and laminin (1 μg/ml; Corning). pNPCs in the form of rosettes developed for another 7 days (week 2). Next, rosettes were manually isolated from surrounding cells and expanded for 7 days (week 3) in pNPC medium, composed of a 1:1 mixture of Neurobasal (Thermo Fisher Scientific) and DMEM/F12, supplemented with 1× N2, 1× B27-RA (Thermo Fisher Scientific), FGF2 (20 ng/ml, Peprotech), human leukemia inhibitory factor (hLIF, 10 ng/ml, Millipore), CHIR99021 (3 μM, Biogems), SB431542 (2 μM), and ROCK inhibitor Y-27632 (10 μM, Tocris).

Then the expanded pNPCs were dissociated into single cells using TrypLE Express (Thermo Fisher Scientific). 10,000 cells were cultured in suspension in the presence of ROCK inhibitor Y-27632 (10 μM) in ultra-low-attachment 96-well plates to form uniform organoids and then those organoids were transferred to ultra-low-attachment 6-well plates. To pattern these organoids to the fate of ventral forebrain, we treated them with sonic hedgehog (SHH) (50 ng/mL, Peprotech) and purmorphamine (1 μM, Cayman Chem), an agonist of sonic hedgehog signal pathway from week 3 to 5 (Figure 1A). The media were replenished every day. Starting from week 5, the cell culture plates were kept on orbital shaker with speed of 80 rpm/min. Maximum 8 organoids were cultured in each well of the ultra-low-attachment 6-well plate in neuronal differentiation medium containing a 1:1 mixture of Neurobasal and DMEM/F12, supplemented with 1× N2 (Thermo Fisher Scientific), 1× B27 (Thermo Fisher Scientific), BDNF (20 ng/ml, Peprotech), GDNF (20 ng/ml, Peprotech), dibutyryl-cyclic AMP (1mM, Sigma), and ascorbic acid (200 nM, Sigma) and media was replenished every other day. For 2D neuronal differentiation, 5,000 dissociated cells were plated onto poly-L-ornithine (0.002%, Sigma) and laminin (10 μg ml^{-1}) pre-coated coverslips in the same neuronal differentiation medium. The neurons cultured in the neuronal differentiation medium for 4–6 weeks were used for experiments.

Cell transplantation

The 5-week-old hiPSC-derived ventral forebrain organoids were dissociated and suspended as single cells at a final concentration of 100,000 cells per μl in PBS. The cells were then injected into the brains of P0 *rag1* -/- immunodeficient mice (B6.129S7-Rag1tm1Mom/J on a C57BL/6 background, Jackson Laboratories). The precise transplantation sites were bilateral from the midline = ± 1.0 mm, posterior bregma = -1.0 mm, and dorsoventral depth = -1.0 or -1.8 mm (Figure 4A and Figure S4A). The mouse pups were anesthetized by placing them on ice for 5 minutes. Once cryo-anesthetized, the pups were placed on a digital stereotaxic device (David KOPF Instruments), equipped with a neonatal mouse adaptor (Stoelting). The pups were then injected with 1 μl of cells into each site by directly inserting Hamilton needles through the skull into the target sites. The pups were weaned at 3 weeks and were kept up to 6 months before they were tested for the engraftment of human cells.

Electrophysiology

Brain slice electrophysiology was carried out as described elsewhere (Liu et al., 2017). Briefly, mice were anesthetized, decapitated, and brains were removed and quickly immersed in cold (4°C) oxygenated cutting solution containing (in mM): 50 sucrose, 2.5 KCl, 0.625 $CaCl_2$, 1.2 $MgCl_2$, 1.25 NaH_2PO_4, 25 $NaHCO_3$, and 2.5 glucose, pH to 7.3 with NaOH. Coronal cerebral cortex slices, 300 μm in thickness, were cut using a vibratome (VT 1200S; Leica). Brain slices were collected in artificial cerebrospinal fluid (ACSF) and bubbled with 5% CO_2 and 95% O_2. The ACSF contained (in mM): 125 NaCl, 2.5 KCl, 2.5 $CaCl_2$, 1.2 $MgCl_2$, 1.25 NaH_2PO_4, 26 $NaHCO_3$, and 2.5 glucose (pH 7.3 with NaOH). After at least 1 hour of recovery, slices were transferred to a recording chamber and constantly perfused with bath solution (30°C) at a flow rate of 2 ml/min. Patch pipettes with a resistance of 8~10 MΩ were made from borosilicate glass (World Precision Instruments) with a pipette puller (PC-10,

Narishige) and filled with pipette solution containing (in mM): 126 K-Gluconate, 4 KCl, 10 HEPES, 4 Mg-ATP, 0.3 Na_2-GTP, 10 phosphocreatine, (pH to 7.2 with KOH) for current and voltage clamp recordings. Dextran Alexa Fluor 594 was included in the intracellular recording solution for cell labeling. After whole-cell patch-clamp was achieved, spontaneous PSCs were recorded under voltage clamp at -70 mV. Input resistance and series resistance were monitored throughout the experiments and recordings were rejected if series resistance increased above 25 MΩ. All data were sampled at 5 kHz and analyzed offline using ClampFit 10.2 (Molecular Devices, USA) software.

RNA isolation and qPCR

Total RNA was prepared from organoids with RNAeasy kit (Qiagen) (Chen et al., 2014). Complementary DNA was prepared with a Superscript III First-Strand kit (Invitrogen). The qPCR was performed with Taqman primers (Life Technologies) on an ABI 7500 Real-Time PCR System. All primers used are listed in Table S4. All experimental samples were analyzed and normalized with the expression level of housekeeping gene glyceraldehyde- 3-phosphate dehydrogenase (GAPDH). Relative quantification was performed by applying the $2^{-\Delta\Delta Ct}$ method(Chen et al., 2014).

ChIP

Chromatin immunoprecipitation (ChIP) was performed using Magna-CHIP™ A Chromatin Immunoprecipitation Kit (Millipore, USA) according to the manufacturer's instructions. Briefly, after being washed with cold PBS, the 5-week-old organoids were incubated in PBS with 1% formaldehyde at room temperature for ten minutes to cross-link chromatin proteins to genomic DNA. Glycine was used to quench unreacted formaldehyde. Following cold PBS washing, organoids were resuspended in lysis buffer with protease inhibitor Cocktail II and subjected to bioruptor sonication to shear DNA length to 200 -1000 bp. 5 µg of anti-OLIG2 (Phosphosolutions 1538), anti-IgG (Kit included) or anti-Acetyl-Histone H3 antibody (positive control, included in the kit) and Protein A magnetic beads were added to the chromatin solution and incubated overnight at 4°C with rotation. After washing and elution, crosslinks of the protein/DNA complexes were reversed to free DNA by the addition of proteinase K and incubation at 62°C for 2 h followed by further incubation at 95°C for 10 min. Then, the DNA fragments were purified and used for PCR. The primers targeting human GAPDH was provided by the kit, working as the positive control. All primer sequences were listed in Table S5. The PCR products were analyzed by agarose gel electrophoresis.

RNA sequencing

Organoids (5-week old) generated from hiPSC lines derived from two DS patients (patient DS1 and DS3 and corresponding cell lines include DS1, control1, isogenic Tri-DS3 and Di-DS3, Tri-DS3+Cont^{shRNA}, and Tri-DS3+OLIG2s^{hRNA} hiPSCs) were used for RNA-sequencing. In order to reduce technical variations among different batches of cultures, a large number of organoids (total 40-60 organoids for each cell line) collected from three batches of organoid cultures were pooled together for RNA extraction and sample preparation.

Total RNA was prepared with RNAeasy kit (Qiagen) (Chen et al., 2014) and libraries were constructed using 600 ng of total RNA from each sample and the TruSeqV2 kit from Illumina (Illumina, San Diego, CA) following manufacturers suggested protocol. The libraries were subjected to 75 bp paired read sequencing using a NextSeq500 Illumina sequencer to generate approximately 30 to 36 million paired-reads per sample. Fastq files were generated using the Bc12Fastq software, version 1.8.4. The genome sequence was then indexed using the rsem-prepare-reference command. Each fastq file was trimmed using the fqtrim program, and then aligned to the human genome using the rsem-calculate-expression (version 1.2.31) command to calculate FPKM (fragments per kilobase of transcript per million mapped reads) values.

In order to analyze the transcripts, FPKM > 1 was set as cutoff to filter transcripts. |Fold change | > 1.5 was set as criteria to filter differential expressed genes (DEGs). Upregulated and downregulated DEGs were mapped to each chromosome and the number of DEGs in each chromosome was counted.

Functional enrichment analysis was performed using DAVID online tool (Huang da et al., 2009a, b) and visualized using GraphPad. Heatmaps were generated using pheatmap package of R. Correlations with BrainSpan data were performed in R using only genes common to both experiments. The average of the Spearman correlation coefficient is presented for all the combinations of organoid sample replicates or BrainSpan samples matching the labeled condition.

Immunostaining and cell counting

Mouse brains and organoids fixed with 4% paraformaldehyde were processed and cryo-sectioned for immunofluorescence staining (Liu et al., 2011; Pasca et al., 2015). The primary antibodies were listed in key resource table. Slides were mounted with the anti-fade Fluoromount-G medium containing 1, 40,6-diamidino-2-phenylindole dihydrochloride (DAPI) (Southern Biotechnology). Diaminobenzidine (DAB) immunostaining was performed with antibody against GFP or a human-specific marker STEM121 as described in our previous study (Chen et al., 2016; Jiang et al., 2013b). Images were captured with Zeiss 710 confocal microscope. Figure 4C, Figures S3E-S3J and Figure S4B scan images were obtained by confocal tile scan and automatically stitched using 10% overlap between tiles by Zen software (Zeiss). The analysis of fluorescence intensity was performed using ImageJ software (NIH Image). The relative fluorescence intensity was presented as normalized value to the control group. The cells were counted with ImageJ software. For organoids, at least three fields of each organoid were chosen randomly and at least 16 organoids from each group were counted. For brain sections, at least five consecutive sections of each brain region were chosen. The number of positive cells from each section was counted after a Z projection and at least 7 mice in each group were counted. Engraftment efficiency and degree of chimerization were assessed by quantifying the percentage of hN^+ cells among total $DAPI^+$ cells in sagittal brain sections, as reported in the previous studies (Chen et al., 2015; Han et al., 2013). The cell counting was performed on every fifteenth sagittal brain section with a distance of 300 µm, covering brain regions from 0.3 to 2.4 mm lateral to the midline (seven to eight sections from each mouse brain were used).

Electron microscopy

The selected vibratome sections that contained DAB-labeled cells were post-fixed and processed for electron microscopy (EM) as described in our previous studies (Chen et al., 2016; Jiang et al., 2016; Jiang et al., 2013a). EM images were captured using a high-resolution charge-coupled device (CCD) camera (FEI).

Western blotting

Western blotting was performed as described previously (Xu et al., 2014). Lysates from organoids or human brain tissue were prepared using RIPA buffer and the protein content was determined by a Bio-Rad Protein Assay system. Proteins were separated on 4-12% SDS-PAGE gradient gel and transferred onto nitrocellulose membrane. Then the membrane was incubated with antibodies (Table S7). Appropriate secondary antibodies conjugated to HRP were used and the ECL reagents (Pierce ECL Plus Western Blotting Substrate, Thermoscientific) were used for immunodetection. For quantification of band intensity, blots from at least three independent experiments for each molecule of interest were used. Signals were measured using ImageJ software and represented as relative intensity versus control. β-tubulin was used as an internal control to normalize band intensity. The human brain tissues used for western blotting analyses are de-identified by encoding with digital numbers and obtained from University of Maryland Brain and Tissue Bank which is a Brain and Tissue Repository of the NIH NeuroBioBank. All the human brain tissues were derived from the cerebral cortex of patients at the ages from 186 to 339 days (Table S3). Additional information on the human brain tissue, including sex, race, and postmortem interval (PMI), was also provided.

Coomassie blue staining

Similar to previous studies involving human tissue for western blotting (Blair et al., 2016), we performed denatured SDS-PAGE and Coomassie blue staining using the human samples, prior to examining the expression of proteins of interest. The sample preparations that exhibited the absence of smear (little or no degradation) and sharp resolution of protein bands were used for experiments. SDS-PAGE gradient gel was stained by staining solution (0.1% Coomassie Brilliant Blue R-250, 50% methanol and 10% glacial acetic acid) with shaking overnight and was de-stained using de-staining solution (40% methanol and 10% glacial acetic acid) for 1 hour.

shRNA knockdown experiments

OLIG2 shRNA (sc-38147-V), non-targeting control shRNA (sc-108080), and copGFP (sc-108084) lentiviral particles were purchased from Santa Cruz Biotechnology. OLIG2 shRNA lentiviral particles carry three different shRNAs that specifically target *OLIG2* gene expression. Undifferentiated hiPSCs were infected with lentivirus and selected with puromycin treatment. The optimal concentration of puromycin for the selection of transduced hiPSC colonies was established by puromycin titration on the specific hiPSC line used for the experiments. Puromycin was added at a concentration of 0.5 μg/ml for two weeks to select transduces hiPSCs. Stable hiPSCs were then used for neural differentiation with puromycin kept in all the media at 0.3 μg/ml as previously described (Mariani et al., 2015). Knockdown of *OLIG2* mRNA expression was confirmed by qPCR after SHH and Pur treatment.

FACS

Sorting of $OLIG2^{+}/GFP^{+}$ cells and data acquisition were performed in a BD FACS Calibur (BD Bioscience). Acquired data were subsequently analyzed by calculating proportions/percentages and average intensities using the FlowJo software (Treestar Inc)(Jiang et al., 2013b).

Cell fractionation

The isolation of cell nuclear and cytosolic fractionation was performed by using Nuclear/Cytosolic Fractionation Kit (Cell Biolabs Inc, AKR171). The lysates of fractions were subjected to western blotting analyses. β-tubulin was used as the cytosolic marker and phospho-Histone H3 was used as the nuclear marker.

Open field test

Mice were placed into a white Plexiglas chamber (60 long×60 wide×30 cm high) under dim ambient light conditions and activity was monitored for 5 min in a single trial. Four squares were defined as the center and the 12 squares along the walls as the periphery. The movements were monitored by an overhead video camera and analyzed by an automated tracking system (San Diego Instruments, CA). Results were averaged for total distance traveled and the number of entries into the center of the field(Belichenko et al., 2009; Ichiki et al., 1995).

Elevated plus maze

The elevated plus maze was made of a black Plexiglas cross (arms 40 cm long × 6 cm wide) elevated 55 cm above the floor. Two opposite arms were enclosed by the transparent walls (40 cm long × 15 cm high) and the two other arms were open. A mouse was placed in the center of the apparatus facing an enclosed arm and allowed to explore the apparatus for 5 min. The total traveling distance and the time spent on the open arms was scored (Walf and Frye, 2007).

Novel object recognition

As previously described (Belichenko et al., 2015; Bevins and Besheer, 2006), two sample objects in one environment were used to examine learning and memory with 24 hours delays. Before testing, mice were habituated in a black Plexiglas chamber (40 long×30 wide×30 cm high) for 10 minutes on 2 consecutive days under ambient light conditions. The activities were monitored by an overhead video camera and analyzed by an automated tracking system (San Diego Instruments, CA). First, two

identical objects, termed as ‘familiar’, were placed in the chamber, and a mouse was placed at the mid-point of the wall opposite the sample objects. After 10 minutes to explore the objects, the mouse was returned to the home cage. After 24 hours, one of the ‘familiar’ objects used for the memory acquisition was replaced with a ‘new’ object similar to the ‘familiar’ one. The mouse was again placed in the chamber for 3 minutes to explore the objects; The total traveling distance and the time spent investigating the objects was assessed. The preference to the novel object was calculated as Time exploring new object / (Time exploring new object + Time exploring familiar object).

Vector construction, transfection, and luciferase reporter assay

Promoter regions of human *DLX1* (from TSS upstream -10 to -1250 bp) or human *LHX*8 (from TSS upstream 0 to -2000 bp) were amplified by PCR from human genomic DNA extracted from control hiPSC-derived pNPCs with the primers shown in Table S6. Then promoter regions were inserted into the pGL3-Basic luciferase-reporter vector (Promega, USA). Control pNPCs were used for luciferase reporter assay. The pNPCs were seeded at $3X10^5$ per well in 24 well plates one day before transfection. The cells were co-transfected with 0.3 µg firefly luciferase-reporter construct (*DLX1*-pGL3, *LHX8*-pGL3 or pGL3-Basic), 0.02 µg pRL-TK Renilla luciferase-reporter plasmid (Promega, USA), and 0.6 µg pLenti-*Olig2*-IRES-GFP vector or control vector using Lipofectamine 3000 (Invitrogen, USA). The luciferase activity was examined using a dual-luciferase reporter assay system (Promega, USA) according to the manufacturer's instructions, and the signal was normalized to the internal Renilla control for transfection efficiency.

CGH array.

CGH array was performed in the cytogenetic laboratory at Rutgers New Jersey Medical School (NJMS). The microarray CGH from NJMS is a customization of the Agilent Technologies 180,000 oligonucleotide probe array including SNPs to detect regions of homozygosity. These arrays provide genome-wide coverage of quantitative variants while as well as providing comprehensive assessment of known deletion/duplication syndromes and detailed coverage of all subtelomeric regions. Data were analyzed by BlueFuse Multi, v3.1 (BlueGnome, Ltd).

QUANTIFICATION AND STATISTICAL ANALYSIS

All data represent mean ± s.e.m. The organoid experiments were replicated at least three times and each experiment was performed in triplicate using organoids derived from the three pairs of DS and control hiPSCs. When only two independent groups were compared, significance was determined by two-tailed unpaired t-test with Welch’s correction. When three or more groups were compared, one-way ANOVA with Bonferroni post hoc test was used. A P value less than 0.05 was considered significant. The analyses were done in GraphPad Prism v.5.

DATA AND SOFTWARE AVAILABILITY SUPPLEMENTAL

The accession number of the RNA sequencing data reported in this study is GEO: GSE124513.

Figure legends:

Figure 1. Generation of ventral forebrain organoids and GABAergic neurons from OLIG2-GFP hPSC reporter lines.

(A) A schematic procedure for deriving ventral forebrain organoids from OLIG2-GFP knockin hiPSCs or hESCs by the treatment of sonic hedgehog (SHH) and purmorphamine (Pur). Insets: representative bright-field and fluorescence images at different stages. Scale bars: 100 μm.

(B) Representatives of Nestin-, FOXG1-, NKX2.1-, PAX6-, OLIG2-, OLIG1- and GFP-expressing cells in 5 to 6-week-old ventral forebrain organoids. Scale bars: 20 μm or 10 μm in the original or enlarged images, respectively.

(C) Quantification of pooled data from OLIG2-GFP hiPSCs and hESCs showing the percentage of Nestin$^+$, FOXG1$^+$, NKX2.1$^+$, PAX6$^+$, GFP$^+$, OLIG2$^+$, OLIG1$^+$, Nestin$^+$/GFP$^+$, FOXG1$^+$/GFP$^+$, NKX2.1$^+$/GFP$^+$, PAX6$^+$/GFP$^+$, OLIG2$^+$/GFP$^+$, and OLIG1$^+$/GFP$^+$ cells in week 5-week-old organoids. The experiments are repeated for four times (n = 4) and for each experiment, 4 to 6 organoids from each cell line (total about 50 organoids) are used. Data are presented as mean ± s.e.m.

(D) 5-week-old ventral forebrain organoids were subjected to subcellular fractionation assay. Western blotting analysis shows that OLIG2 is localized in the nuclear fraction (nuc), whereas OLIG1 localized in the cytosolic fraction (cyto). β-tubulin is used as a cytosolic marker and Histone 3 is used as a nuclear fraction marker.

(E) qPCR analysis of *OLIG2* and *OLIG1* mRNA expression in the organoids at different stages. The experiments are repeated for four times (n = 4) and for each experiment, 20 to 30 organoids derived from OLIG2-GFP hESCs and hiPSCs are used. One-way ANOVA test. $^{**}P < 0.01$, $^{***}P < 0.001$, and *NS* represents no significance. Data are presented as mean ± s.e.m.

(F) Representatives of βIIIT-, GABA-, S100β-, and GFP-expressing cells in 8-week-old ventral forebrain organoids. Scale bars: 20 μm or 10 μm in the original or enlarged images, respectively.

(G) Quantification of pooled data from OLIG2-GFP hiPSCs and hESCs showing the percentage of βIIIT$^+$, GABA$^+$, S100β$^+$, βIIIT$^+$/GFP$^+$, GABA$^+$/GFP$^+$, and S100β$^+$/GFP$^+$ cells in 8-week-old organoids (n = 4, and for each experiment, 4 to 6 organoids from each cell line are used). Data are presented as mean ± s.e.m.

(H) A schematic showing that 5-week-old ventral forebrain organoids derived from OLIG2-GFP hPSC-derived are disaggregated to single cells and then subjected to FACS. The purified GFP$^+$ cells were further cultured under 3D conditions to form organoids.

(I) FACS analysis showing that in 5-week-old organoids, the percentage of GFP$^+$ cells is much higher in the group treated with SHH and Pur than that in the control group treated with DMSO. The experiments are repeated for four times (n = 4) and for each experiment, 40 to 60 organoids derived from OLIG2-GFP hiPSCs and hESCs are used to collect GFP$^+$ cells.

(J) Representatives of GABA-, calbindin (CB)-, calretinin (CR)-, parvalbumin (PV)-, somatostatin (SST), and neuropeptide Y (NPY)-expressing GABAergic neurons in 8-week-old GFP$^+$ cell-derived organoids. Scale bars: 20 μm.

(K) Quantification of pooled data from OLIG2-GFP hiPSCs and hESCs showing the percentage of GABA$^+$, CR$^+$, CB$^+$, SST$^+$, PV$^+$, and NPY$^+$ neurons in 8-week-old GFP$^+$ cell-derived organoids (n = 4 and for each experiment, 4 to 6 organoids from each cell line are used). Data are presented as mean ± s.e.m.

See also Figure S1.

Figure 2. Abnormal expression of OLIG2 in DS hiPSC-derived ventral forebrain organoids.

(A) Fluorescence in situ hybridization (FISH) analysis confirms that three pairs of control (Cont1, Cont2, and Di-DS3) and DS (DS1, DS2, and Tri-DS3) pNPCs stably maintain disomy and trisomy of HAS21, respectively. Scale bar represents 10 μm.

(B) Representatives of Ki67, SOX2, and βIIIT immunostaining, showing ventricular zone (VZ)-like areas found in both control and DS hiPSC-derived 6-week-old organoids after SHH and Pur treatment. Scale bars: 100 μm.
(C) Representatives of Nestin-, NKX2.1-, FOXG1-, PAX6-, and OLIG1-expressing cells in control and DS iPSC-derived 5-week-old ventral forebrain organoids after SHH and Pur treatment. Scale bars: 20 μm.
(D) Quantification of pooled data showing the percentage of Nestin-, NKX2.1-, FOXG1-, PAX6-, and OLIG1-expressing cells from three pairs of control and DS hiPSCs derived 5-week-old ventral forebrain organoids. The experiments are repeated for four times (n = 4) and for each experiment, 4 to 6 organoids from each cell line (total around 70 control and 70 DS organoids) are used. Student's *t* test. *NS* represents no significance. Data are presented as mean ± s.e.m.
(E) Representatives of OLIG2-expressing cells from three pairs of control (Cont1, Cont2, and Di-DS3) and DS (DS1, DS2, and Tri-DS3) iPSC-derived 5-week-old ventral forebrain organoids after SHH and Pur treatment. Scale bars: 20 μm.
(F) Quantification of the percentage of $OLIG2^+$ cells in control or DS hiPSC-derived 5-week-old ventral forebrain organoids. The experiments are repeated for four times (n = 4) and for each experiment, 4 to 6 organoids from each cell line were used. Student's *t* test. ***$P < 0.001$, comparison between DS and corresponding control organoids. Data are presented as mean ± s.e.m.
(G) qPCR analysis of *OLIG2* and *OLIG1* mRNA expression in 5 to 6-week-old control and DS organoids. The experiments are repeated for four times (n = 4) and for each experiment, 20 to 30 organoids respectively derived from control and DS hiPSC lines are used. Student's *t* test, ***$P < 0.001$, comparison between DS and corresponding control organoids. Data are presented as mean ± s.e.m.
(H) Western blotting analysis of OLIG2 and OLIG1 expression in 5 to 6-week-old control and DS organoids.
(I) Quantification of pooled data showing OLIG1 and OLIG2 expression by western blot in the organoids. The experiments are repeated for three times (n = 3) and for each experiment, 30 to 40 organoids respectively derived from three pairs of control and DS hiPSCs are used. Student's *t* test. **$P < 0.01$. Data are presented as mean ± s.e.m.
(J-L) Transcriptome correlation between 5-week-old organoids and post-mortem human brain samples from the BrainSpan project. The x axis shows the post-conception age in weeks or the brain region of the BrainSpan post-mortem brain samples. The y axis shows the mean spearman correlation. AMY, amygdala; CBC, cerebellar cortex; DFC, dorsolateral frontal cortex; HIP, hippocampus; ITC, inferolateral temporal cortex; MFC, medial prefrontal cortex; OFC, orbital frontal cortex; STC, superior temporal cortex; STR, striatum. In (H) x axis shows BrainSpan agglomerated brain regions (i.e., more brain regions were merged into a single ''larger'' region): VF (i.e., VF, CGE, LGE, MGE, STR), ventral forebrain; NCX (i.e., DFC, ITC, MFC, OFC, STC), neocortex; HIP, hippocampus; AMY, amygdala; URL (i.e., CBC, CB, URL), upper rhombic lip.
See also Figure S2, S5 and Table S1, S2.

Figure 3. Overproduction of GABAergic neurons in DS ventral forebrain organoids and DS human brain tissue.
(A) Representatives of MAP2 expression in 8-week-old control (Cont) and DS ventral forebrain organoids. Scale bar: 50 μm.
(B) Representatives of NeuN- and S100β-expressing cells in 8-week-old control and DS organoids. Scale bar: 20 μm.
(C) Quantification of pooled data from three pairs of control and DS hiPSCs showing the percentage of $NeuN^+$ and $S100\beta^+$ cells in 8-week-old control and DS organoids. The experiments are repeated for four times (n = 4) and for each experiment, 4 to 6 organoids from each cell line (total around 70 control and 70 DS organoids) are used. Student's *t* test. *NS* represents no significance. Data are presented as mean ± s.e.m.

(D) Representatives of GABA-expressing neurons from three pairs of control (Cont1, Cont2, and Di-DS3) and DS (DS1, DS2, and Tri-DS3) hiPSC-derived 8-week-old organoids. Scale bar: 20 μm.
(E) Quantification data showing the fluorescence intensity (FI) of GABA in 8-week-old control and DS organoids. The experiments are repeated for four times (n = 4) and for each experiment, 4 to 6 organoids from each cell line are used. Student's *t* test. *$P < 0.05$, ** < 0.01, comparison between DS and corresponding control organoids. Data are presented as mean ± s.e.m.
(F) Representatives of CR-, CB-, SST-, PV-, NPY-, and ChAT-expressing neurons in 8-week-old control and DS organoids. Scale bar: 20 μm.
(G) Quantification data showing the percentage of $GABA^+$, CR^+, SST^+, CB^+, PV^+, NPY^+, and $ChAT^+$ neurons in control and DS hiPSC-derived 8-week-old ventral forebrain organoids. The experiments are repeated for four times (n = 4) and for each experiment, 4 to 6 organoids from each cell line are used. Student's *t* test. **$P < 0.01$, ***$P < 0.001$ and *NS* represents no significance, comparison between DS and corresponding control organoids. Data are presented as mean ± s.e.m.
(H) Western blotting analysis of GAD65/67, CR, and SST expression in postmortem cerebral cortex tissue from control and DS patients at ages less than one-year old.
(I) Quantification of GAD65/67, CR, and SST expression in postmortem cerebral cortex tissue from control and DS patients. Student's *t* test. *$P < 0.05$ and *NS* represents no significance. Data are presented as mean ± s.e.m.
See also Figure S2 and Table S3.

Figure 4. Human neuronal chimeric mice engrafted with DS ventral forebrain NPCs show overabundance of donor-derived GABAergic neurons and abnormal behavior.
(A) A schematic diagram showing that hiPSC-derived ventral forebrain organoids are dissociated into single cells and then engrafted into the brains of P0 *rag*$1^{-/-}$ mice.
(B) Representatives of engrafted human cells at two months post-transplantation. Anti-human nuclei antibody (hN) staining selectively labels engrafted human cells. Engrafted cells are found in the brain regions overlying the lateral ventricles (LV; B1) and the cerebral cortex (B2). Scale bars: 100 μm.
(C) Representatives of hN^+ donor-derived cells at 6 months post-transplantation, showing wide distribution of donor-derived cells in the cerebral cortex. Areas in C1 and C2 are enlarged to show the different cell density in the cerebral cortex and the distribution of donor-derived cells in the hippocampus (HIP), respectively. The images were from confocal stitched tile scan. Scale bars: 100 μm.
(D) A representative image of engrafted lenti-GFP-labeled hiPSC-derived ventral forebrain NPCs. Notably, the GFP^+ neural processes are widely dispersed in the hippocampus. Scale bar: 50 μm.
(E) Representatives of NeuN-, GFAP-, MBP-, and OLIG2-expressing cells differentiated from engrafted control and DS ventral forebrain NPCs in the cerebral cortex at 6 months post-transplantation. Scale bars: 50 μm.
(F) A representative image showing high fluorescence intensity of GABA staining in areas enriched of donor-derived hN^+ cells. Scale bar: 50 μm.
(G) Representatives of GABA staining in the cerebral cortex at 6 months after transplantation of control or DS NPCs. Scale bars: 50 μm.
(H) Representatives of CR-, SST-, CB-, PV-, NPY-, and ChAT-expressing donor-derived hN^+ cells in the cerebral cortex at 6 months post-transplantation. Scale bars, 50 μm.
(I) Quantification of pooled data from control (Cont1 and Di-DS3) and DS (DS1 and Tri-DS3) hiPSCs showing the percentage of $NeuN^+$, $GFAP^+$, MBP^+, and $OLIG2^+$ cells among the total hN^+ cells in the cerebral cortex at 6 months post-transplantation (n = 7 mice for each group). Student's *t* test. **$P < 0.01$, ***$P < 0.001$, and *NS* represents no significance. Data are presented as mean ± s.e.m.
(J) Quantification data from control and DS groups showing the fluorescence intensity (FI) of GABA staining in the cerebral cortex at 6 months post-transplantation (n = 7 mice for each group). Student's *t* test. **$P < 0.01$, ***$P < 0.001$, comparison between DS and corresponding control groups. Data are presented as mean ± s.e.m.

(K) Quantification data from control and DS groups showing percentage of CR^+, SST^+, CB^+, PV^+, NPY^+, and $ChAT^+$ cells among the total hN^+ cells in the cerebral cortex at 6 months post-transplantation (n = 7 mice for each group). Student's *t* test. ***$P < 0.001$, comparison between DS and corresponding control groups. Data are presented as mean ± s.e.m.
(L) Representative images of a human donor-derived neuron filled with Dextran Alexa Fluor 594 during whole-cell patch-clamp recording and visualized by post hoc labeling with hN staining. Scale bars: 10 μm.
(M) Representative current-clamp (I-clamp) recording traces from the cell labeled in (L). Within a pulse stimulation ramping from 0 to 200 pA, the cell can fire action potentials (APs). Six hN^+ cells recorded showed similar response.
(N) Representative voltage-clamp (V-clamp; upper panel) and I-clamp recording traces (lower panel) showing spontaneous postsynaptic currents (sPSCs) and spontaneous postsynaptic potentials (sPSPs) recorded from the cell labeled in (L). The enlarged area in the upper panel shows the presence of both excitatory and inhibitory postsynaptic currents, EPSCs and IPSCs, based on their respective kinetics. Seven hN^+ cells recorded showed sPSCs and sPSPs.
See also Figure S3, S4, S5, S6.

Figure 5. Abnormal gene expression in DS ventral forebrain organoids.
(A) A heatmap showing the differentially expressed genes (DEGs) in 5-week-old organoids derived from control (Cont1 and Di-DS3) and DS (DS1 and Tri-DS3) hiPSCs. Notably, the two disomic control organoids and two trisomic DS organoids cluster closer to each other, respectively.
(B) Venn diagram showing the numbers of DEGs in 5-week-old control and DS organoids. Among these genes, 398 and 212 DEGs are commonly upregulated and downregulated, respectively in the two pairs of control and DS organoids.
(C) The total number of DEGs, percentage of DEGs, and number of up-regulated or down-regulated DEGs on each chromosome in 5-week-old control and DS organoids.
(D) A heatmap showing the DEGs in 5-week-old control (Cont1 and Di-DS3) organoids, DS (DS1 and Tri-DS3) organoids, and organoids derived from Tri-DS3 hiPSCs infected with lentivirus that carry control shRNA (Tri-DS3 + $Cont^{shRNA}$) or OLIG2 shRNA (Tri-DS3 + $OLIG2^{shRNA}$).
(E) Venn diagram showing the numbers of rescued genes after OLIG2 knockdown (KD). Among these genes, 255 and 166 genes are the overlapping DEGs identified from the two pairs of control and DS organoids.
(F) GO analyses of the overlapping down-regulated DEGs and the rescue effects after OLIG2 knockdown.
(G) GO analyses of the overlapping up-regulated and the rescue effects after OLIG2 knockdown.
(H) A heatmap showing the expression of genes critical for GABAergic neuron differentiation and specification in the 5-week-old organoids.
(I) qPCR analysis of *OLIG2*, *DLX1*, *DLX2*, *DLX5*, *DLX6*, *LHX6*, *LHX8*, and *SOX6* mRNA expression in 5-week-old organoids. The experiments are repeated for four times (n = 4) and for each experiment, 20 to 30 organoids are used in each group. One-way ANOVA test. ***$P < 0.001$ and *NS* represents no significance. Data are presented as mean ± s.e.m.
(J) ChIP assay showing that OLIG2 directly interacts with the promotor of *DLX1* and *LHX8*. The regions highlighted in red are the only ones that are immunoprecipitated by OLIG2 antibody.
(K) Luciferase reporter assay showing that OLIG2 expression vector is capable of upregulating *DLX1* or *LHX8* luciferase activity, compared with control vector. The experiments are repeated for three times (n = 3). Student's t test. * $P < 0.01$, ** $P < 0.05$. Data are presented as mean ± s.e.m.
See also Figure S7 and Table S4-6.

Figure 6. Inhibiting OLIG2 expression rescues overproduction of GABAergic neurons in DS organoids and chimeric mice.

(A) Representatives of GABA-expressing cells in 8-week-old DS + Cont^{shRNA} and DS + OLIG2^{shRNA} organoids. Scale bars: 20 μm.
(B) Quantification of the percentage of GABA^{+} cells and FI of GABA staining in 8-week-old control (Cont) organoids, DS + Cont^{shRNA} organoids, and DS + OLIG2^{shRNA} organoids. The data are pooled from control (Cont1 and Di-DS3) hiPSCs, DS (DS1 and Tri-DS3) hiPSCs, and the two lines of DS hiPSCs infected with lentiviruses that carry control shRNA or OLIG2 shRNA. The experiments are repeated for four times (n = 4) and for each experiment, 4-6 organoids from each cell line are used. One-way ANOVA test, $^{**}P < 0.01$ and $^{***}P < 0.001$. Data are presented as mean ± s.e.m.
(C) Representatives of CR-, SST-, CB-, PV-, NPY-, and ChAT-expressing cells in 8-week-old DS + Cont^{shRNA} and DS + OLIG2^{shRNA} organoids. Scale bars: 20 μm.
(D) Quantification of pooled data showing the percentage of CR^{+}, SST^{+}, CB^{+}, PV^{+}, NPY^{+}, and ChAT^{+} cells in 8-week-old disomic Cont organoids, DS + Cont^{shRNA} organoids, and DS + OLIG2^{shRNA} organoids (n = 4 and for each experiment, 4 to 6 organoids from each cell line are used). One-way ANOVA test, $^{***}P < 0.001$, *NS* represents no significance. Data are presented as mean ± s.e.m.
(E) Representatives of GABA-expressing donor-derived hN^{+} cells in the cerebral cortex at 6 months after transplantation of DS + Cont^{shRNA} or DS + OLIG2^{shRNA} ventral forebrain NPCs. Scale bars: 50 μm.
(F) Quantification of FI of GABA staining in the cerebral cortex at 6 months after transplantation of Cont, DS + Cont^{shRNA} or DS + OLIG2^{shRNA} ventral forebrain NPCs (n = 6-8 mice for each group). The data are pooled from mice received transplantation of the NPCs derived from control (Cont1 and Di-DS3) hiPSCs, DS (DS1 and Tri-DS3), and the two lines of DS hiPSCs infected with lentiviruses that carry control shRNA or OLIG2 shRNA. One-way ANOVA test, $^{**}P < 0.01$ and $^{***}P < 0.001$. Data are presented as mean ± s.e.m.
(G) Representatives of CR-, SST-, CB-, PV-, NPY-, and ChAT-expressing donor-derived hN^{+} cells in the cerebral cortex at 6 months after transplantation of DS + Cont^{shRNA} or DS + OLIG2^{shRNA} ventral forebrain NPCs. Scale bars: 50 μm.
(H) Quantification of percentage of CR^{+}, SST^{+}, CB^{+}, PV^{+}, NPY^{+}, and ChAT^{+} cells among total hN^{+} donor-derived cells in the cerebral cortex at 6 months after transplantation of Cont, DS + Cont^{shRNA} or DS + OLIG2^{shRNA} ventral forebrain NPCs (n = 6-8 mice for each group). The data are pooled from mice received transplantation of the NPCs derived from control (Cont1 and Di-DS3) hiPSCs, DS (DS1 and Tri-DS3), and the two lines of DS hiPSCs infected with lentiviruses that carry control shRNA or OLIG2 shRNA. One-way ANOVA test, $^{**}P < 0.01$ and $^{***}P < 0.001$. Data are presented as mean ± s.e.m. See also Figure S7.

Figure 7. DS chimeric mice exhibit impaired cognitive functions.
(A) Open filed test showing the traveling distance and the percentage of time that PBS control mice, Cont chimeric mice, DS chimeric mice, DS + Cont^{shRNA} chimeric mice, and DS + OLIG2^{shRNA} chimeric mice spend in the center area of (n = 10-15 mice for each group). One-way ANOVA test. *NS* represents no significance. Data are presented as mean ± s.e.m.
(B) *Left,* a schematic diagram showing novel object recognition test. *Right,* quantification of the traveling distance and the preference ratio to the novel object of the five groups of chimeric mice (n = 10-15 mice for each group). One-way ANOVA test. $^{***}P < 0.001$, $^{**}P < 0.01$. *NS* represents no significance. Data are presented as mean ± s.e.m.
(C) Elevated plus-maze test showing the traveling distance, the number of entries, and the time that the chimeric mice spend on open arms (n = 10-15 mice for each group). One-way ANOVA test. *NS* represents no significance. Data are presented as mean ± s.e.m.

Supplemental figure legends

Figure S1. Related to Figure 1. Ventral forebrain organoids derived from OLIG2-GFP hPSCs and OLIG2$^+$ ventral forebrain NPCs mainly give rise to CR$^+$ GABAergic neurons under 2D culture conditions.

(A) Representative bright-field and fluorescence images of OLIG2-GFP hPSC-derived ventral forebrain organoids at different stages. Scale bar: 200 μm.

(B) Representatives of SOX2, βIIIT and GFP immunostaining, showing ventricular zone (VZ)-like areas in 6-week-old OLIG2-GFP hPSC-derived ventral forebrain organoids. Scale bars: 50 μm.

(C) Representatives of MBP-expressing mature oligodendrocytes in 8-week-old OLIG2-GFP hPSC-derived ventral forebrain organoids cultured under glial differentiation condition. Scale bars: 10 μm.

(D) Representatives of OLIG2-, Nestin-, NKX2.1-, and OTX2- expressing cells among the GFP$^+$ cells after FACS purification. Scale bars: 50 μm.

(E) Representative bright-field and fluorescence images showing OLIG2$^+$/GFP$^+$ cell-derived organoids at different time points. Scale bar: 500 μm.

(F) Representatives of NeuN-, S100β-, NG2-, and PDGFRα-expressing cells in 8-week-old OLIG2$^+$/GFP$^+$ cell-derived organoids cultured under neuronal differentiation condition. Scale bars: 20 μm.

(G) Quantification of pooled data from OLIG2-GFP hiPSCs and hESCs showing the percentage of NeuN$^+$, S100β$^+$, NG2$^+$, and PDGFRα$^+$ in 8-week-old GFP$^+$ cell-derived organoids (n = 3 and for each experiment, 4 to 6 organoids from each line are used). Data are presented as mean ± s.e.m.

(H) Representatives of GABA-, CR-, and MAP2-expressing neurons differentiated from OLIG2$^+$ ventral forebrain NPCs under neuronal differentiation condition in 2D cultures. Scale bar: 50 μm.

(I) Quantification of pooled data from OLIG2-GFP hiPSCs and hESCs showing the percentage of GABA$^+$, CR$^+$, PV$^+$, and SST$^+$ cells among total MAP2$^+$ neurons (n = 4). Data are presented as mean ± s.e.m.

Figure S2. Related to Figure 2 and 3. Overabundance of GABAergic neurons in DS organoids. (A) Comparative genomic hybridization (CGH) array of isogenic pair of Di-DS3 and Tri-DS3 demonstrates a gain of one chromosome 21 (red arrow) in Tri-DS3. No significant deletions or insertions were detected between the isogenic pair.

(B) Close-up of Chr21 CGH of Tri-DS3 shows full chromosome 21 trisomy with no deletions or duplications.

(C) qPCR results from genomic DNA showing the relative *OLIG1* and *OLIG2* DNA copy numbers in control (Cont1, Cont2, and Di-DS3) and DS (DS1, DS2, and Tri-DS3) pNPCs. *$P < 0.05$, comparison between Cont1 vs. DS1, Cont-2 vs. DS2, or Di-DS3 vs. Tri-DS3 pNPCs.

(D) Representative bright-field images of control (Cont) and DS hiPSC-derived ventral forebrain organoids at different stages. Scale bars: 200 μm.

(E) Quantification of size of control (Cont) and DS hiPSC-derived ventral forebrain organoids at different stages. Scale bars: 200 μm. Student's *t* test. *NS* represents no significance. Data are presented as mean ± s.e.m.

(F) Representative low magnification images of organoids showing GABA-, CR- and SST-expressing neurons in 8-week-old control and DS organoids. Scale bar: 50 μm.

(G) Coomassie blue staining of the human samples after running denatured SDS-PAGE showing high sharpness and resolution of protein bands and the absence of smear (little or no degradation) of protein bands.

Figure S3. Related to Figure 4. Distribution and characterization of donor-derived cells after transplantation to the sites overlying lateral ventricles.

(A) Representatives of NKX2.1-expressing donor-derived hN^+ cells in the cerebral cortex at 2 months post-transplantation of control or DS NPCs. Arrows indicate the donor-derived hN^+ cells expressing NKX2.1 and arrowhead indicates the NKX2.1-negative endogenous mouse cell. Scale bars, 20 μm.
(B) Quantification of pooled data from control (Cont1 and Di-DS3) and DS (DS1 and Tri-DS3) hiPSCs showing the percentage of $NKX2.1^+$ cells among the total hN^+ cells in the cerebral cortex at 2 months post-transplantation (n = 7 mice for each group). Student's *t* test. *NS* represents no significance. Data are presented as mean ± s.e.m.
(C) Representatives of LHX6-expressing donor-derived hN^+ cells in the cerebral cortex at 6 months post-transplantation of control or DS NPCs. Arrows indicate the donor-derived hN^+ cells expressing LHX6. Scale bars, 20 μm.
(D) Quantification of pooled data from control (Cont1 and Di-DS3) and DS (DS1 and Tri-DS3) groups showing the percentage of $LHX6^+$ cells among the total hN^+ cells in the cerebral cortex at 6 months post-transplantation (n = 7 mice for each group). Student's *t* test. *NS* represents no significance. Data are presented as mean ± s.e.m.
(E and F) Representative images from sagittal brain sections showing the wide distribution of hN^+ donor-derived cells in the cerebral cortex at 6 months post-transplantation. Areas in E1 and F1 are enlarged. The images were from confocal stitched tile scan. Scale bars: 1mm or 500 μm as indicated.
(G) A schematic diagram showing the relative positions of the sagittal sections shown in (E) and (F).
(H-J) Representative images from coronal brain sections showing the wide distribution of hN^+ donor-derived cells in the cerebral cortex at 6 months post-transplantation. The sections were collected after whole-cell patch-clamp recording and visualized by post hoc labeling with hN staining. Areas in H1, I1 and J1 are enlarged. The images were from confocal stitched tile scan. Scale bars: 1mm or 500 μm as indicated.
(G) A schematic diagram showing that relative positions of coronal sections shown in (H), (I), and (J).
(L) Representatives of DCX-expressing donor-derived hN^+ cells in the cerebral cortex at 4 months post-transplantation. Arrows indicate the bipolar processes of DCX^+/hN^+ cells. Scale bars, 20 μm.

Figure S4. Related to Figure 4. Characterization of donor-derived cells after transplantation to the sites near subventricular zone.
(A) A schematic diagram showing that control hiPSC-derived ventral forebrain NPCs are engrafted into the brains of P0 *rag*$1^{-/-}$ mice into the sites near the subventricular zone (SVZ).
(B) Representatives showing that donor-derived hN^+ cells have migrated along the rostral migratory stream to the olfactory bulb at 6 months after transplantation. Scale bar, 1 mm or 100 μm as indicated.
(C) Representatives of NeuN-, GFAP-, MBP-, OLIG2- and CR-expressing donor-derived hN^+ cells in the olfactory bulb at 6 months post-transplantation. Arrows indicate the donor-derived hN^+ cells expressing the indicated markers. Scale bars, 50 μm.
(D) Representatives of NeuN-, GFAP-, MBP-, CR-, SST-, CB-, PV-, NPY-, and ChAT-expressing donor-derived hN^+ cells in the regions near injection sites at 6 months post-transplantation. Arrows indicate the donor-derived hN^+ cells expressing the indicated markers. Scale bars, 50 μm.
(E) Representatives of DCX-expressing donor-derived hN^+ cells at 3 months post-transplantation in the cerebral cortex. CC, corpus callosum. Scale bars, 50 μm.
(F) Quantification of pooled data from control (Cont1 and Di-DS3) hiPSCs showing NeuN-, GFAP-, MBP-, OLIG2- and CR-expressing donor-derived hN^+ cells among the total hN^+ cells in the olfactory bulb at 6 months post-transplantation (n = 7 mice for each group). Data are presented as mean ± s.e.m.
(G) Quantification of pooled data from control (Cont1 and Di-DS3) hiPSCs showing NeuN-, GFAP-, MBP-, CR-, SST-, CB-, PV-, NPY-, and ChAT-expressing donor-derived hN^+ cells in the regions near injection sites among the total hN^+ cells at 6 months post-transplantation (n = 7 mice for each group). Data are presented as mean ± s.e.m.

Figure S5. Related to Figure 2 and Figure 4. Proliferation of the cells before and after transplantation and interneuron identity after transplantation.

(A) Representatives of Ki67-expressing proliferating cells in control and DS 5-week-old ventral forebrain organoids. Arrows indicate OLIG2$^+$/Ki67$^+$ cells and arrowheads indicate OLIG2$^+$/Ki67$^-$ cells. Scale bars: 10 μm.
(B) Representatives of Ki67-expressing donor-derived hN$^+$ cells in the cerebral cortex at 2 and 6 months post-transplantation. Arrows indicate the donor-derived hN$^+$ cells expressing Ki67. The images were from confocal stitched tile scan. Scale bars, 20 μm.
(C) Quantification of pooled data from three pairs of control and DS hiPSCs showing the percentage of Ki67$^+$ cells in the total cells, as well as the percentage of Ki67$^+$/OLIG2$^+$ in total OLIG2$^+$ cells in 5-week-old control and DS ventral forebrain organoids (n = 4 and for each experiment, 4 to 6 organoids from each cell line are used). Student's *t* test. $^{**}P < 0.01$ and *NS* represents no significance. Data are presented as mean ± s.e.m
(D) Quantification of pooled data from control (Cont1 and Di-DS3) and DS (DS1 and TriDS3) hiPSCs showing the percentage of Ki67$^+$ cells among the total hN$^+$ cells in the cerebral cortex at 2 and 6 months post-transplantation (n = 7 mice for each group). Student's *t* test. *NS* represents no significance. Data are presented as mean ± s.e.m.
(E) Representatives of PDGFRα-expressing donor-derived hN$^+$ cells in the cerebral cortex at 6 months post-transplantation. Scale bars, 20 μm.
(F) Quantification of pooled data from control (Cont1 and Di-DS3) and DS (DS1 and Tri-DS3) hiPSCs showing the percentage of PDGFRα$^+$ cells among the total hN$^+$ cells in the cerebral cortex at 6 months post-transplantation (n = 7 mice for each group). Student's *t* test. $^*P < 0.05$. Data are presented as mean ± s.e.m.
(G) Representative images showing strong GABA staining in areas enriched of donor-derived hN$^+$ cells in the cerebral cortex at 6 months after transplantation. The cells are labeled by lenti-CMV-GFP, prior to transplantation. Scale bar, 20 μm.
(H) A representative image from DS chimeric mice showing high fluorescence intensity of GABA staining in areas enriched of donor-derived hN$^+$ cells in the cerebral cortex at 6 months after transplantation. Scale bar, 50 μm.
(I) Representative images showing GFP$^+$ donor-derived cells also express VGAT in the cerebral cortex at 6 months after transplantation. The cells are labeled by lenti-CMV-GFP, prior to transplantation. Scale bar, 10μm.

Figure S6. Related to Figure 4. Overabundance of GABAergic neurons in DS chimeric mouse brains and integration of donor cell-derived neurons into the brain.
(A), (F) Representatives and quantification of GAD65/67staining in the cerebral cortex at 6 months after transplantation of control or DS hiPSC-derived ventral forebrain NPCs. Scale bar, 50 μm. Quantification of pooled data from control (Cont1 and Di-DS3) and DS (DS1 and Tri-DS3) showing the fluorescence intensity (FI) of GAD65/67 staining (n = 7 mice for each group). Student's *t* test. $^*P < 0.05$. Data are presented as mean ± s.e.m.
(B) Representatives of SST, CR, and hN triple-staining in the cerebral cortex at 6 months after transplantation of DS hiPSC-derived ventral forebrain NPCs. Notably, few hN$^+$ human cells co-express SST and CR. Arrows indicate the donor-derived hN$^+$ cells co-expressing SST and CR. Arrowheads indicate the donor-derived hN$^+$ cells only expressing SST or CR. Scale bar, 50 μm or 10 μm in the original or enlarged images, respectively.
(C) Representatives of the hN$^+$ cell nuclei surrounded by the staining of presynaptic marker synapsin I in the cerebral cortex at 6 months after transplantation of control or DS hiPSC-derived ventral forebrain NPCs. Scale bar, 10 μm.
(D) Representatives of human-specific MAP2 (hMAP2)-expressing dendrites that co-localize with puncta of PSD-95 staining, a postsynaptic marker, in the cerebral cortex at 6 months after transplantation of control or DS hiPSC-derived ventral forebrain NPCs. Scale bar, 5 μm.

(E) Representatives of c-Fos-expressing donor-derived hN^+ cells in the cerebral cortex at 6 months post-transplantation of control or DS NPCs. Arrows show engrafted hN^+ cells expressing c-Fos. Scale bars, 20 μm.
(G) Quantification of pooled data from control (Cont1 and Di-DS3) and DS (DS1 and Tri-DS3) hiPSCs showing the percentage of c-Fos^+ cells among the total hN^+ cells in the cerebral cortex at 6 months post-transplantation (n = 7 mice for each group). Student's *t* test. *NS* represents no significance. Data are presented as mean ± s.e.m.
(H) Representative electron microscopy images of synaptic terminals formed between human neurons labeled by DAB staining against GFP or a human-specific marker STEM121 and mouse neurons that were not labeled by the DAB staining. (a) synaptic contacts from human transplant to mouse host tissue and (b) synapse from mouse neurons to human neurons at 6 months post-transplantation. Synaptic cleft structure was seen in the synaptic terminals. "H" denotes human neurons, "M" denotes mouse neurons, and arrowheads indicate DAB electron-dense precipitates. Scale bar represents 100 nm.

Figure S7. Related to Figure 5 and Figure 6. Reversed expression of differentially expressed genes (DEGs) in Tri-DS3 organoids by OLIG2 knockdown and differentiation of DS ventral forebrain NPCs after OLIG2 knockdown in the organoids and chimeric mouse brains.
(A) Venn diagrams showing 438 upregulated and 388 downregulated DEGs are reversed after *OLIG2* knockdown (KD) in 5-week-old Di-DS3 and Tri-DS3 organoids.
(B) The total number of reversed DEGs, percentage of reversed DEGs, and number of up-regulated or down-regulated of DEGs that are reversed after OLIG2 knockdown on each chromosome in 5-week-old Di-DS3 and Tri-DS3 organoids.
(C) qPCR analysis of *OLIG2* mRNA expression in 5-week-old control, DS, DS + $Cont^{shRNA}$ and DS + $OLIG2^{shRNA}$ organoids. The data are pooled from control (Cont1 and Di-DS3) hiPSCs, DS (DS1 and Tri-DS3) hiPSCs, and the two lines of DS hiPSCs infected with lentiviruses that carry control shRNA or OLIG2 shRNA. The experiments are repeated for three times (n = 3) and for each experiment, 20 to 30 organoids from each line are used. Student's *t* test. $^{**}P < 0.01$, $^{*}P < 0.05$. Data are presented as mean ± s.e.m.
(D) Western blotting analysis of OLIG2 expression in 5-week-old control, DS, DS + $Cont^{shRNA}$ and DS + $OLIG2^{shRNA}$ organoids.
(E) Quantification data showing OLIG2 expression by western blotn in 5-week-old control, DS, DS + $Cont^{shRNA}$ and DS + $OLIG2^{shRNA}$ organoids. The data are pooled from control (Cont1 and Di-DS3) hiPSCs, DS (DS1 and Tri-DS3) hiPSCs, and the two lines of DS hiPSCs infected with lentiviruses that carry control shRNA or OLIG2 shRNA. The experiments are repeated for three times (n = 3) and for each experiment, 30 to 40 organoids from each line are used. Student's *t* test. $^{**}P < 0.01$, $^{*}P < 0.05$. Data are presented as mean ± s.e.m.
(F) Representatives of NeuN-, S100β-, NG2-, and PDGFRα-expressing cells in 8-week-old DS + $Cont^{shRNA}$ and DS + $OLIG2^{shRNA}$ organoids. Scale bars: 20 μm.
(G) Representatives of NeuN-, GFAP-, and MBP-expressing donor-derived hN^+ cells in the cerebral cortex at 6 months after transplantation of DS + $Cont^{shRNA}$ and DS + $OLIG2^{shRNA}$ ventral forebrain NPCs. Scale bars, 50 μm.
(H) Quantification of percentage of $NeuN^+$, $S100\beta^+$, $NG2^+$, and $PDGFR\alpha^+$ in 8-week-old control (Cont), DS + $Cont^{shRNA}$, and DS + $OLIG2^{shRNA}$ organoids. The data are pooled from control (Cont1 and Di-DS3) hiPSCs, DS (DS1 and Tri-DS3) hiPSCs, and the two lines of DS hiPSCs infected with lentiviruses that carry control shRNA or OLIG2 shRNA. The experiments are repeated for three times (n = 3) and for each experiment, 8 to10 organoids from each line are used. Data are presented as mean ± s.e.m.
(I) Quantification of the percentage of $NeuN^+$, $GFAP^+$, and MBP^+ expressing cells among total hN^+ cells in the cerebral cortex at 6 months after transplantation of control (Cont), DS + $Cont^{shRNA}$, or DS + $OLIG2^{shRNA}$ ventral forebrain NPCs (n = 7 mice for each group). The data are pooled from mice received transplantation of the NPCs derived from control (Cont1 and Di-DS3) hiPSCs, DS (DS1 and

Tri-DS3) hiPSCs, and the two lines of DS hiPSCs infected with lentiviruses that carry control shRNA or OLIG2 shRNA. One-way ANOVA test, *$P < 0.05$, **$P < 0.01$, and *NS* represents no significance. Data are presented as mean ± s.e.m.

(J) Quantification of the percentage of hN^+ cells in total $DAPI^+$ cells in the cerebral cortex at 6 months post-transplantation in control (Cont), DS + $Cont^{shRNA}$, or DS + $OLIG2^{shRNA}$ chimeric mouse groups (n = 7-8 mice for each group). The data are pooled from mice received transplantation of the NPCs derived from control (Cont1 and Di-DS3) hiPSCs, DS (DS1 and Tri-DS3) hiPSCs, and the two lines of DS hiPSCs infected with lentiviruses that carry control shRNA or OLIG2 shRNA. One-way ANOVA test. *NS* represents no significance. Data are presented as mean ± s.e.m.

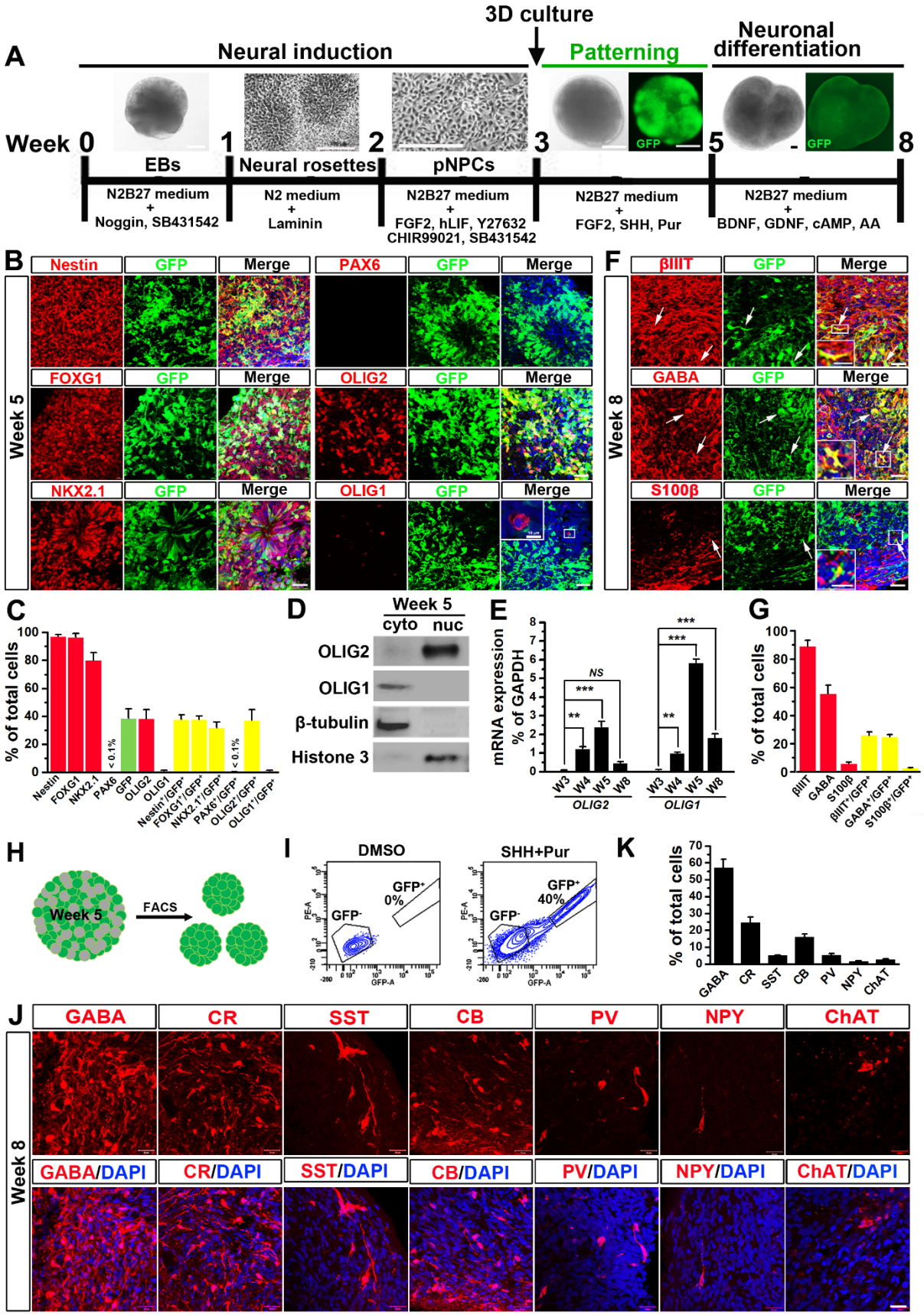
A
3D culture
Neural induction
Patterning
Neuronal differentiation
Week 0
1
2
3
5
8
EBs
Neural rosettes
pNPCs
N2B27 medium + Noggin, SB431542
N2 medium + Laminin
N2B27 medium + FGF2, hLIF, Y27632 CHIR99021, SB431542
N2B27 medium + FGF2, SHH, Pur
N2B27 medium + BDNF, GDNF, cAMP, AA
GFP
B
Week 5
Nestin
PAX6
FOXG1
OLIG2
NKX2.1
OLIG1
GFP
Merge
F
Week 8
βIIIT
GABA
S100β
C
% of total cells
Nestin
FOXG1
NKX2.1
PAX6
GFP
OLIG2
OLIG1
Nestin+/GFP+
FOXG1+/GFP+
NKX2.1+/GFP+
PAX6+/GFP+
OLIG2+/GFP+
OLIG1+/GFP+
< 0.1%
D
Week 5
cyto
nuc
OLIG2
OLIG1
β-tubulin
Histone 3
E
mRNA expression % of GAPDH
NS
***
**
W3
W4
W5
W8
OLIG2
OLIG1
G
βIIIT
GABA
S100β
βIIIT+/GFP+
GABA+/GFP+
S100β+/GFP+
H
Week 5
FACS
I
DMSO
SHH+Pur
GFP-
GFP+
0%
40%
PE-A
GFP-A
K
% of total cells
GABA
CR
SST
CB
PV
NPY
ChAT
J
Week 8
GABA/DAPI
CR/DAPI
SST/DAPI
CB/DAPI
PV/DAPI
NPY/DAPI
ChAT/DAPI

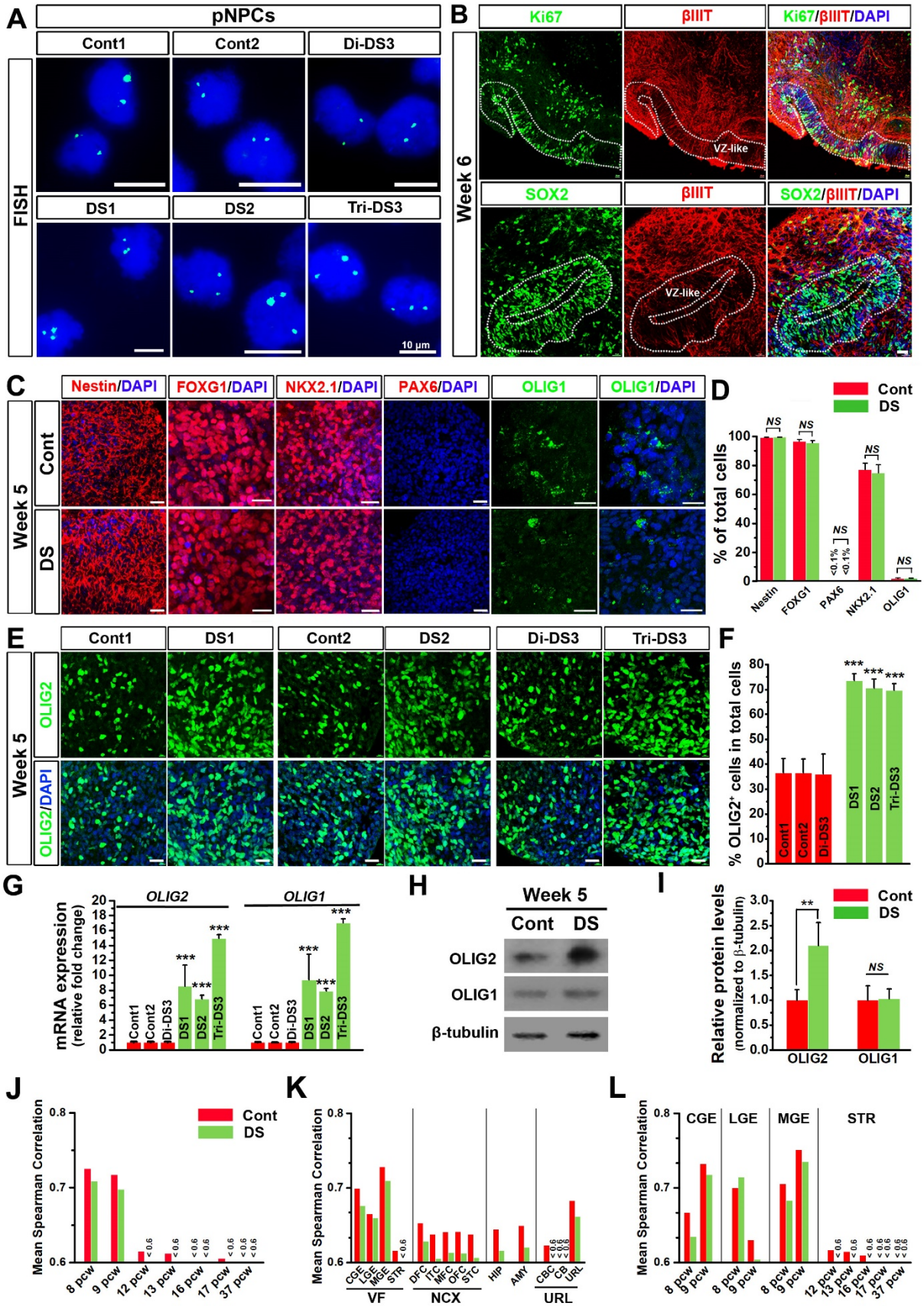
A
pNPCs
Cont1
Cont2
Di-DS3
FISH
DS1
DS2
Tri-DS3
10 μm
B
Ki67
βIIIT
Ki67/βIIIT/DAPI
Week 6
VZ-like
SOX2
SOX2/βIIIT/DAPI
C
Nestin/DAPI
FOXG1/DAPI
NKX2.1/DAPI
PAX6/DAPI
OLIG1
OLIG1/DAPI
Week 5
Cont
DS
D
% of total cells
NS
<0.1%
Nestin
FOXG1
PAX6
NKX2.1
OLIG1
E
OLIG2
OLIG2/DAPI
F
% OLIG2+ cells in total cells
***
G
mRNA expression (relative fold change)
OLIG2
OLIG1
H
Week 5
β-tubulin
I
Relative protein levels (normalized to β-tubulin)
**
J
Mean Spearman Correlation
8 pcw
9 pcw
12 pcw
13 pcw
16 pcw
17 pcw
37 pcw
K
CGE
LGE
MGE
STR
DFC
ITC
MFC
OFC
STC
HIP
AMY
CBC
CB
URL
VF
NCX
L

Xu et al., Figure 3

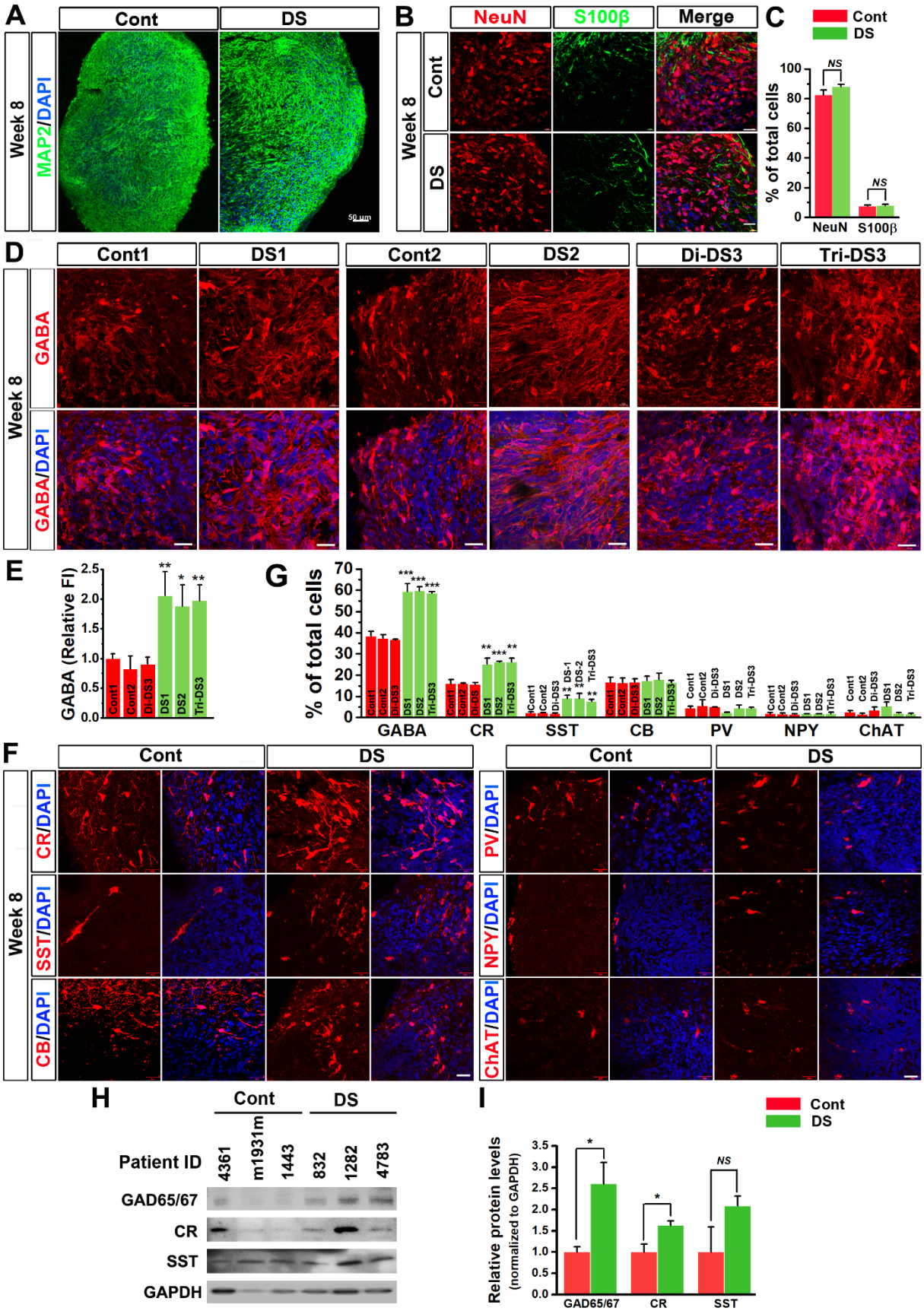

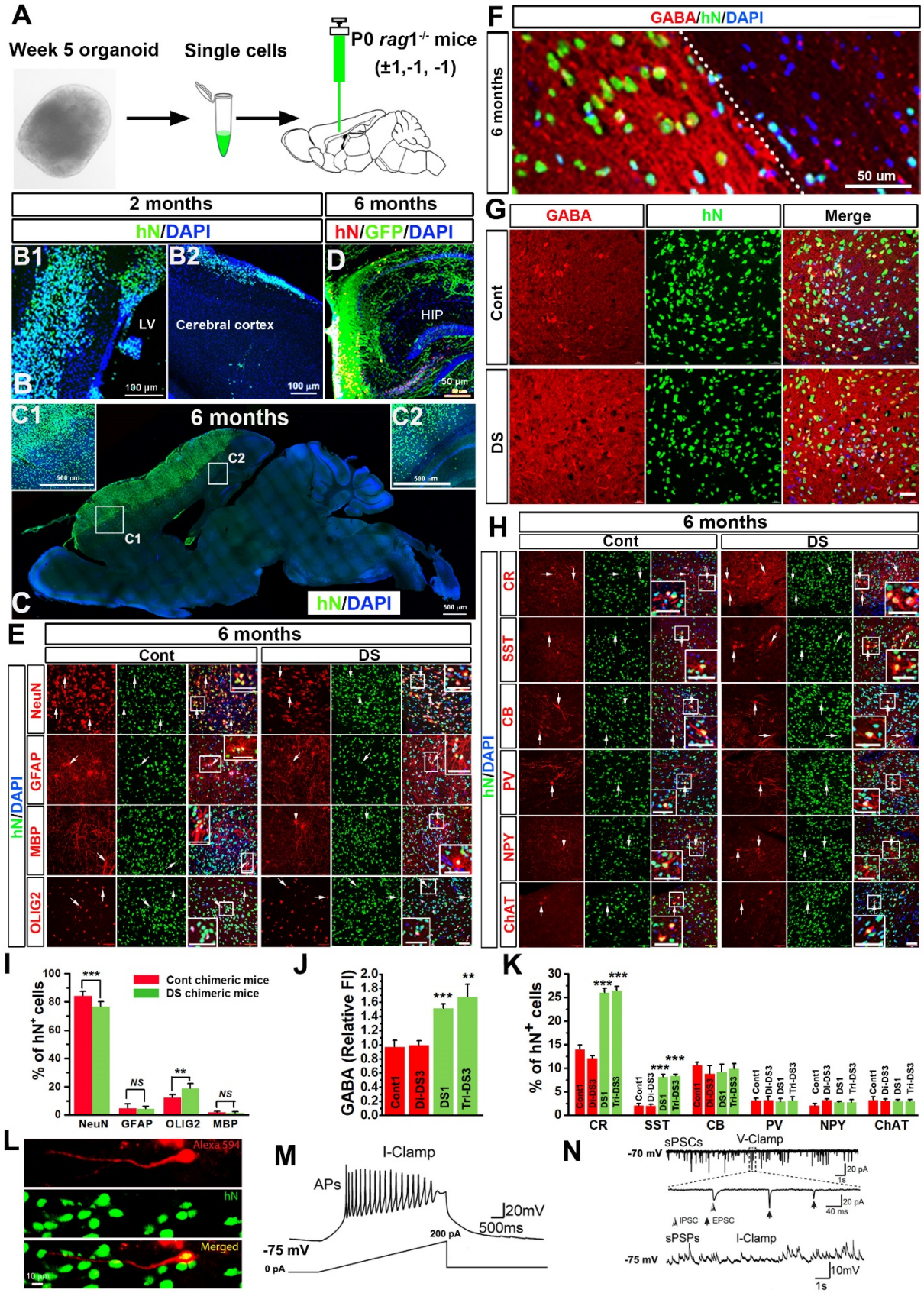
A
Week 5 organoid
Single cells
P0 rag1-/- mice
(±1,-1, -1)
2 months
6 months
hN/DAPI
hN/GFP/DAPI
B1
B2
D
LV
Cerebral cortex
HIP
100 µm
50 µm
C1
C2
6 months
C
hN/DAPI
500 µm
E
6 months
Cont
DS
NeuN
GFAP
MBP
OLIG2
F
GABA/hN/DAPI
6 months
50 um
G
GABA
hN
Merge
Cont
DS
H
6 months
Cont
DS
CR
SST
CB
PV
NPY
ChAT
I
% of hN+ cells
Cont chimeric mice
DS chimeric mice
NeuN
GFAP
OLIG2
MBP
NS
J
GABA (Relative FI)
Cont1
Di-DS3
DS1
Tri-DS3
K
% of hN+ cells
CR
SST
CB
PV
NPY
ChAT
L
Alexa 594
hN
Merged
10 µm
M
I-Clamp
APs
20mV
500ms
-75 mV
200 pA
0 pA
N
sPSCs
V-Clamp
-70 mV
20 pA
1s
IPSC
EPSC
40 ms
sPSPs
I-Clamp
-75 mV
10mV
1s

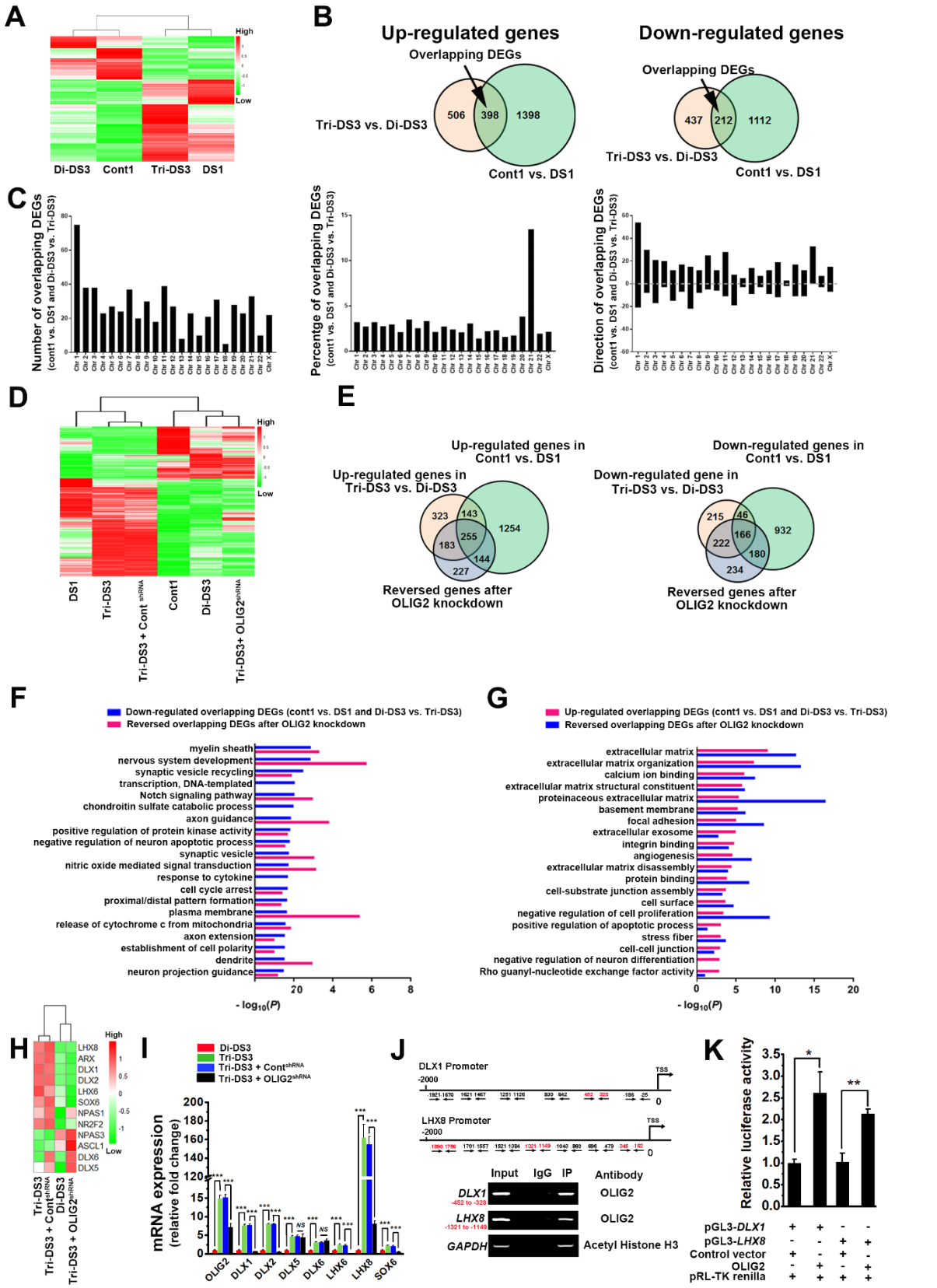
A
High
Low
Di-DS3
Cont1
Tri-DS3
DS1
B
Up-regulated genes
Overlapping DEGs
Tri-DS3 vs. Di-DS3
506
398
1398
Cont1 vs. DS1
Down-regulated genes
Overlapping DEGs
437
212
1112
Tri-DS3 vs. Di-DS3
Cont1 vs. DS1
C
Number of overlapping DEGs (cont1 vs. DS1 and Di-DS3 vs. Tri-DS3)
Percentge of overlapping DEGs (cont1 vs. DS1 and Di-DS3 vs. Tri-DS3)
Direction of overlapping DEGs (cont1 vs. DS1 and Di-DS3 vs. Tri-DS3)
D
High
Low
DS1
Tri-DS3
Tri-DS3 + Cont shRNA
Cont1
Di-DS3
Tri-DS3+ OLIG2shRNA
E
Up-regulated genes in Cont1 vs. DS1
Up-regulated genes in Tri-DS3 vs. Di-DS3
323
143
1254
255
183
144
227
Reversed genes after OLIG2 knockdown
Down-regulated genes in Cont1 vs. DS1
Down-regulated gene in Tri-DS3 vs. Di-DS3
215
46
166
932
222
180
234
Reversed genes after OLIG2 knockdown
F
Down-regulated overlapping DEGs (cont1 vs. DS1 and Di-DS3 vs. Tri-DS3)
Reversed overlapping DEGs after OLIG2 knockdown
myelin sheath
nervous system development
synaptic vesicle recycling
transcription, DNA-templated
Notch signaling pathway
chondroitin sulfate catabolic process
axon guidance
positive regulation of protein kinase activity
negative regulation of neuron apoptotic process
synaptic vesicle
nitric oxide mediated signal transduction
response to cytokine
cell cycle arrest
proximal/distal pattern formation
plasma membrane
release of cytochrome c from mitochondria
axon extension
establishment of cell polarity
dendrite
neuron projection guidance
- log10(P)
G
Up-regulated overlapping DEGs (cont1 vs. DS1 and Di-DS3 vs. Tri-DS3)
Reversed overlapping DEGs after OLIG2 knockdown
extracellular matrix
extracellular matrix organization
calcium ion binding
extracellular matrix structural constituent
proteinaceous extracellular matrix
basement membrane
focal adhesion
extracellular exosome
integrin binding
angiogenesis
extracellular matrix disassembly
protein binding
cell-substrate junction assembly
cell surface
negative regulation of cell proliferation
positive regulation of apoptotic process
stress fiber
cell-cell junction
negative regulation of neuron differentiation
Rho guanyl-nucleotide exchange factor activity
- log10(P)
H
High
Low
LHX8
ARX
DLX1
DLX2
LHX6
SOX6
NPAS1
NR2F2
NPAS3
ASCL1
DLX6
DLX5
Tri-DS3
Tri-DS3 + Contshrna
Di-DS3
Tri-DS3 + OLIG2shrna
I
Di-DS3
Tri-DS3
Tri-DS3 + Contshrna
Tri-DS3 + OLIG2shrna
mRNA expression (relative fold change)
OLIG2
DLX1
DLX2
DLX5
DLX6
LHX6
LHX8
SOX6
J
DLX1 Promoter
LHX8 Promoter
TSS
Input
IgG
IP
Antibody
DLX1
OLIG2
LHX8
OLIG2
GAPDH
Acetyl Histone H3
K
Relative luciferase activity
pGL3-DLX1
pGL3-LHX8
Control vector
OLIG2
pRL-TK renilla

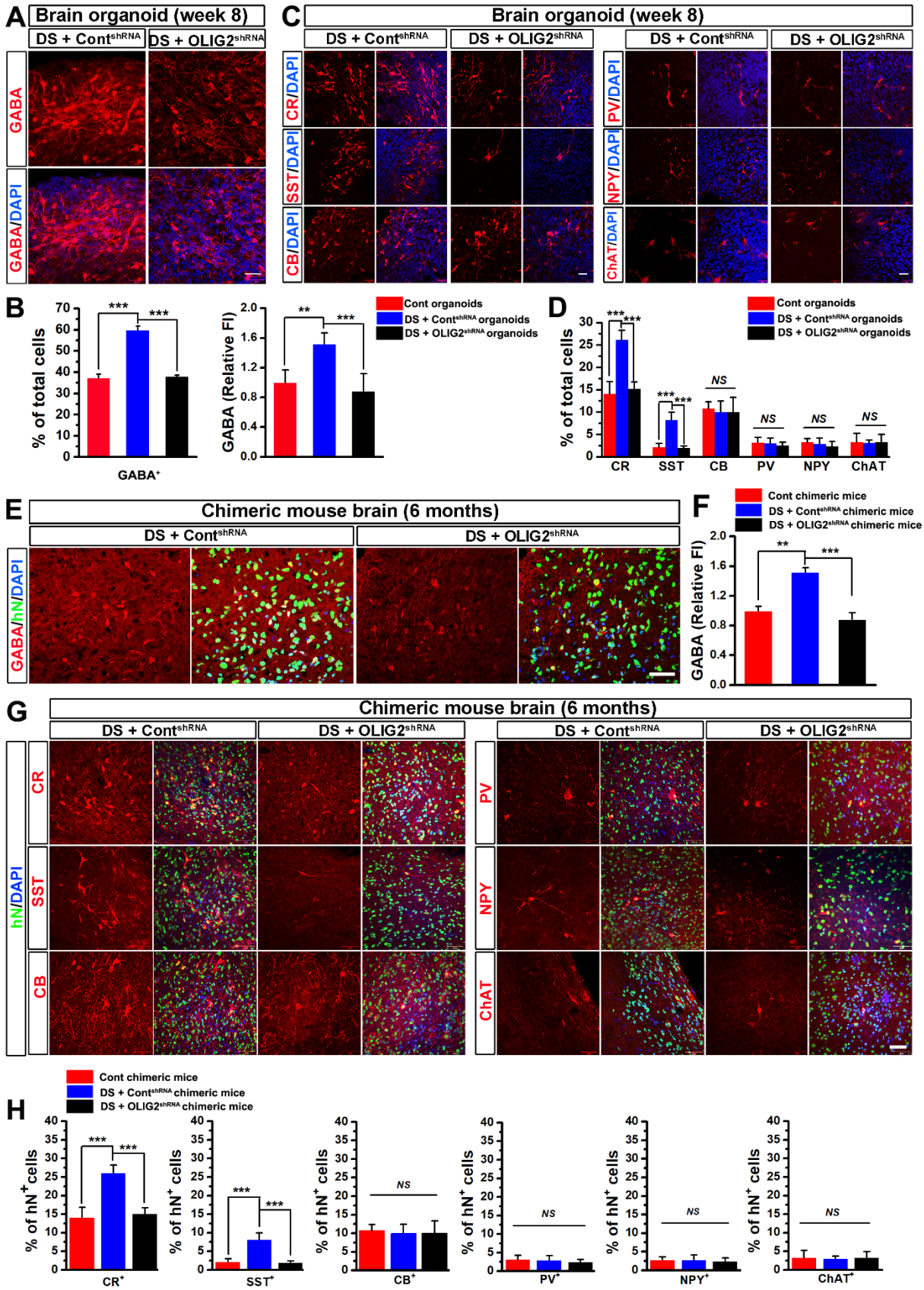
A
Brain organoid (week 8)
DS + Cont shRNA
DS + OLIG2 shRNA
GABA
GABA/DAPI
C
Brain organoid (week 8)
DS + Cont shRNA
DS + OLIG2 shRNA
CR/DAPI
SST/DAPI
CB/DAPI
PV/DAPI
NPY/DAPI
ChAT/DAPI
B
% of total cells
GABA+
GABA (Relative FI)
Cont organoids
DS + Cont shRNA organoids
DS + OLIG2 shRNA organoids
D
% of total cells
CR
SST
CB
PV
NPY
ChAT
NS
E
Chimeric mouse brain (6 months)
DS + Cont shRNA
DS + OLIG2 shRNA
GABA/hN/DAPI
F
Cont chimeric mice
DS + Cont shRNA chimeric mice
DS + OLIG2 shRNA chimeric mice
GABA (Relative FI)
G
Chimeric mouse brain (6 months)
DS + Cont shRNA
DS + OLIG2 shRNA
hN/DAPI
CR
SST
CB
PV
NPY
ChAT
H
Cont chimeric mice
DS + Cont shRNA chimeric mice
DS + OLIG2 shRNA chimeric mice
% of hN+ cells
CR+
SST+
CB+
PV+
NPY+
ChAT+
NS

A Open field

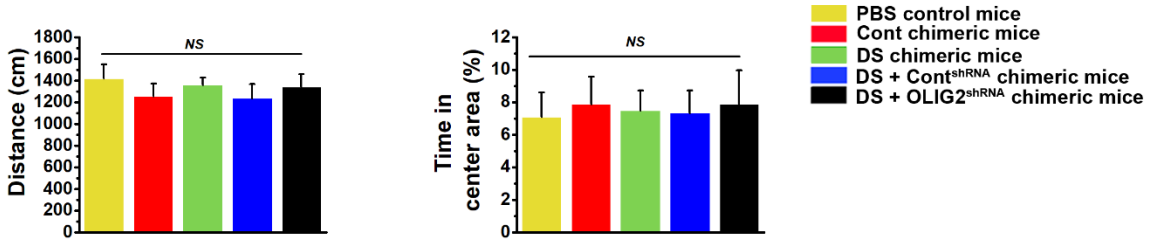

B Novel object recognition

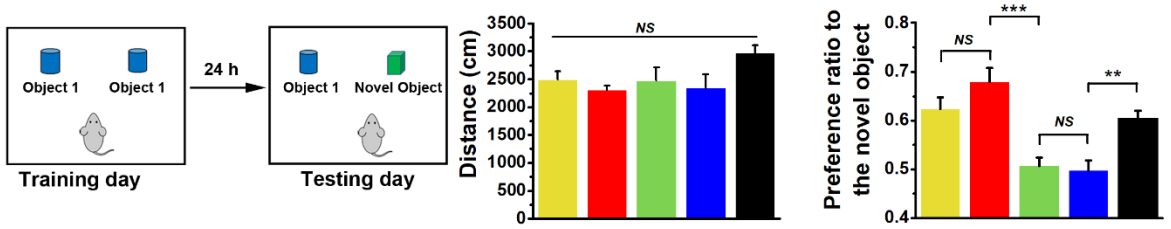
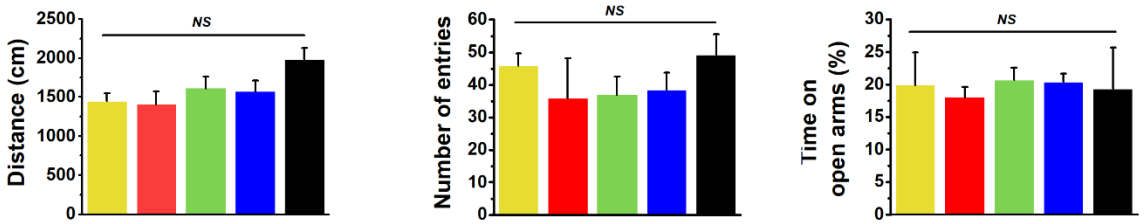
C Elevated plus maze